Superhydrophobic Engineered Cementitious Composites for Highway Bridge Applications: Phase II

CFIRE

CFIRE 05-10
June 2013

National Center for Freight & Infrastructure Research & Education
Department of Civil and Environmental Engineering
College of Engineering
University of Wisconsin–Madison

Authors:
Konstantin Sobolev, Habib Tabatabai, Jian Zhao, Ismael Flores-Vivian, Scott Muzenski
University of Wisconsin, Milwaukee

Michael G. Oliva, Rehan Rauf
University of Wisconsin, Madison

Principal Investigators:
Konstantin Sobolev (PI), Habib Tabatabai (co-PI), Jian Zhao (co-PI)
University of Wisconsin-Milwaukee

Michael G. Oliva (co-PI)
University of Wisconsin-Madison

DISCLAIMER

This research was funded by the National Center for Freight and Infrastructure Research and Education. The contents of this report reflect the views of the authors, who are responsible for the facts and the accuracy of the information presented herein. This document is disseminated under the sponsorship of the Department of Transportation, University Transportation Centers Program, in the interest of information exchange. The U.S. Government assumes no liability for the contents or use thereof. The contents do not necessarily reflect the official views of the National Center for Freight and Infrastructure Research and Education, the University of Wisconsin-Milwaukee, the University of Wisconsin-Madison, the Wisconsin Department of Transportation, or the USDOT's RITA at the time of publication.

Technical Report Documentation Page

1. Report No. CFIRE 05-10	2. Government Accession No.	3. Recipient's Catalog No. **CFDA 20.701**
4. Title and Subtitle **Development of an Engineered Cementitious Composite to Enhance Bridge Approach Slab Durability**		5. Report Date **June 2013** 6. Performing Organization Code
7. Author/s Konstantin Sobolev, Habib Tabatabai, Jian Zhao, Ismael Flores, Scott Muzenski University of Wisconsin, Milwaukee Michael G. Oliva, Rehan Rauf, University of Wisconsin, Madison		8. Performing Organization Report No. **CFIRE 05-10**
9. Performing Organization Name and Address National Center for Freight and Infrastructure Research and Education (CFIRE) University of Wisconsin-Madison 1415 Engineering Drive, 2205 EH Madison, WI 53706		10. Work Unit No. (TRAIS) 11. Contract or Grant No. **344k304**
12. Sponsoring Organization Name and Address Research and Innovative Technology Administration United States Department of Transportation 1200 New Jersey Ave, SE Washington, D.C. 20590		13. Type of Report and Period Covered **Final Report [10/1/2011 to 9/28/2012]** 14. Sponsoring Agency Code
15. Supplementary Notes **Project completed for the USDOT's RITA by CFIRE.**		

16. Abstract

The strength and durability of highway bridges are two of the key components in maintaining a high level of freight transportation capacity on the nation's highways.

The CFIRE project 04-09 demonstrated the feasibility of a new hybrid engineered cementitious composite (SECCs), engineered cement based concrete combined with polyvinyl alcohol fibers and hydrophobic compounds, to create a substitute concrete material which can provide the strength and durability demanded in key regions of highway bridges. The Phase II project investigated the durability of the developed SECCs.

17. Key Words engineered cementitious concrete, mix design, fibers, superhydrophobicity, approach slab, durability, ductile concrete, crack distribution	18. Distribution Statement **No restrictions. This report is available through the Transportation Research Information Services of the National Transportation Library.**		
19. Security Classification (of this report) **Unclassified**	20. Security Classification (of this page) **Unclassified**	21. No. Of Pages 80	22. Price **-0-**

Form DOT F 1700.7 (8-72) **Reproduction of form and completed page is authorized.**

Table of Contents

List of Figures

List of Tables

SUPERHYDROPHOBIC ENGINEERED CEMENTITIOUS COMPOSITES FOR HIGHWAY APPLICATIONS: PHASE II

EXECUTIVE SUMMARY

America's infrastructure is in urgent need of restoration/repair, especially in parts of the country exposed to freezing. Freezing and thawing cycles in northern regions lead to loss of performance, demanding urgent repairs and attention or bridge failures. The key elements that are especially prone to deterioration in these regions are bridge approach slabs, which are intended to provide a smooth transition between the roadway and the bridge. A "bump" forms at the junction of the bridge and approach slab due to differential settlement of the two structures, load or temperature deformations, or damage due to exposure of detrimental agents, such as chlorides from de-icing salts and other compounds causing driver discomfort or damage to their vehicle and excessive dynamic loading. Strategically connecting the approach slab to the bridge could eliminate damage due to such loading. However, in this system, the approach slab would undergo increased bending which should be accommodated without excessive cracking. Large cracks can result in water and deicing chemicals filtrating through the integral approach slab-bridge joint and be a cause for early maintenance.

An engineered high-performance and durable material is required for these elements of infrastructure in order to increase the service life of roadways and to minimize the need for repair. A material capable of superior performance for 120 or more years would drastically improve sustainability by reducing the amounts of raw materials required for bridge renovation/new construction and reducing the carbon emissions produced by vehicles that are delayed in traffic due to closures for maintenance. Moreover, the sue of concrete that incorporates supplementary cementitious materials or byproducts is desired to reduce the carbon emission resulting from the production of portland cement.

An early CFIRE study (CFIRE Report 04-09) demonstrated the improved flexural behavior of engineered cementitious composites with superhydrophobic admixtures. The design of superhydrophobic engineered cementitious composites is based on the following:

1. Micromechanical design of ECC with 1 to 4 % (by volume) of polyvinyl alcohol fibers to realize ductile performance.
2. Application of small quantities (0.01 to 0.1% of cement weight) of siloxane-based hydrophobic admixtures (e.g., based on polymethyl- hydrosiloxane, PEHS/PMHS) modified by super-fine submicro- or nano-sized materials (such as nano-silica, nano-clay additives or SiO_2-rich reactive powders) and use of an effective superplasticizer to form a controlled air-void structure (Figs. 2,3).
3. Inclusion of selected by-product or mineral additives (also known as supplementary cementitious materials, SCMs) to decrease cement content and improve the sustainability of the material.

The optimal performance of developed material was achieved by creating a fiber-reinforced composite with "desired" small, evenly spaced air voids throughout the cementitious matrix that act as artificial flaws to initiate a multi-cracking response and strain hardening behavior. This enables the material to have high ductility while still maintaining high load carrying capacity. Moreover, the void surfaces have a water repellant nature that improves durability. In the previous report several parameters were considered in order to obtain the best mixture proportions, including the dosages of fibers and admixtures, sand-to-cement and water-to-cement ratios, and mixing procedures to create very ductile material while still maintaining high compressive strengths. Additionally,

different types of polyvinyl alcohol fibers at different volumes were investigated to determine the best performing mixtures. The best performing mixture incorporated 2.75% by volume RECS 15 x 12 mm with a water-to-cement ratio of 0.30 and a sand-to-cement ratio of 0.5. The mixture also incorporated a single dose (0.25 g of PMHS to 1 liter of SECC mixture) and 0.125% of cementitious material weight polycarboxylate ether superplasticizer. It was also determined that mixing fibers and sand prior to adding cementitious materials provides the necessary abrasion to disperse fibers.

This report focuses on durability aspects of engineered cementitious composites with superhydrophobic admixtures. To achieve improved performance, the admixtures developed in the previous study (CFIRE Report 04-09) were further enhanced by incorporating nano-particles which helped to increase the stability of the admixture and the surface roughness of the voids, thus improving hydrophobicity and creating superior water repellant surfaces. Many durability tests were performed on composites with 50% supplementary cementitious materials. Based on results from the previous study, 45% ground granulated blast furnace slag (slag cement) and 5% silica fume provided the optimal performance. Later, mixtures were designed with 50% slag cement to visualize the added benefits of superhydrophobic admixtures.

Air void analysis, mechanical behavior, freeze-thaw testing, water absorption, rate of absorption, and rapid chloride permeability were all tested for the durability investigation. Air-void analysis was performed to determine air content, spacing factor, and size distribution of air voids throughout the cementitious matrix in order to achieve well-spaced, well-distributed small air voids. Freeze-thaw analysis was performed on samples both with and without hydrophobic and superhydrophobic admixtures for up to 700 cycles in fresh and salt water (5% NaCl) using an accelerated testing regime at temperatures ranging from -50°C to 20°C (-58°F to 68°F). Freezing and thawing tests were performed on specimens with different water-to-cement ratios to investigate effects of this factor. Rapid chloride permeability was tested to determine the effect of superhydrophobic admixtures and water-to-cement ratios. Rate of absorption and absorption of engineered cementitious composites, both with and without superhydrophobic admixtures were also tested. Research data demonstrated that the addition of silica fume imparts exceptional durability for all engineered cementitious composites. As a consequence, the durability study focused on the performance of engineered cementitious composites with 50% ground granulated blast furnace slag to demonstrate the improved performance of materials with superhydrophobic admixtures. Even though it was not tested in the majority of durability tests, the replacement of 5% silica fume along with superhydrophobic admixtures will provide exceptional durability.

It was ultimately determined that the engineered cementitious composites with superhydrophobic admixtures were shown to successfully improve durability. Superhydrophobic hybridization reduces permeability and absorption, providing a beneficial contribution as the water repellent nature of the voids allow less water to occupy the capillary voids. Although specimens with superhydrophobic admixtures at a lower water-to-cement ratio displayed similar performance for freeze-thaw testing through 700 cycles, it can be postulated that, if tested for longer periods, with a greater accumulation of deterioration, the specimens with superhydrophobic admixtures will exhibit a significantly improved performance, as was demonstrated for composites with a higher water-to-cement ratio.

1. Introduction

The strength and durability of highway bridges are the key components in maintaining a high level of freight transportation capacity on the nation's highways [1] [2] [3] [4] [5]. Highways, bridges, and other critical transportation infrastructure works are rapidly deteriorating due to loading and deformation, aging, de-icing, and other detrimental factors in addition to rebar corrosion [1] [2] [3] [4] [5]. The average service life of concrete infrastructure in Wisconsin is 40-50 years, with up to 10% of bridge decks reinforced by uncoated rebar needing replacement after 30 years [3] [4] [5] [6] [7]. The direct costs for roadway improvements are escalating because the price of key materials needed for highway and bridge construction has increased rapidly (~46% from 2004) [3] [4] [5] [6] [7]. Indirect costs of highway bridge construction, in the form of environmental damage, are being realized in relation to the production and recycling of basic concrete materials. The time is right for a paradigm change to address the urgent need for highly durable and more sustainable materials to meet the challenges that future freight transportation will demand.

The durability of concrete bridges is often limited by the performance of connection regions or joints between bridge components, especially in decks. Recent CFIRE project investigated the use of precast bridge approach slabs that could reduce the early distress noted in service [8]. The connection between an approach slab and bridge deck, or joints in the bridge deck, or the portion of bridge deck bending in a negative curvature above mid-span bridge piers, are critical bridge locations where durability problems are apparent and premature deterioration occurs. This results in regular maintenance demands or early replacement. A high-performance material that does not exhibit early age shrinkage cracking, withstands the deformation from truck loading, and provides durability is required for these susceptible elements of bridges.

1.1 Design of Engineered Cementitious Composites

Engineered cementitious composite (ECC) materials exhibit very ductile performance under tension, like steel, as shown in Figure 1. The strain capacity of ECC may be increased by a factor of 200 when high-strength reinforcing fibers such as polyvinyl alcohol (PVA/Kuralon K-II) are three-dimensionally dispersed in the mortar [9] [10] [11]. The engineered fiber composite controls initial shrinkage cracking while providing extreme deformation and strain enhancement, as illustrated in our research team's previous results in Figure 1, left.

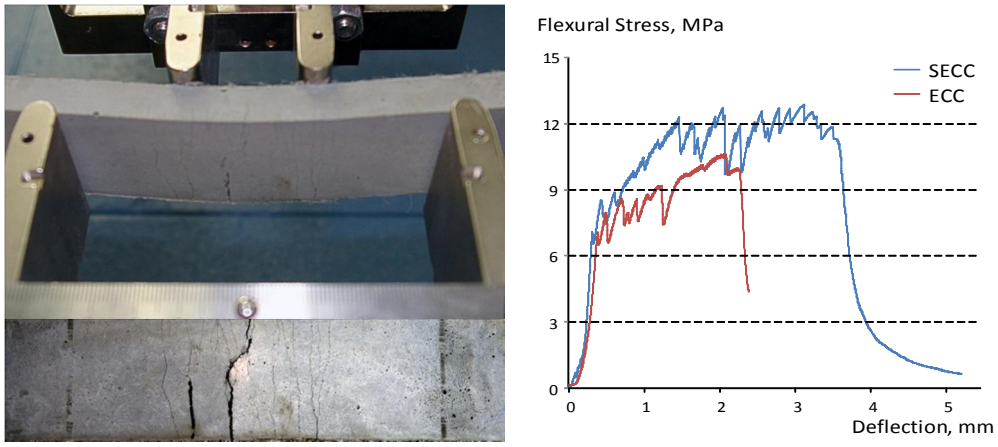

Figure 1: The Bending Test Demonstrating High Ductility and Multi-Cracking Fracture Performance of SECC

The use of Polyvinyl Alcohol (PVA) fibers in engineered cementitious composite (ECC) proves to be a very effective method to not only improve the ductility of concrete, but to drastically improve its durability. Conventional reinforced concrete is a relatively brittle material which, when loaded, typically causes large cracks. These large cracks allow water to penetrate through the concrete, reaching the reinforcing steel and, in turn, cause the steel to corrode, ultimately leading the failure of the reinforced concrete. PVA-ECC when loaded, allows for small width multiple micro cracking. In conventional reinforced concrete, when a crack forms the entire load is transferred directly to the reinforcing steel bridging the crack. This single crack is typically large enough to allow water to penetrate while at the same time small enough to not allow for much ductility in the reinforcing steel. Since conventional reinforced concrete does not allow for large ductility it will not be able to survive large deformations caused by loading, impact, or freezing and thawing actions. Moreover, the large cracks allowing water to penetrate can be extremely detrimental to its performance under freezing and thawing, and chemical attack due to penetration of chlorides. This, in turn, requires much maintenance on the concrete and results in a much shorter than expected lifespan of the structure.

When PVA-ECC is loaded, the initial crack is bridged by the PVA fibers. These PVA fibers have very high tensile strength. The bond between the PVA fibers and the cement matrix is also strong unlike the bond in conventional reinforced concrete. These features allow for multi-cracking fracture in ECC. Instead of one crack forming and the entire load is transferred to the material bridging this one crack, load can be distributed throughout several cracks. This allows for a much larger ductility while at the same time maintaining small enough cracks that will allow very little if no water to penetrate.

1.2 Comparison of Conventional Fiber Reinforced Concrete and ECC

1.2.1 The Need for Efficient Approach Systems

There are approximately 600,000 bridges in the United States, 35% of which are deficient and the cost of repair is estimated around $78 billion. A part of this infrastructure degradation is a problem known as “bump” at the end of the bridge. This problem alone requires a yearly expense of $100 million for repair nationwide [12].

The primary objective of the bridge approach slab is to provide a smooth transition between the roadway and the bridge. This bump causes discomfort to the drivers and a potential safety hazard to motorists. Engineers and researchers have been working on this problem for the past 20 years and they regard the differential settlement between the approach slab and the bridge to be the root cause of this problem [13]. Figure 2 shows typical elements of a bridge approach system.

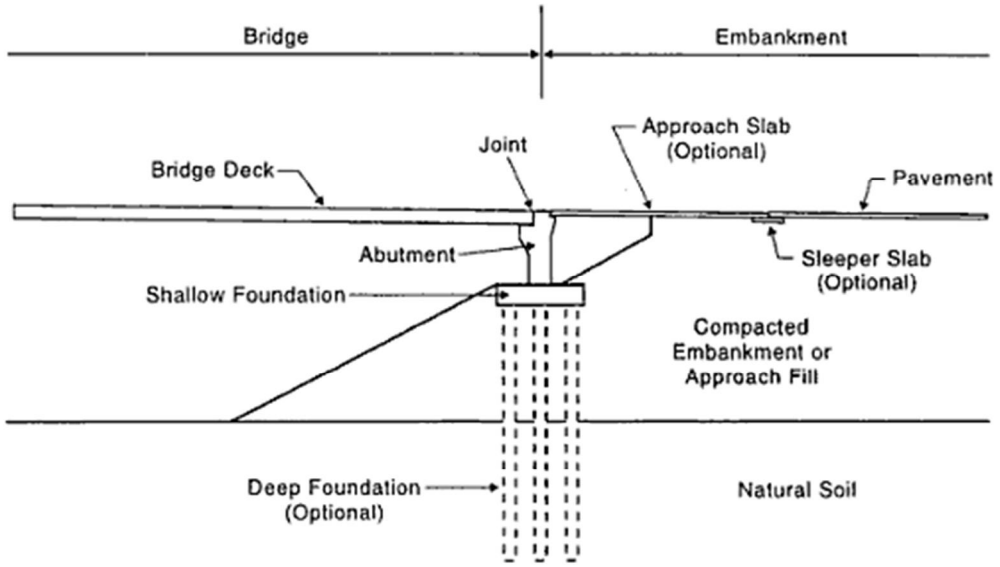

Figure 2: Bridge Approach System [12]

Most commonly reported causes of the differential settlement problems in order of their importance are [12] [13]

- Compression of the fill material
- Settlement of the natural soil under the embankment
- Poor construction practices
- High traffic loads
- Poor drainage
- Poor fill material
- Loss of fill by erosion
- Poor joints
- Temperature cycles

The implications of the differential settlement vary. Roadway users start to feel the bump once the differential settlement reaches a half inch [14]. Once differential settlement reaches one inch, it can become a costly problem for the Department of Transportation (DOT) as repair or even replacement of the approach slab is recommended [15]. If differential settlement is allowed to reach two inches, the roadway user will experience serious discomfort [16].

In order to get rid of the aforementioned problem and improve the performance of the bridge approach system, one of the solutions is to ensure a smooth transition between the approach slab and the bridge deck (Figure **3**). In order to provide a smooth transition, the approach slab should be integrally connected to the bridge deck and should be able to deform in order to take care of the differential settlement at the end of the pavement [17]. The deformation must be achieved without any large cracks (> 0.05 inch) in the slab in order to avoid water infiltration, thus avoiding erosion of soil below and enhancing durability. The finite element modeling was used to analyze the approach slab and it was concluded that the approach slab at the abutment could rotate 0.002 radians [18], Figure **4**.

1.2.2 Objectives to Address the Deficiencies of Concrete Approach Slabs

The objectives include:

- Design an ECC mix that can be used in the bridge approach slabs allowing it to rotate a minimum of 0.002 radians [18] at the approach slab – bridge deck joint as shown in Figure 3**,** Figure 4, and Figure 5;
- Obtain small sized cracks in the slabs when bent, instead of large cracks;
- Obtain a mix that is workable and easy to use in the field;

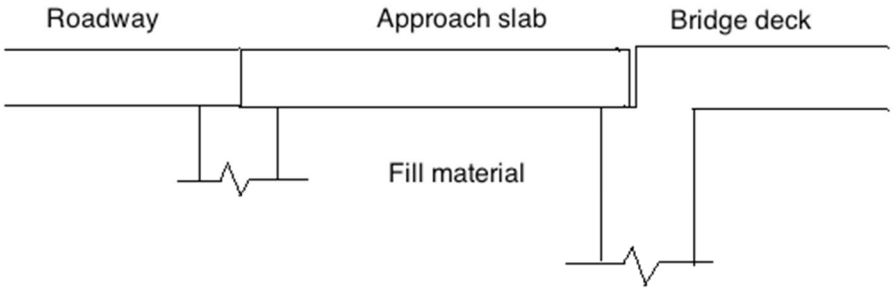

Figure 3: Typical Bridge Approach Slab

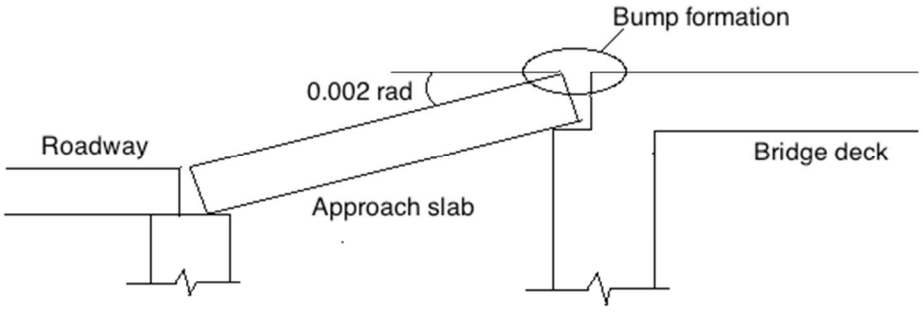

Figure 4: Bridge Approach Slab with Differential Settlement of Soil

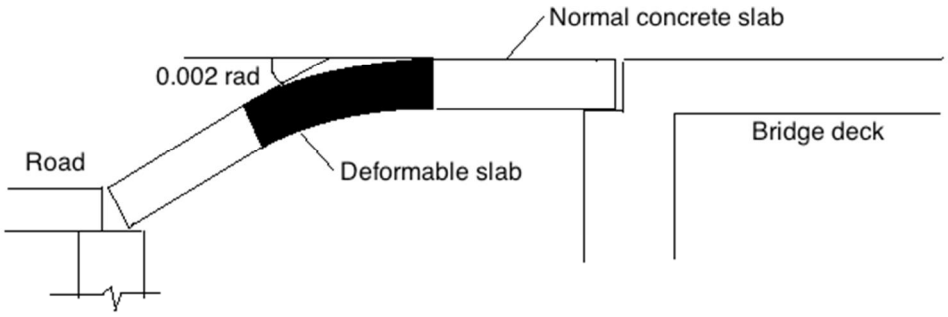

Figure 5: Proposed Solution of Bridge Approach Slab when Differential Settlement of Soil Occurs

1.2.3 Fiber Reinforced Concrete

An effective fiber reinforced cementitious composite (FRCC) uses steel fibers for tensile reinforcement. They can be classified into three different groups based upon the volume of fibers in the matrix. First, low volume fractions FRCC (< 1%) can greatly reduce the effects of shrinkage cracking [19]. Next, moderate volume fractions FRCC (between 1% and 2%) can improve mechanical properties such as modulus of rupture (MOR), fracture toughness, and impact resistance. FRCCs in this group can even be used as secondary reinforcement such as partial replacement of shear steel stirrups [20] [21] [22] or for crack width control [23] [24]. Within the past couple decades, a new class named high performance FRCC (HPFRCC) was introduced. This class uses high volume fractions (> 2%) and typically exhibits tensile strain-hardening behavior (1.5% or more) [11]. While FRCCs provide enhanced performance, their use in pavements is limited by the possibility of rapid corrosion and loss of section in the small steel fibers when subjected to high chloride concentrations from application of salt on roads.

Reserachers at the University of Michigan have developed and fine-tuned a new type of FRCC called ECC [9]. Rather than a strain-softening behavior seen in most FRCC and the brittle failure of plain concrete, the bridging effect of the fibers encourages a pseudo strain-hardening response [25]. Comprised of portland cement, fly ash, fine-grained silica sand, water, small amounts of admixtures, and synthetic microfibers, this concrete displays a high amount of tensile strain (3% to 7%) while utilizing polyvinyl alcohol fibers in the moderate volume fractions [9] [26].

Some examples of polymeric fibers that have been used for ECC applications are polyethylene (PE), and polyvinyl alcohol (PVA). This research will primarily focus on PVA fibers because of its potential to balance cost and effectiveness.

1.2.4 ECC Material Design Basis

Extensive research has shown that the most fundamental properties of fiber reinforced cementitious materials is the fiber bridging across a matrix crack, generally referred to as the σ-δ curve [27]. This is he averaged tensile stress (σ) transmitted across a crack with uniform crack opening (δ) as envisioned in a uniaxial tensile specimen. The σ-δ curve (Figure 6**)** can be thought of as a spring law describing the behavior of non-linear springs connecting the opposite

surfaces of a crack, representing the averaged forces of the bridging fibers acting against the opening of the crack when the composite is in tension loading [28].

One of the criteria for multiple cracking is that the matrix cracking strength (including the first crack strength) must not exceed the maximum bridging stress (σ_{cu}). This may be labeled as the strength criterion for multiple cracking. A second criterion for multiple cracking is concerned with the mode of crack propagation, which, in turn, is governed by the energetics of the crack extension. This may be labeled as the energy criterion of the multiple cracking.

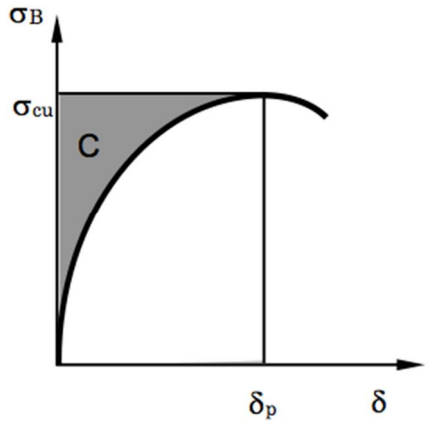

Figure 6: Stress-Deflection Curve to Determine Complimentary Energy (C)

High bridging strength (σ_{cu}) and large complementary energy (C) are conducive to composite strain-hardening [28]. When the fiber-matrix interface is too weak, pullout of fibers occurs, resulting in a σ-δ curve with low peak strength. When the interface is too strong, the springs cannot stretch, resulting in rupture and a small value of critical opening (δ_p). In either case, the complementary energy shown as the shaded area C to the left of the σ-δ curve in Figure 6 will be small. Steady state crack analysis [29] reveals that when the complementary energy is small in comparison to crack tip toughness (the energy needed to break down the crack tip material to extend the bridged crack), the crack will behave like a typical Griffith crack in Figure 7a.

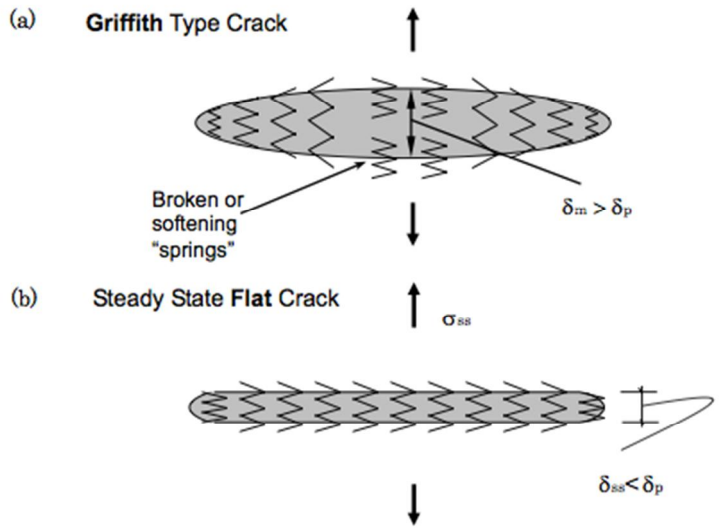

Figure 7: Griffith (a) and Steady State Flat (b) Crack

As the crack propagates, unloading of the springs will initiate at the middle of the crack, where the opening is maximum and δ_m exceeds δ_p (Figure 6). An expanding traction free or tension-softening region will follow the crack tip as the crack continues to propagate. After the passage of this crack, the composite will fail with reduced load carrying capacity, resulting in the tension-softening behavior of a normal FRC [28].

Steady state crack analysis [29] reveals two crack propagation scenarios: First, low complementary energy in comparison to crack tip toughness results in Griffith type cracking. Next, high complementary energy results in a flat crack propagation configuration [28].In contrast, if the complementary energy is large, the crack will remain flat as it propagates so that the steady state crack opening where $\delta_{ss} < \delta_p$ (Figure 7b), and maintains tensile load carrying capacity after its passage. As a result, load can be transferred from this crack plane back into the matrix and cause the formation of another crack, which may initiate from a different matrix defect site. Repetition of this process creates the well-known phenomenon of multiple cracking. The shape of the σ-δ curve therefore plays a critical role in determining whether a composite strain-hardens as in ECC, or tension-softens, as in normal FRC, under uniaxial tensile load [28]. Rather than failing under modified Griffith cracking, ECC tends to be governed by steady-state cracking [29].

1.2.5 PVA Fiber Behavior

The selection of a synthetic fiber for an ECC is based upon several parameters such as tensile strength, modulus of elasticity, chemical bond interaction between the fiber and the concrete matrix, and cost [30]. With polyvinyl-alcohol (PVA) fiber's high strength, high modulus of elasticity, and low cost (Table 1), it is considered to have excellent potential for ECC [26]. Its cost is about 1/8 that of the high-modulus polyethylene fiber and is even lower than steel fibers on an equal volume basis [17] [26].

Table 1: Properties of RECS 15 X 8 mm PVA Fibers [17]

Diameter (μm)	40
Thickness (dtex)	15
Cut Length (mm)	8
Tensile Strength (MPa/ksi)	1600/232.1
Elongation (%)	7
Young's Modulus (GPa/ksi)	40/5801
Specific Gravity	1.3

1.2.6 Tailoring Fiber and Matrix Interface

It is clear that a low critical fiber volume fraction in the mix is desirable [28]. Since this parameter is associated with fiber and interface properties, micromechanics provide guidelines to tailoring the fiber and the interface to minimize the critical fiber volume fraction. Figure 8 illustrates the dramatic effect of tailoring the interfacial bond on the tensile strain capacity. While Figure 9 shows the influence of surface coating on protecting the fiber from damage during the pullout process. The tailoring is implemented via control of the surface coating of the PVA fiber [28]. For this hydrophilic fiber, the untreated fiber has a chemical and frictional bond with cementitious material that is too high. A surface coating (oil) content between 0.8% and 1.2% by weight of fibers tends to lower the interface chemical and frictional bond properties to a level that causes the critical fiber volume fraction to drop to a minimum of about 2% [30].

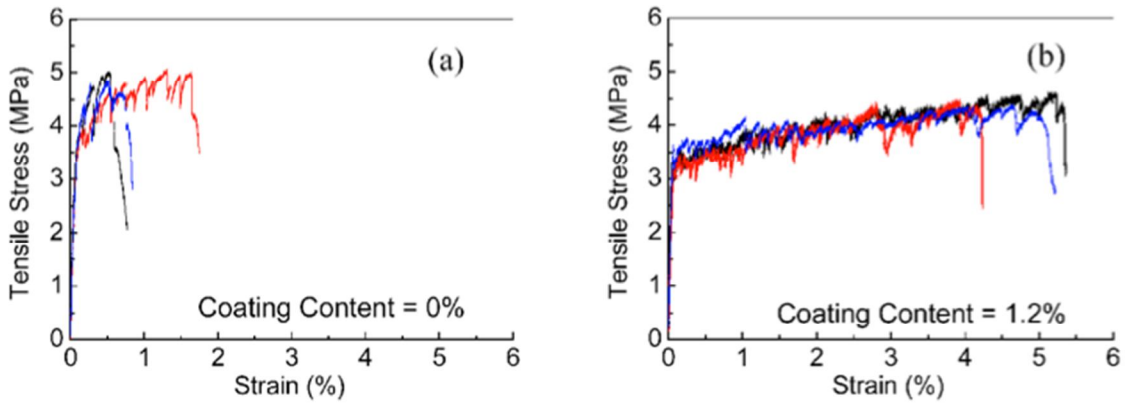

Figure 8: Effect of Fiber Oil Coating on Tensile Strain Capacity of Mix [30]

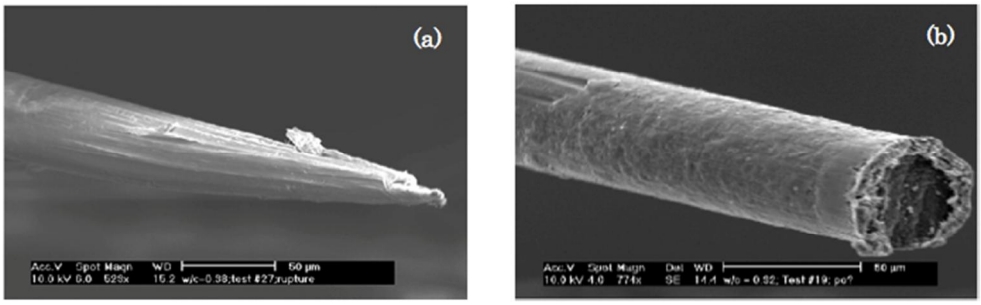

Figure 9: Magnified Image of Fibers from Composite Fracture Surface [30]

1.3 Addition of Superhydrophobic Admixtures

In addition to improved deformability and crack control provided by ECC, a new high-performance material with improved long-term durability can be realized by combining ECC with superhydrophobic admixtures. The use of PVA fibers along with superhydrophobic emulsions not only generates multiple micro-cracking when loaded, but allows for air voids to be created within the cement matrix to allow for extremely good resistance to freezing and thawing while maintaining its high strengths unlike typical air entraining approach. This allows structures that incorporate superhydrophobic emulsions along with PVA-ECC to have a vastly extended lifespan with little to no maintenance required. This is extremely cost effective as well, considering that the small price increase for materials will be drastically offset by the reduction of labor costs for maintenance and early replacement over the entire life span of the bridge. The feasibility of SECC was proven with CFIRE project 04-09.

Superhydrophobic hybridization of concrete is a novel concept developed at UW-Milwaukee, which engages interdisciplinary work combining biomimetics (lotus effect), chemistry (siloxane polymers) and nanotechnology (nano-SiO_2 particles) to resolve fundamental problems of concrete such as insufficient durability and corrosion protection for internal reinforcing [31] [32] [33] [34]. The use of a superhydrophobic admixture helps to tailor the volume, size, and distribution of air voids in the concrete, and the bond with PVA fibers to realize controlled pullout behavior. Furthermore, controlled air void structures can be used to realize the "preferred" fracture modes. These synergetic effects were verified by the research program under CFIRE project 04-09. The design of hybrid superhydrophobic ECC (SECC) is based on three principles:

4. Micromechanical design of ECC with 1 to 4 % (by volume) of polyvinyl alcohol fibers to realize ductile performance.
5. Application of small quantities (0.01 to 0.1% of cement weight) of siloxane-based hydrophobic admixtures (e.g., based on polyethyl/polymethyl-hydrosiloxane, PEHS/PMHS) modified by super-fine submicro- or nano-sized materials (such as nano-silica, nano-clay additives or SiO_2-rich reactive powders) and use of an effective superplasticizer to form a controlled air-void structure (Figure 10, Figure 11).
6. Inclusion of selected by-product or mineral additives (also known as supplementary cementitious materials, SCMs) to decrease cement content and improve the sustainability of the material.

Superhydrophobic surfaces, or surfaces that have a water contact angle Θ larger than 150° (Figure 11), have generated much interest due to their potential in industrial applications (mainly for self-cleaning), and have been tested for enhancing concrete durability. This nature-inspired approach improves the performance of hydrophobic materials that control wettability [32] [33] [34].

The superhydrophobic admixtures were manufactured by combination of the hydrogen containing siloxane admixture (e.g., PMHS) with small quantities of super-fine, submicro- or nano-sized particles such as nano-silica, nano-clay additives, or SiO_2-rich reactive powders (Figure 11).

A modified PEHS/PMHS admixture (used at a dosage of 0.01…0.1% of cement weight) releases hydrogen and forms a small (10 - 100 μm), uniform air void evenly distributed within the cement paste (Figure 11, left). The volume, size, and distribution of the air void within the hardened cement phase are precisely tailored by preparing the water-based emulsion of siloxane with a certain droplet size. For optimal performance, more than 70% of the PEHS must be dispersed to the size of less than 10 μm [31]. As a result, the hydrophobic particles cover the surface of the voids, providing the superhydrophobic hybridization effect.

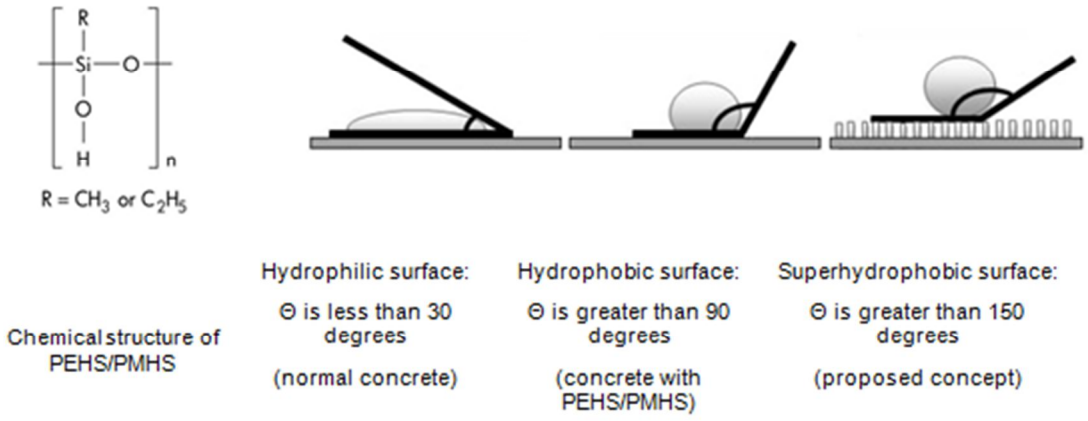

Figure 10: The Concept of Superhydrophobic Hybidization of Concrete Pore Surface

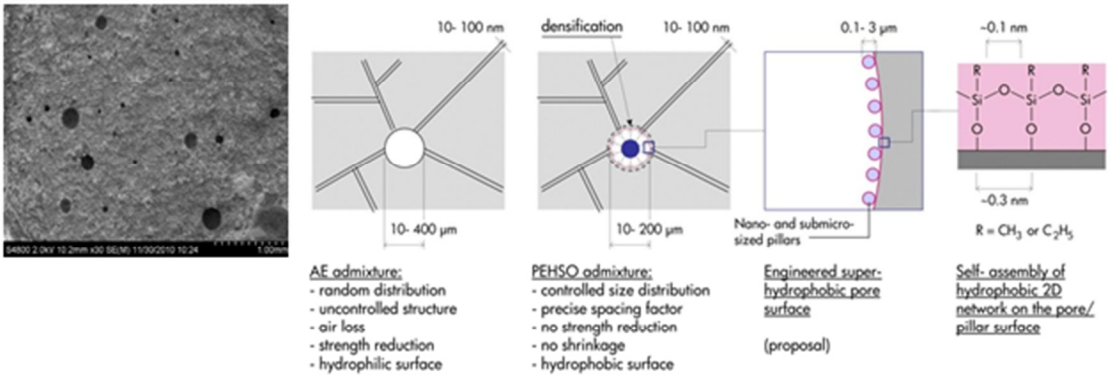

Figure 11: How The Superhydrophobic Hybridization of Concrete Works

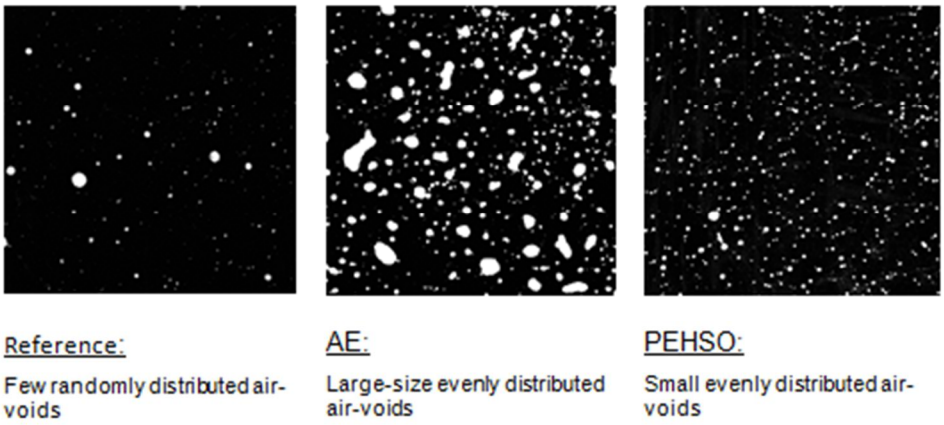

Figure 12: The Design Preferred Microstructure Using PEHSO Admixture

2. Research Objectives

This project investigated the durability of developed superhydrophobic engineered cementitious composite (SECC) with a service life of 120+ years as required to replace the conventional concrete in critical elements of highway/bridge infrastructure. The investigated concept resulted in a new generation of concrete with significantly improved ductility, durability, and sustainability through a longer life and less maintenance. Furthermore, the proposed approach considers the use of significant amounts of supplementary cementitious materials (SCMs) to reduce the detrimental impact of cement production on the environment.

The principal objectives of the project are to:

1. Evaluate the durability of SECC in respect to freeze-thaw and salt scaling resistance;
2. Evaluate the permeability of SECC;
3. Investigate the effect of air void structure in the hardened concrete on freeze-thaw and salt scaling resistance;

4. Investigate the mechanical behavior of SECC after durability testing to confirm the deformability performance required in critical regions of highway bridges to allow heavy freight traffic without brittle damage or undesirable cracking and investigate the fracture modes of aged SECC;
5. Evaluate the combined effects of PVA fibers, siloxane-based admixtures, superplasticizer, and supplementary cementitious materials (SCMs) on durability performance of SECC.

3. Materials

The mechanical and geometrical properties of the Kuralon K-II PVA Fibers from Kuraray Japan used in this study are shown in Table 2. Commercially available polyacrilate/polycarboxylate superplasticizer (PAE/SP, 31% concentration, supplied by Handy Chemicals) was used as modifying admixtures.

Commercial Type I ordinary portland cement (OPC) from Lafarge, fly ash Class F (FA F) from We Energies, metakaolin (Mk) from Burgess Optipozz, silica fume (SF) from Elkem, lime (L) from Western Lime and blast furnace slag (BFS) from Lafarge were used as cementitious materials. The chemical and physical properties of OPC and FA F are shown in Table 3 and Table 4, respectively.

X-ray diffraction for OPC, FA F, SF and BFS are presented in Figure 13 and Figure 14. The morphology of Mk, SF, L, FA F, BFS and OPC were analyzed using SEM (Figure 15). ASTM-graded quartz sand and tap water were used to produce mortar specimens.

Table 2: Properties of PVA Fibers

Fiber	Length (mm)	Thickness (dtex)	Diameter (mm)	Young's Modulus (kN/sq. mm)	Tensile Strength (GPa)
RECS 7x6mm	6	7	0.027	39	1.6
RECS 15x8mm	8	15	0.040	40	1.6
RECS 15x12mm	12	15	0.040	40	1.6

Note: 1 dtex= 1 x 10^{-7} kg/m =0.9 denier

Table 3: Properties of Portland Cement Type I And ASTM C-150 Requirements

CHEMICAL

Item	Spec. Limit	Test Result
SiO_2, %	--------	20.6
Al_2O_3, %	--------	4.7
Fe_2O_3, %	--------	2.7
CaO, %	--------	63.9
MgO, %	6.0 max	2.3
SO_3, %	3.0 max	2.4
Ignition loss, %	3.0 max	2.1
Insoluble residue, %	0.75 max	0.36
Free lime, %	--------	1.1
CO_2, %	--------	1.3
Limestone, %	--------	3.4
$CaCO_3$ in limestone, %	--------	93.0
Potential, %		
C_3S	--------	55.0
C_2S	--------	17.6
C_3A	--------	8.0
C_4AF	--------	8.2
$C_4AF+2(C_3A)$	--------	24.2
$C_3S+4.75(C_3A)$	--------	93.0
Na_2O_{equi}	0.6 max	0.55

PHYSICAL

Item		Spec. Limit	Test Result
Air content, % (C-185)		12 max	7.5
Blaine fineness, m^2/kg (C-204)		260 min	380
Autoclave expansion, % (C-151)		0.8 max	0.02
Compressive strength, MPa			
	1 day	--------	12.4
	3 days	12.0 min	21.7
	7days	19.0 min	27.6
	28 days	28.0 min	37.9
Time of setting, minutes			
	Initial	45 min	110
	Final	375 max	225
Heat of hydration at 7 days, kJ/kg		--------	411
Percent Passing 325 Mesh (C-430)		--------	95.4

Table 4: Chemical Composition and Performance of Fly Ash Class F

Chemical composition, %	Class F	ASTM C618 limits
Silicon Oxide, SiO_2	49.9	-----
Aluminum Oxide, Al_2O_3	24.0	-----
Iron Oxide, Fe_2O_3	14.4	-----
Total, $SiO_2+Al_2O_3+Fe_2O_3$	88.0	70 min
Sulfur Trioxide, SO_3	0.88	5.0 max
Calcium Oxide, CaO	3.23	-----
Magnesium Oxide, MgO	0.98	-----
Potassium Oxide, K_2O	2.46	-----
Moisture Content	0.11	3.0 max
Loss on Ignition	3.50	6.0 max

Physical Tests	Class F	ASTM C618 limits
Fineness, % Retained on #325 Sieve	25.7	34 max
Pozzolanic Activity Index with Portland Cement, 28 days, %	93	75 min
Water Requirement, % of Control	103	105 max
Soundness, Autoclave Expansion, %	0.08	0.8 max
Specific Gravity	2.30	-----

Note: 1 psi = 0.0069 MPa

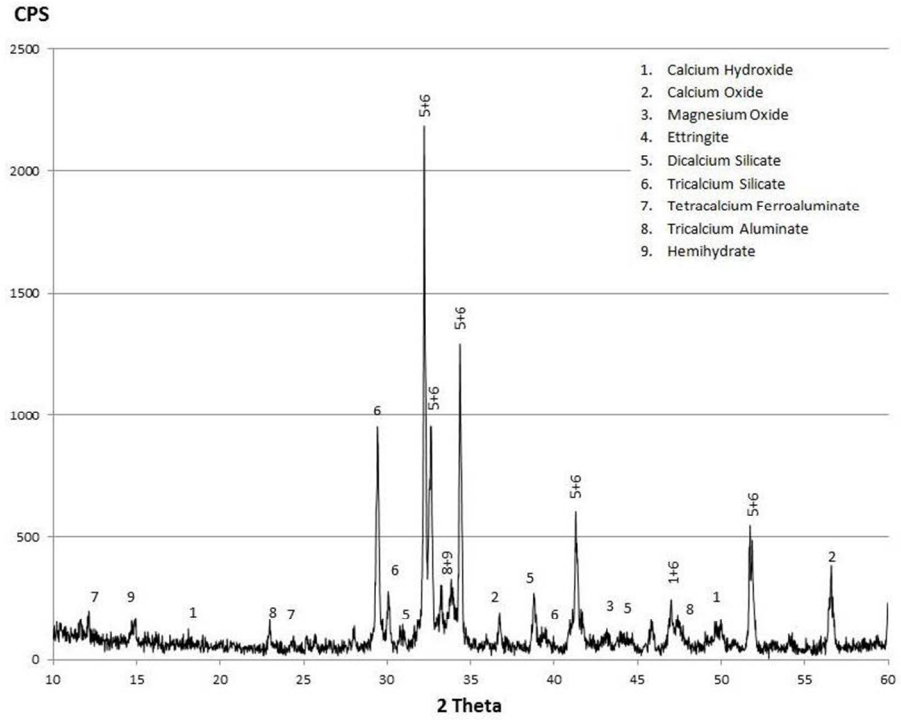

Figure 13: X-Ray Diffraction of Ordinary Portland Cement

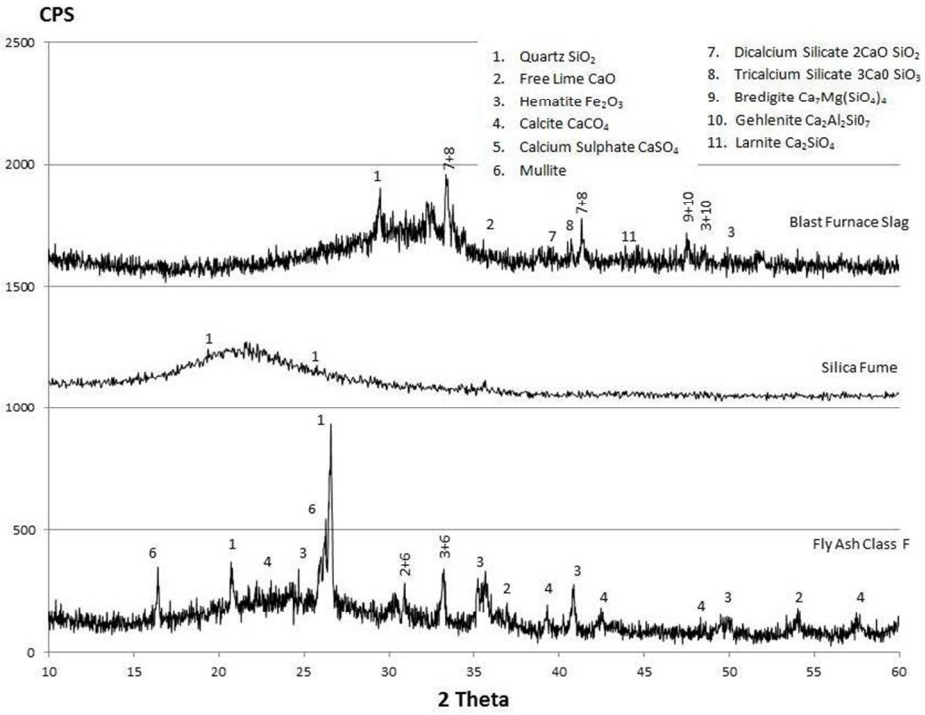

Figure 14: X-Ray Diffraction of Fly Ash Class F, Silica Fume, and Blast Furnace Slag

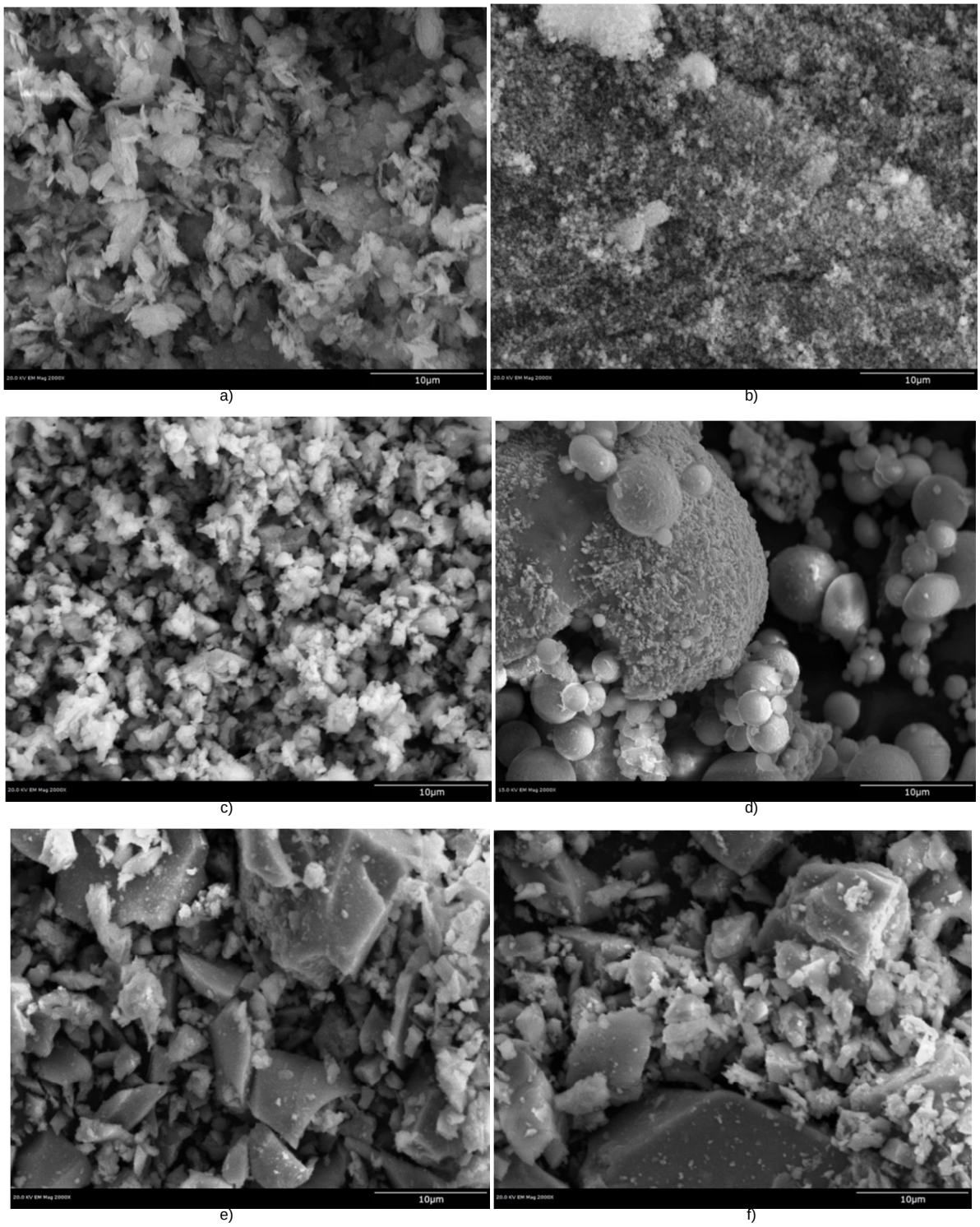

Figure 15: SEM Images at 2000x Magnification for Particles of: a) Metakaolin; b) Silica Fume; c) Lime; and d) Fly Ash Class F; e) Blast Furnace Slag; and f) Portland Cement

4. Experimental Procedures

4.1 Design of Superhydrophobic Emulsions

4.1.1. Raw Materials

Polyvinyl alcohol (PVA), 98% hydrolyzed with molecular weight of 16,000 (Across Chemicals) was used as a surfactant for emulsions. Deionized water (DI water) was used as the dispersion medium for production of emulsion. A polymethyl hydrogen siloxane oil (XIAMETER MHX-1107) from Dow Corning with a specific gravity of 0.997 (at 25°C) and a viscosity of 30 cSt was used as hydrophobic agent. This product contains 85-100% of methyl-hydrogen siloxane as an active agent. Metakaolin (Mk) from Burgess Optipozz and nano-SiO_2 (NS) were used for preparation of the emulsion.

4.1.2. Superhydrophobic Emulsions and Coatings

The concentration of siloxane, surfactant, metakaolin and nano-SiO_2 was kept constant at 25, 4.4, 0.40 and 0.10 % by weight of the emulsion. The PVA was gradually added to de-ionized water and stirred for 10 minutes at 23±3°C temperature, using a magnetic stirrer on a hot plate. Then, temperature was increased to 90°C, and kept constant for 40 minutes while stirring the solution. The solution was allowed to repose in water bath until 23±3°C was archived. Siloxane was slowly added to the PVA-DI water solution and mixed for 10 min at 10,000 rpm. Then, the metakaolin was slowly added and mixed for 10min at 5,000 rpm.Nano-SiO_2 was added to the emulsion following the same procedure as the addition of metakaolin. High speed mixer (HSM, from Silverson model L5M-A) was used to produce the emulsion. Z-potential and particle size distribution were used for characterization of the emulsion. PE, ME and 10NE were used as a notation for the emulsions with no powders (plain), metakaolin and metakaolin and nano-SiO_2 particles where used, respectively.

4.1.3. Characterization of Particles

The morphology of MK and NS were analyzed using SEM and TEM techniques (Figure 16). Rough and flaky particles with sizes from 0.8 to 12 μm with a certain degree of agglomeration were found in metakaolin. Round particles with sizes from 10 to 25 nm with a certain degree of agglomeration were representing nano-SiO_2.

4.1.4. Characterization of Emulsions

The magnitude of zeta potential gives an indication of the potential stability of the system. A negative zeta potential is associated with an acidic solution (pH<7), while a positive zeta potential is associated with a basic solution (pH>7). Low Zeta potential values are an indication that the repulsion forces are not sufficient to prevent the particles from coming together and flocculating. Table 4 shows the average droplet size and the Z-potential of the emulsions. The addition of metakaolin increase the Z-potential of the emulsion, but addition of nano-SiO_2 induces a bigger increment. The results indicate that the addition of powders, especially nano-particles, produce a more stable emulsion. The droplet size distribution of the emulsion are shown in Figure 17. The droplet sizes were reduced with the addition of powders. A more uniform and with an overall reduction of 0.5 μm on the droplet size from PE to ME was observed when metakaolin was used. More spread from 0.4 to 2.5 μm droplet sizes were formed when nano-particles were added into the emulsion.

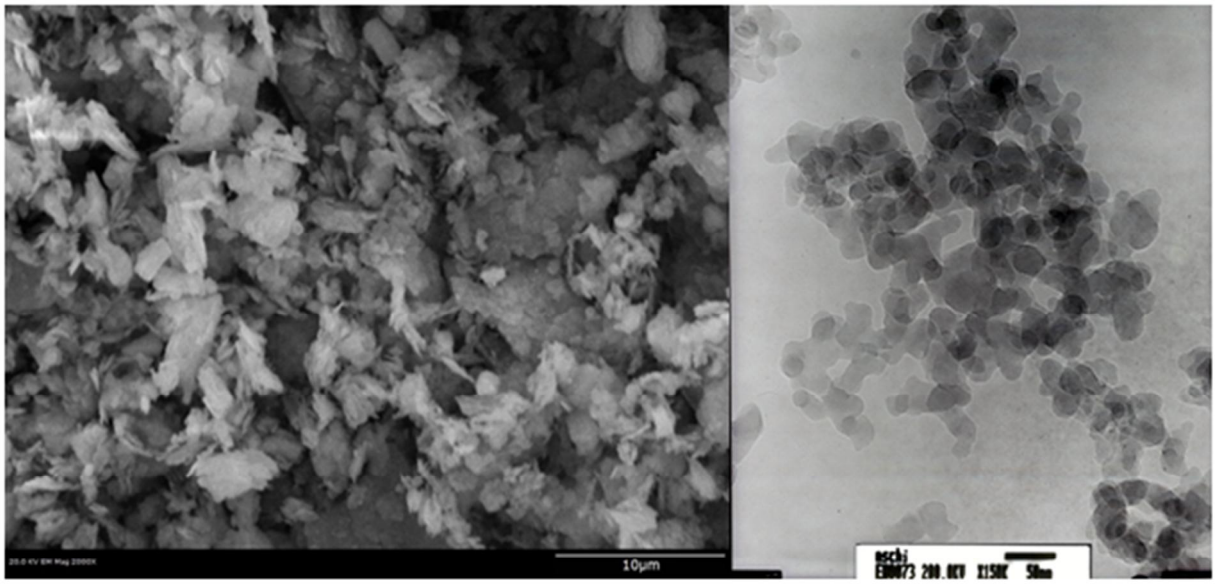

Figure 16: SEM and TEM Images for Particles of: a) Metakaolin (Mk); and b) Nano-SiO_2 (NS)

Table 5: Average Droplet Size and Z-potential of Emulsions

Emulsion	Powder Addition	Average, nm	Std. Dev., nm	Z-potential, mV
PE	None	1651.0	180.1	-10.450
ME	0.5% Metakaolin	895.8	32.2	-13.085
10NE	0.4% Metakaolin + 0.1Nano-SiO_2	1313.9	56.7	-13.540

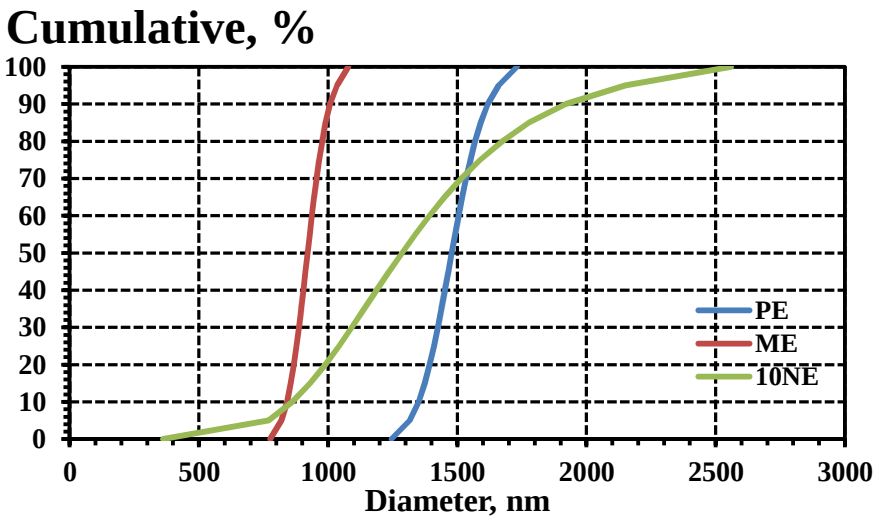

Figure 17: Droplet Size Distribution of the Emulsions with/without Particles

4.2 Experimental Setup and Design of ECC/SECC

4.2.1 Fiber Type and Volume Study

Several different types of PVA fibers were considered to determine the best performing SECC. In this study, RECS 15x8 mm and RECS 15x12 mm fibers were tested (Table 6). Each of these types of fibers was considered at 2.0, 2.25, 2.5, 2.75, and 3% by volume of the mixture. The w/cm ratio for this study was kept constant at 0.3, and the s/cm was 0.5. Even though no hydrophobic/superhydrophobic emulsions were added to these mixes, it is safe to say that the ECC used in this study can demonstrate the effects of fiber types and fiber volumes. It was assumed that with superhydrophobic emulsions added, the performance can be further improved. Flow, compressive strength, and flexural properties were considered in analyzing the performance of different fibers and fiber volumes.

Table 6: Properties of PVA Fibers

Fiber	Length (mm)	Thickness (dtex)	Diameter (mm)	Young's Modulus (kN/mm^2)	Tensile Strength (GPa)
RECS 7x6mm	6	7	0.027	39	1.6
RECS 15x8mm	8	15	0.04	40	1.6
RECS 15x12mm	12	15	0.04	40	1.6

Additional tests were performed on ECC with a combination of different types of fibers. The experimental matrix for this can be seen in Table 7.

Table 7: Experimental Setup for Combinations of Fiber Types

Specimen ID	Volume of RECS 7x6 mm (%)	Volume of RECS 15x12 mm (%)	Total Volume of Fiber (%)
PVA_16	0.25	2.75	3.00
PVA_17	0.50	2.50	3.00
PVA_18	1.00	2.00	3.00
PVA_19	0.25	2.25	2.50
PVA_20	0.50	2.00	2.50
PVA_21	0.50	2.25	2.75

4.2.2 Durability Investigation: Phase A

Durability research with the addition of 50% SCM (GGBFS) was conducted based on results from previous studies. These mixtures consisted of a fiber volume of 2.75% of RECS 15x12 mm fibers, which was determined to be the optimal fiber content and fiber type. Results from the supplementary cementitious materials study demonstrated that the addition of silica fume provides very high strengths. Knowing this, silica fume can be used as a replacement for portland cement at a content of up to 10-15%. One concern of making a durable ECC/SECC,

was to use up to 50% of SCM in order to create environmentally friendly material. Considering this, the use of ground granulated blast furnace slag in supplementary cementitious materials study demonstrated very good ductility response. Based on these results, it was determined that the addition of 5% silica fume and 45% ground granulated blast furnace slag would not only be more environmentally friendly since the burden on production of portland cement would be cut in half, but both strength and ductility could be improved. Moreover, the varying size of cementitious particles in the mixtures will allow for a better packing degree and a stronger interfacial transition zone to improve both durability by reducing permeability and strength. The use of a single dose (250 g of siloxane per 1 liter of mixture) of hydrophobic emulsion was considered to be the best in the hydrophobic emulsion study (CFIRE Phase I report). This optimal admixture incorporated 25% siloxane emulsion in water with 4.4% PVA as emulsifier mixed at 10,000 rpm was used in this study.

An experimental matrix was designed incorporating the above features. Along with these features, two different w/cm ratios were considered at 0.30 and 0.45. In previous studies it was determined that the optimal w/cm ratio was 0.30; however, water to cementitious ratio of 0.45 was also considered for this study to prove the contribution of w/cm ratio. A sand to cementitious ratio of 0.5 was used with the lower w/cm ratio and a s/cm ratio of 1.0 was used with the higher w/cm ratio. Additionally, a single dose of hydrophobic emulsion was used in both w/cm ratios and compared against the reference mixtures (without any added air). Table 8 below shows the experimental setup for the main research program.

Table 8: Experimental Setup of SECC for Durability Testing (Phase A)

Specimen ID	w/cm	s/cm	SCM	Emulsion
REF 30	0.30	0.5	5% silica fume, 45% GGBFS	None
REF 45	0.45	1.0	5% silica fume, 45% GGBFS	None
E 30	0.30	0.5	5% silica fume, 45% GGBFS	E5_P4F1
E 45	0.45	1.0	5% silica fume, 45% GGBFS	E5_P4F1

To test the durability aspects of the above materials, compressive strengths and flexural behavior was analyzed in the same way as previous studies. Rapid chloride permeability of the material was also determined to see the effects of both w/cm ratio and addition of hydrophobic emulsions on permeability. Next, freezing and thawing tests were performed with temperatures oscillating between -50°C and 20°C in both fresh water and salt water (5% solution). To determine the quantity of air within the specimens, air content in the fresh state was measured and an air void analysis was performed on hardened specimens to determine the size and spacing of the air voids.

4.2.3 Durability Investigation: Phase B

Another experiment was performed in a similar fashion as the one mentioned above. One of the only differences being that mixtures with 50% of ground granulated blast furnace slag were

used without silica fume. Along with this, new superhydrophobic emulsions with the addition of nano-particles as described in 4.1 were used.

For this set of tests rapid chloride permeability, freeze-thaw testing (with temperatures dropping to -50˚C), water absorption and rate of absorption, and abrasion resistance tests were performed on selected specimens. The freeze-thaw tests that were performed on the samples also included embedded strain gages which allow for the deformations during the freezing and cycles to be displayed in addition to manual testing in the thawed state. The experimental matrix for the Phase B sets of tests can be seen in Table 9 below.

Table 9: Experimental Setup of SECC for Durability Testing (Phase B)

Specimen ID	w/cm	s/cm	SCM	Emulsion
REF 30	0.30	0.5	50% GGBFS	None
REF 45	0.45	1.0	50% GGBFS	None
E 30	0.30	0.5	50% GGBFS	Superhydrophobic Emulsion with nano SiO_2
E 45	0.45	1.0	50% GGBFS	Superhydrophobic Emulsion with nano SiO_2

4.3 Preparation of ECC/SECC

Several different methods of mixing ECC/SECC were considered in this research. Mixing of material is of extreme importance so that fibers are distributed evenly throughout the samples. Also of equal importance, voids created by the siloxane-based emulsions must be distributed evenly throughout the samples. A detailed explanation of the different methods for mixing can be found in the Phase I report to CFIRE (CFIRE, 2011). The ECC/SECC were mixed in a 20 quart Hobart HL-200 mixer. The final mixing procedure that was used for the majority of the work in this research is as follows: 75% of drinking water at room temperature was added to the mixing bowl along with the superplasticizer. Next, standard graded silica sand was added and mixed at low speed (107 rpm) for 30 seconds. Half of the PVA fibers were then added and mixed for 30 seconds followed by the remaining PVA fibers mixed for another 30 seconds. Next, half of the cementitious materials were added and mixed for 1 minute, followed by the remainder of the cementitious materials mixed for another minute. Finally, the remainder of the water along with the emulsion was added and mixed at low speed for 1 minute, followed by 30 seconds of mixing on medium speed (198 rpm). The SECC was then tested for flow, followed by mixing for 30 seconds at medium speed before being placed in the molds.

The materials were then placed in several different molds. 50.8 mm x 50.8 mm x 50.8 mm cube specimens were used for compressive testing, 14 mm tall x 40 mm wide x 160 mm long beams were used for 4-point flexural testing, 40 mm x 40 mm x 160 mm beams were used for dynamic modulus testing during freezing and thawing cycles, as well as the same specimens with steel inserts to test for deformation during freezing and thawing cycles. Finally, specimens were cast in 75 mm diameter x 150 mm tall cylinders for air void analysis, as well as 100 mm diameter x 200 mm tall cylinders for rapid chloride permeability.

4.4 Investigation of Microstructure

4.4.1 Requirements for Air Void Freezing and Thawing Structure

To minimize the deterioration due to freezing and thawing, air voids have to be incorporated into concrete to reduce the hydraulic pressure during freezing. These air voids not only provide an escape for excess water, but also more space for the volume expansion; therefore they increase the resistance of concrete to freeze thawing. In order to ensure enough air voids in concrete, ASTM requires the use of an air entraining admixtures. These chemicals entrain voids in hardened concrete by stabilizing the shell of the void to the cement paste. However, the amount of air entrained, or voids created, have been limited to approximately a 5-7% of the volume of concrete. More than 7% of air may create large air voids, which reduces compressive strength because air can't take any load. Table 10 shows the classification and some characteristics of voids in concrete samples.

Table 10: Classification and Characteristics of Voids in Portland Cement Concrete Materials

Type of voids	Size range	Shape	Formation
Gel pores	1- 5 nm	Irregular	-
Capillary Voids	10-1000 nm	Irregular	Spaces left by mixed water
Entrained Air Voids	100 µm-1 mm	Spherical	AEA
Entrapped voids	1-10 mm	Spherical	Mixing of concrete
Micro- Cracks	0.01-0.2 mm	Irregular	-
Cracks	0.5-2 mm	Irregular	-

The air void system, however, is critically important in concrete, and can be described using several characteristics, or parameters, such as volume, number of bubbles, bubble size distribution, and spatial distribution within the paste. Of these parameters, the most important factors regarding freeze thaw resistance is the presence of an optimal number of well-distributed air voids which is most commonly described in terms of specific surface and spacing factor. These two last factors are correlated. On one hand, the specific surface, the ratio of total bubble surface area to total air volume, normally expressed in mm^2/mm^3, reflects the relative number and sizes of the air voids. For a given volume of air, a greater number of smaller air voids results in a higher specific surface area and thus provide more protection than larger voids, as the number of bubbles will be higher and the distance between them will be less. In addition, small bubbles will not compromise strength of concrete. Specific surface, then, is an indicator of air void system effectiveness, and it has been established that 25 mm^{-1} (630 in^{-1}) of air volume [35].

On the other hand, the spacing factor is an empirical quantity intended to represent the maximum distance that water would have to travel in the cement paste to reach a contiguous air void. If this distance is more than the critical maximum distance, the concrete should be adequately protected. This theoretical distance has been reported by several researches like Pigeon [35] and was established a "flow length" which should be between 200 to 250 µm. As shown in Figure 18, durability factor decreases abruptly as soon as the spacing factor surpasses the 0.2 mm (0.008 in).

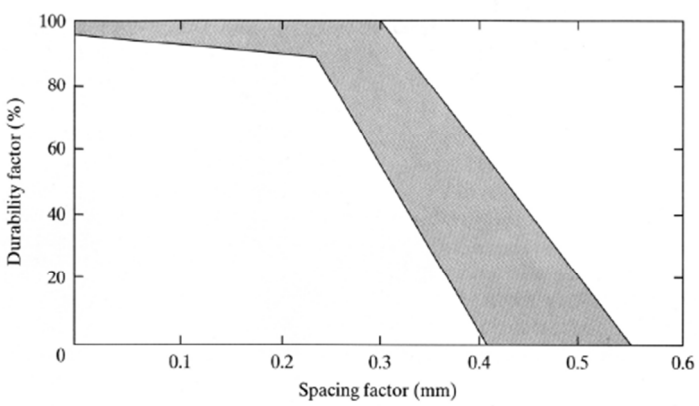

Figure 18: Relationship between Frost Durability and Bubble Spacing Factor [36]

These limits however, do not restrict or limit the good resistance of concrete over freeze thaw cycles. Tanesi and Meininger (2006) [37] found that all of the samples tested had a spacing factor larger than the recommended (in fact, larger than 0.36mm) and specific surface lower than 24 mm^{-1} and, all of them except non-air entrained samples showed a durability factor of 80% or above. In these set of samples, sections with spacing factor of 0.5 mm or smaller demonstrated satisfactory freeze thaw resistance, as well as samples with specific surface above 10 mm^{-1}. Further research by Aitcin (1998) [38], established a recommended and a maximum permitted spacing factor depending on the water to cement ratio. The results are summarized in Table 11.

Table 11: Recommended Spacing Factor Depending on Water to Cement Ratio [38]

w/c	Recommended L	Permitted Max. L (for scaling resistance)
>0.4	230 μm	260 μm
0.35<w/c≤0.4	350 μm	400 μm
0.30<w/c≤0.35	450 μm	550 μm
≤0.3	Same as 0.35	

4.4.2 Air Content and Air Void Analysis Procedure

Air content in the fresh state was tested to determine the effect of siloxane-based emulsions. Since the emulsions release hydrogen to create air voids within the specimen, it is important to determine if the emulsion have begun to create the voids while still in the fresh state. The voids created by entrapped air can also be measured through this test. Since SECC is not as workable as typical mortars, it is more likely that there will be more entrapped air within the specimen.

Air content was tested using an air meter as per ASTM C231 and AASHTO T152. In this test, the cementitious material is placed within the container and the lid is placed on and sealed. The container is then pressurized to allow all voids within the container to be accessible to the air that will be presented in the next step. A valve is then released, allowing air to flow into the container and causing a pressure decrease which is then proportional to the amount of air the

was originally in the specimen. This air content can then be read on the apparatus and recorded.

For Phase A experiment, air void analysis of SECC was performed on hardened specimens. Cylindrical specimens (75 mm x 150 mm) were molded and used for the analysis of air void system according to Zalocha's method [39]. Each specimen was cut down the middle from top to bottom with a diamond blade saw to create two flat surfaces. Surfaces were then polished using a series of increasing diamond grit platens followed by 800 grit of silicon carbide. Next, the surface was cleaned and scanned. The surface was then blackened using a black permanent marker and then a 2-μm wollastonite white powder was placed on the surface and spread to fill the voids. After repeatedly spreading wollastonite until all voids have been filled, the specimens were scanned at a resolution of 10 x 10 μm (4800 dpi). Air void structures of scanned images were analyzed using Image J software and compared against one another for spacing and size of air voids.

For Phase B experiment, the characterization of the air void system of SECC specimens was performed using the modified point count procedure of ASTM C 457 [40], (

Figure **19**). Results were obtained from a slab sawn from the center of 40x40x160 mm specimens, carefully smoothed and polished with a series of silicon carbide abrasive papers (No. 220, 320, 600, and 800) until it was suitable for microscopical observation. The point count was performed using Leica Wild M420 microscope, a Sony Exwave Had camera and a software MS Bubble 3.0. In addition to air void and microstructure characterization, microphotographs of the surface of specimens were taken. Using the area of the specimen to be analyzed and the maximum size of aggregates as parameters, the software determines the grid in the specimens for the analysis expressed in lines and points, and calculates the content of phases.

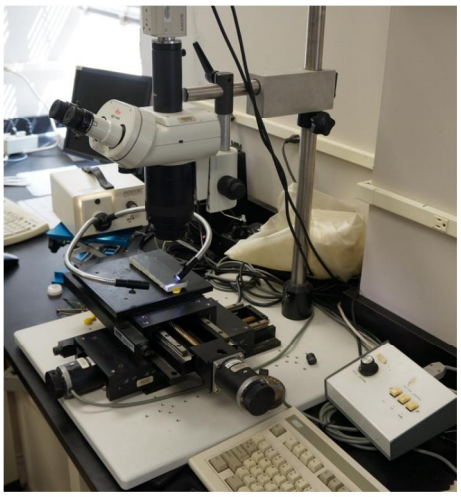

Figure 19: Investigation using Modified Point Count Procedure of ASTM C457

4.4.3 Micro CT scanning of SECC

X-ray microscopy (XRM) based on advanced 3D imaging solutions using X-ray computed tomography (CT) scanning technology of SECC was performed to visualize the 3D distribution of fibers and air-voids using the MicroXCT platform VersaXRM-500 from Xradia. Additionally, micro CT scans were performed at the Center for Advanced Radiation Sources at the Advanced Photon Source at Argonne National Laboratory with the help of Dr. Mark Rivers. Both

approaches allow for a micro scale view of air voids, fibers, and the interfacial transition zone within the samples. Although, these results were not quantitatively measured, future work may utilize these scans as a way to analyze air void size, or to model the exact structure of the sample using finite element approaches. A similar approach was used in a previous CFIRE report produced by UW-Milwaukee [41] in which aggregate was analyzed using micro CT scanning to analyze the internal shape, connectivity, and distribution of voids within the sample.

Figure 20 below, shows the internal view of SECC with micro CT scanning utilizing MicroXCT platform from Xradia and Figure 21 shows the internal view of SECC obtained at Argonne National Laboratory.

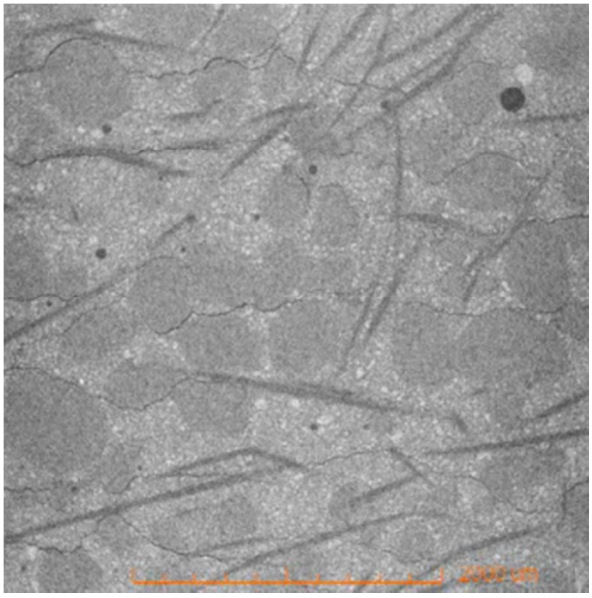

Figure 20: Micro CT Scans of SECC (using VersaXRM-500 from Xradia)

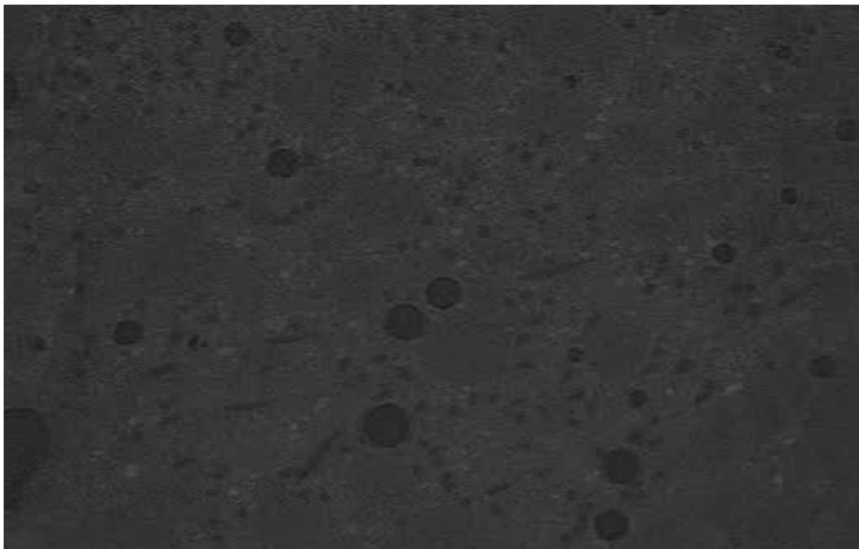

Figure 21: Micro CT Scans (Tests at Argonne National Laboratory)

4.5 Mechanical Tests

4.5.1 Compressive Strength

Compressive tests were performed on 50.8 x 50.8 x 50.8 mm cubes in accordance with ASTM C109. These specimens were tested with an ADR-Auto ELE compression machine and loaded at a rate of 0.9 kN/sec. The maximum load and maximum compressive stress was then recorded.

4.5.2 Four-Point Bending Test Procedures

Four-point flexural testing was performed in order to determine the flexural behavior of ECC/SECC (Figure 22). This test allows quantifying the material's ability to withstand large deformations while still maintaining a high load carrying capacity. This test was performed the most throughout this research since a material's ability to withstand large deformations is vital for a durable material. Flexural tests were then performed on the 160 mm long x 14 mm tall x 40 mm wide beams using four-point bending test. The end supports were 120 mm apart with the middle loading supports 40 mm apart. The beams were then loaded at a rate of 1.2 mm/min to observe the stress-strain behavior after initial cracking. After the beams were tested under flexure they were investigated under a magnifying glass to view the cracking patterns. Typically, only the failure crack was observed by the naked eye, therefore the magnification helps to observe smaller cracks in the material.

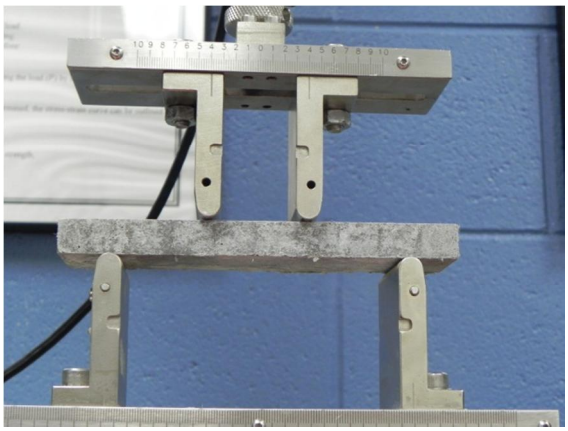

Figure 22: Investigation of Flexural Behavior of ECC/SECC using 4-Point Bending

4.6 Durability Tests

4.6.1 Absorption and Rate of Absorption

Absorption tests were performed on SECC specimens using ASTM C642. This standard procedure provides density, absorption and voids in hardened concrete. The test was performed on SECC samples that have cured to the desired age. At the desired age the samples were oven dried until 24-hour sequential readings were within a 0.5% tolerable range. Next, the samples were immersed in water until 24-hour sequential readings were within a 0.5% tolerable range. This test allows the absorption of the specimen to be determined.

The rate of absorption of the specimens was performed using ASTM C1585 standard procedure. This procedure is conducted by allowing samples to properly cure for a given age and then conditioning the sample for 3 days in an environmental chamber at 50°C and 80% relative humidity. Next the samples were sealed on the sides and covered with plastic on the top so that moisture would only be able to enter the specimen through the bottom. Next, the samples were placed in water on supports so that approximately 3 mm of the sample was under water. Weights of the sample were periodically taken and the provided equations allowed for the rate of absorption to be determined.

4.6.2 Rapid Chloride Permeability

Rapid chloride permeability of ECC/SECC was performed on 100 mm x 200 mm cylinders. These cylinders were cast and cured in lime water, then tested after 28 days. The procedure to determine the material's resistance to permeability conforms to ASTM C1202. Specimens were first cut to create 100 mm diameter by 51 mm tall samples. Each sample was then painted with two coats of waterproof epoxy along its sides to ensure that any solution within the specimen will enter or exit only through the top or bottom and not the sides. Specimens were then placed in a vacuum for 3 hours, and then distilled water was allowed into the vacuum chamber, completely submerging the specimens. After 1 hour of the specimens being submerged in distilled water and vacuum-sealed, the vacuum was released and the pressure was able to return to atmospheric pressure. The specimens remained in this condition for 16 to 20 hours. Next, solutions were then prepared consisting of 12 g of NaOH per liter of distilled water and 30 g of NaCl per liter of distilled water. After removing specimens from the distilled water they were placed in the apparatus for rapid chloride permeability testing and the NaOH and NaCl solutions were placed on each end of the apparatus. A power supply was turned on to 60 volts and current was allowed to pass through the specimen. After 6 hours, the current passed through the specimen is directly correlated to the permeability of the specimen. To calculate the charge passed, the following equation was used:

$$Q=900(I_0+2I_{30}+2I_{60}+\ldots+2I_{300}+2I_{330}+I_{360})$$

where: Q=charge passed (coulombs)

I_t=current passed (amperes) at time t after voltage is applied

The lower the charge passed the lower the chloride ion permeability is. The specimen can then be characterized using Table 12.

Table 12: Chloride Ion Penetrability Based on Charge Passed

Charge Passed (coulombs)	Chloride Ion Penetrability
>4,000	High
2,000–4,000	Moderate
1,000–2,000	Low
100–1,000	Very Low
<100	Negligible

4.6.3 Freeze-Thaw Testing

Freeze-thaw testing on ECC/SECC was mainly performed using an accelerated method as compared with typical freeze-thaw testing. Typical ASTM C666 freeze-thaw test methods place specimens in fresh water and temperatures are oscillated between 4.4°C and -17.8°C (40°F and 0°F) with no specified duration for temperatures to be held at this point. Standards state that freezing and thawing cycles must continue for 300 cycles or until the durability factor (DF) has dropped to 60% of its initial values. The procedure used in this research uses freezing down to -50°C (-58°F) as an accelerated test method to evaluate the freeze-thaw durability.

After de-molding specimens were placed in a curing container with lime water at the age of 24 hours and left for an additional 13 days so that specimens would be placed in the freeze-thaw chamber at 14 days age. Initial readings of cross-section, deformation, mass, and fundamental frequency were recorded. Through this point the accelerated freeze-thaw testing method is identical to ASTM C666 procedures. Next, the specimens were placed in the freeze thaw chamber. Instead of placing the specimens in fresh water and having temperature oscillate between 4.4 and -17.8°C, specimens were placed in both fresh water and salt water (5% solution) and the temperature oscillated between 20°C to -50°C. This process consisted of holding temperatures at 20°C for 2 hours with a relative humidity of 95%. Next, the temperature was rapidly changed to -50°C with 0% of relative humidity. This environmental condition was held for 2 hours and then rapidly changed to 20°C with 95% of relative humidity and then repeated. Mass, cross-sectional area, deformation, and fundamental frequency were periodically tested (typically every 50 or 100 cycles) during cycling. Specimens were tested for up to 700 cycles.

Evaluation of specimen performance under ASTM C666 testing can be assessed by use of ASTM C215. In this standard, the dynamic modulus is used to calculate a durability factor (DF) of concrete. Here, the relative dynamic modulus of elasticity and durability factor are calculated from the following equations.

$$P_c = \left(\frac{n_1^2}{n^2}\right) * 100$$

where: P_c=relative dynamic modulus of elasticity;

n_1=frequency after n cycles;

n=initial frequency.

$$DF = \frac{P_c * N}{M}$$

where: N=the number of cycles at which P reaches the specified minimum value for discontinuing the test or the specified number of cycles at which the exposure is to be determinate;

M=specified number of cycles at which the exposure is to be terminated.

ASTM C215 states that a DF less than 40 results in an undesirable material, and a DF greater than 60 is an acceptable material. Standards state that a material is only required to maintain a durability factor greater than 60 for up to 300 cycles to be considered durable; however, 300

cycles may not be a sufficient minimum value for northern regions such as Wisconsin. Moreover, it is known the durability of PVA-ECC is very high, and the material would easily maintain a high durability factor through 300 cycles. For this reason, durability factors were calculated for each test period.

Young's dynamic moduli of elasticity values were also considered through up to 550 cycles. The value was calculated based on ASTM C215 and the following equations:

$$\text{Dynamic E} = \text{CMn}^2, \text{(Pa)}$$

$$C = 0.9464\left(\frac{L^3T}{bt^3}\right)$$

where: M=mass of specimen (kg);
n=fundamental transverse frequency (Hz);
L=length of specimen (m; d=diameter of cylinder, (m);
t, b=dimensions of cross section of prism (m); t being in the direction in which it is driven,
T=correction factor that depends on K, L and on Poisson's ratio=0.17.

Since the variations in cross sectional area and length remained negligible throughout testing, the value for C was simplified to 2089.65 m^{-1}.

The majority of -50°C (-58°F) freezing and thawing experience is related to Russian standards (GOST-10060) for methods of frost resistance determination. There are three different methods of freezing and thawing in this standard. The first, closely resembles ASTM C666 with specimens immersed in water and temperatures oscillating between 5 and -20°C. The second method is different from the first in that instead of fresh water, 5% NaCl solution is used as the thawing medium and freezing occurs in air. Temperatures range from 10°C to -50°C in the second method as well. The third method is similar to the second except both freezing and thawing occurs in 5% NaCl solution. Materials are then classified as F300, F400, etc. based on how many cycles the material withstands freezing and thawing based on the first method (e.g. a material classified as F300 will withstand 300 freezing and thawing cycles based on the first method). The following table is provided to demonstrate equivalent classifications from the second and third methods.

Table 13: Equivalent Freeze-Thaw Classifications based on GOST 10060

		Concrete Grade						
Method	Use	F25	F100	F200	F400	F600	F800	F1000
I	Structural Concrete	25	100	200	400	600	800	1000
II		-	20	45	110	200	300	450
III		-	3	5	12	19	27	35

Based on Table 13 above, 35 freeze-thaw cycles corresponding to a method similar to the one used within this research (temperatures dropping to -50°C, in salt water) would correspond to 1000 freeze-thaw cycles using standard methods. This means that specimens that were

subjected to 400 freeze-thaw cycles in this research would be an equivalent of over 11,000 standard freeze-thaw cycles. The above table was designed for conventional concrete, therefore ECC/SECC mixtures used within this research will be tested in the future using both methods to determine the proper equivalency.

For specimens that were placed in the freezing and thawing environment in fresh water with temperature ranging from 20°C to -50°C, an earlier report can be used to equate and equivalent freeze-thaw performance to specimens tested under standard ASTM C666 methods. In this report, specimens with siloxane-based admixtures were tested similar to the first method of GOST with the exception of temperature ranging from 20°C to -50°C. In this study, specimens survived over 140 cycles which correspond to 700 freeze-thaw cycles when temperatures only drop to -20°C. To obtain this equivalent value a multiplication factor of 5 was used.

4.7 Abrasion Resistance

Abrasion resistance of SECC on selected specimens was determined in accordance with ASTM C944. This procedure utilizes small cutting blades that are placed on the flat surface of the sample and rotated at a speed of 200 rev/min. The standard also states that the blades should be exerting a normal force on the surface of the sample of either 98N or 197N. For the case of SECC a normal force of 197 N was used. A slight modification to the standard procedure was also used in this analysis as well. The standard states that three 2-minute abrasion periods shall be performed on separate areas of the sample. For testing of SECC, five 2-minute abrasion periods were performed on the same area. This allows for more deterioration to be seen on the sample.

Since, it was not originally intended to perform abrasion resistance procedures on SECC, no duplicate samples were made, meaning that there was only one indicative data value for each sample. Because of the lack of sample duplicates, results from this test cannot be used for statistical analysis on the abrasion resistance of SECC, but may provide a useful indication on how SECC may perform under abrasion resistance.

5. Results and Discussion

5.1 Fiber Type Study

As can be seen in Figure 23, the flow of each mixture decreased as the fiber volume increased. In general, with the exception of 2.0% of RECS 15x8 mm fibers, the largest fibers (RECS 15x12 mm) displayed the best flow when comparing fibers of the same volume. This is most likely due to the fact that compared with smaller fibers at the same volume; there are a lesser number of fibers, allowing for better workability of the material. Interestingly these same larger fibers actually showed the best flexural behavior as well. This is most likely because the fibers had the best chance to distribute themselves evenly throughout the mixture. This is true up until 3.0% by volume of fibers is used, where there is a significant decrease in flexural behavior, showing that this volume may be excessive. The compressive strengths for each of the different types of fibers remained roughly the same as seen in Figure 24. This demonstrates

that fiber type and fiber volume (within a reasonable range) have no effect on the compressive strengths of the material.

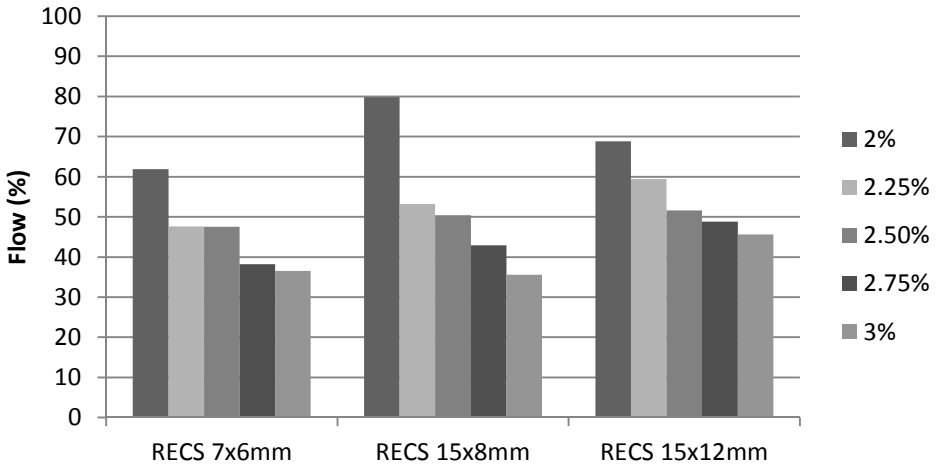

Figure 23: Flow of ECC with Different Fibers and Varying Volumes

Flexural test results show that the largest fibers (RECS 15x12 mm) outperformed the other fibers when considering the same volume. However, when these fibers were used at a volume of 3.0%, there was a considerable reduction in performance. Based on these results the ideal fiber type and volume incorporates the largest fiber at a volume of 2.75%. This being said, fibers types were combined in an attempt to even further increase properties. Since 3.0% of the largest fibers lost some flexural behavior and 3.0% of the smallest fibers still performed quite well, a majority of large fibers were combined with a small amount of RECS 7x6 mm fibers in order to achieve superior performance at a total fiber volume of 3.0%.

The below figures show the flow and flexural behavior of selected mixtures compared to the same total volume of fibers of just the largest size fiber alone. As can be seen in these figures, the performance only slightly increased; therefore it would not be beneficial to combine the two different types of fibers. This approach would also lead to a much difficult mixing process.

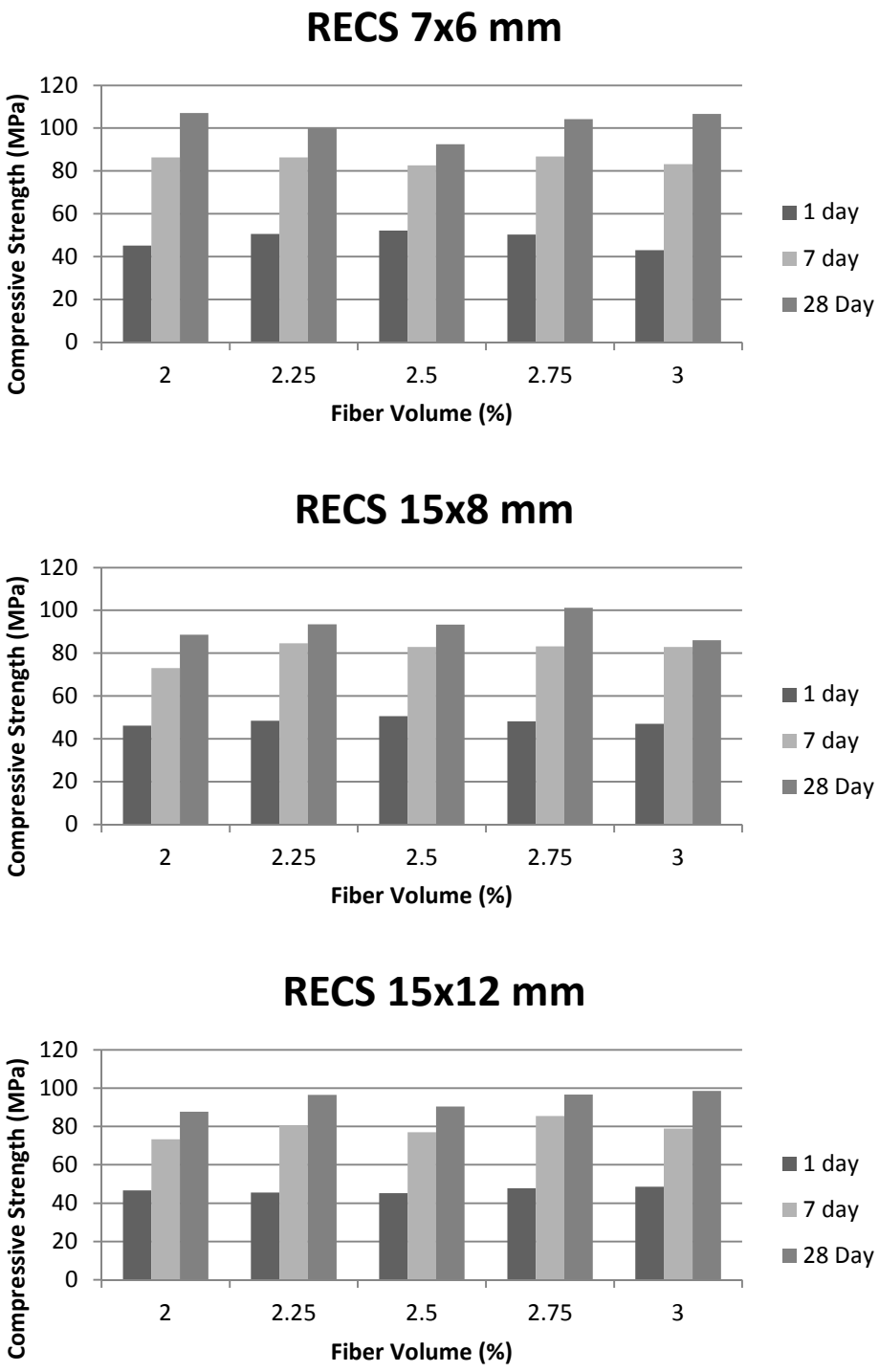

Figure 24: Compressive Strength of ECC with Different Fiber Types and Varying Fiber Volumes

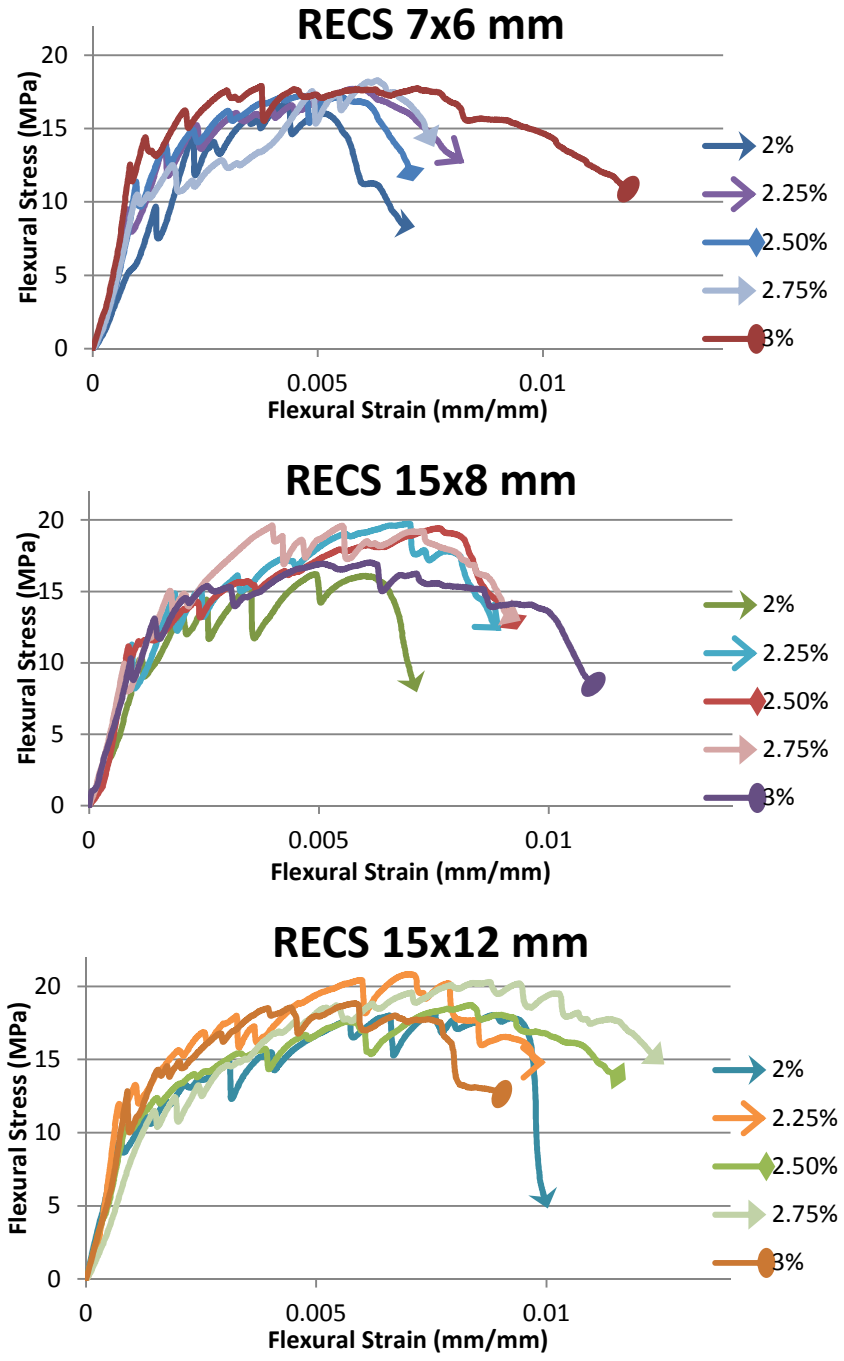

Figure 25: Flexural Behavior of ECC with Different Fiber Types and Varying Fiber Volumes

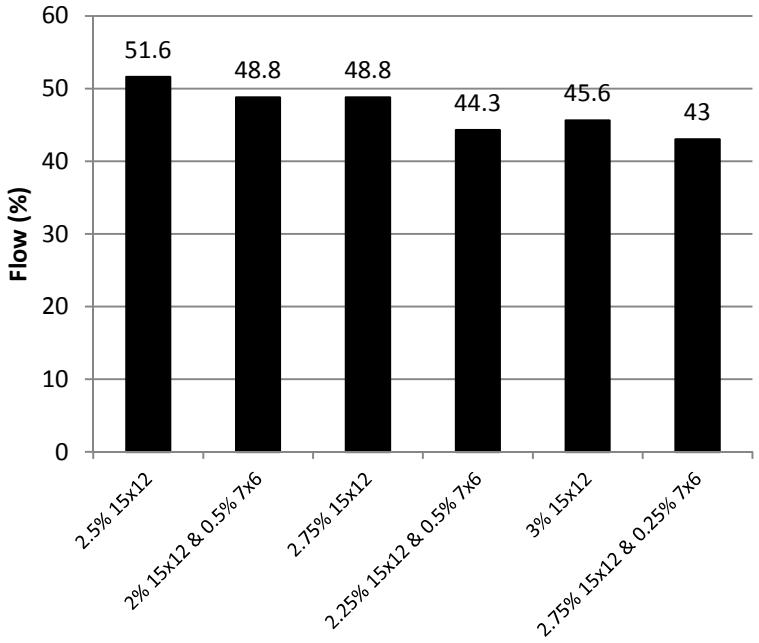

Figure 26: Flow of ECC based on Combined Fiber Types

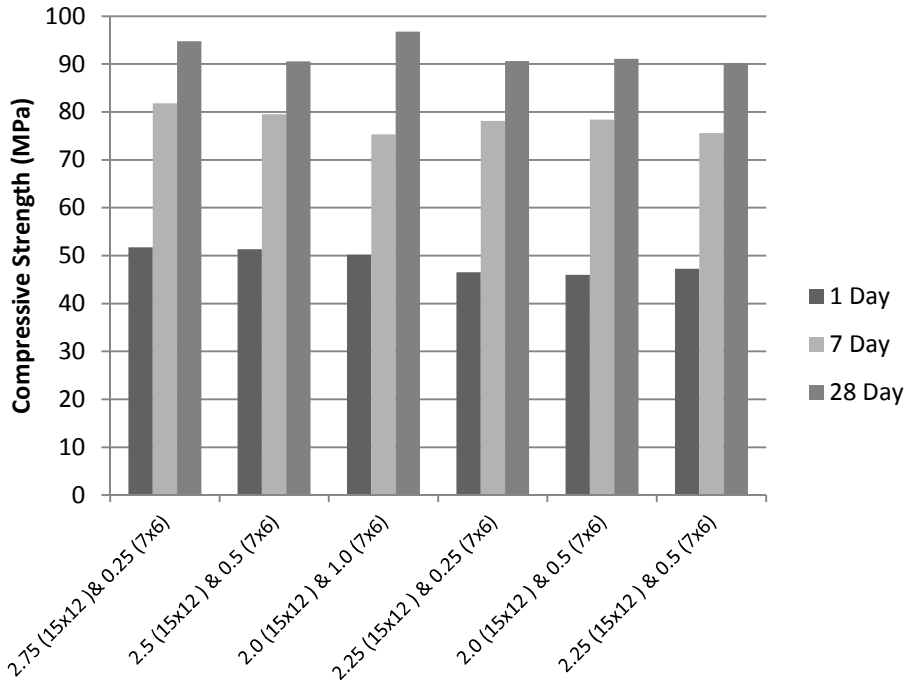

Figure 27: Compressive Strength of ECC based on Combined Fiber Types

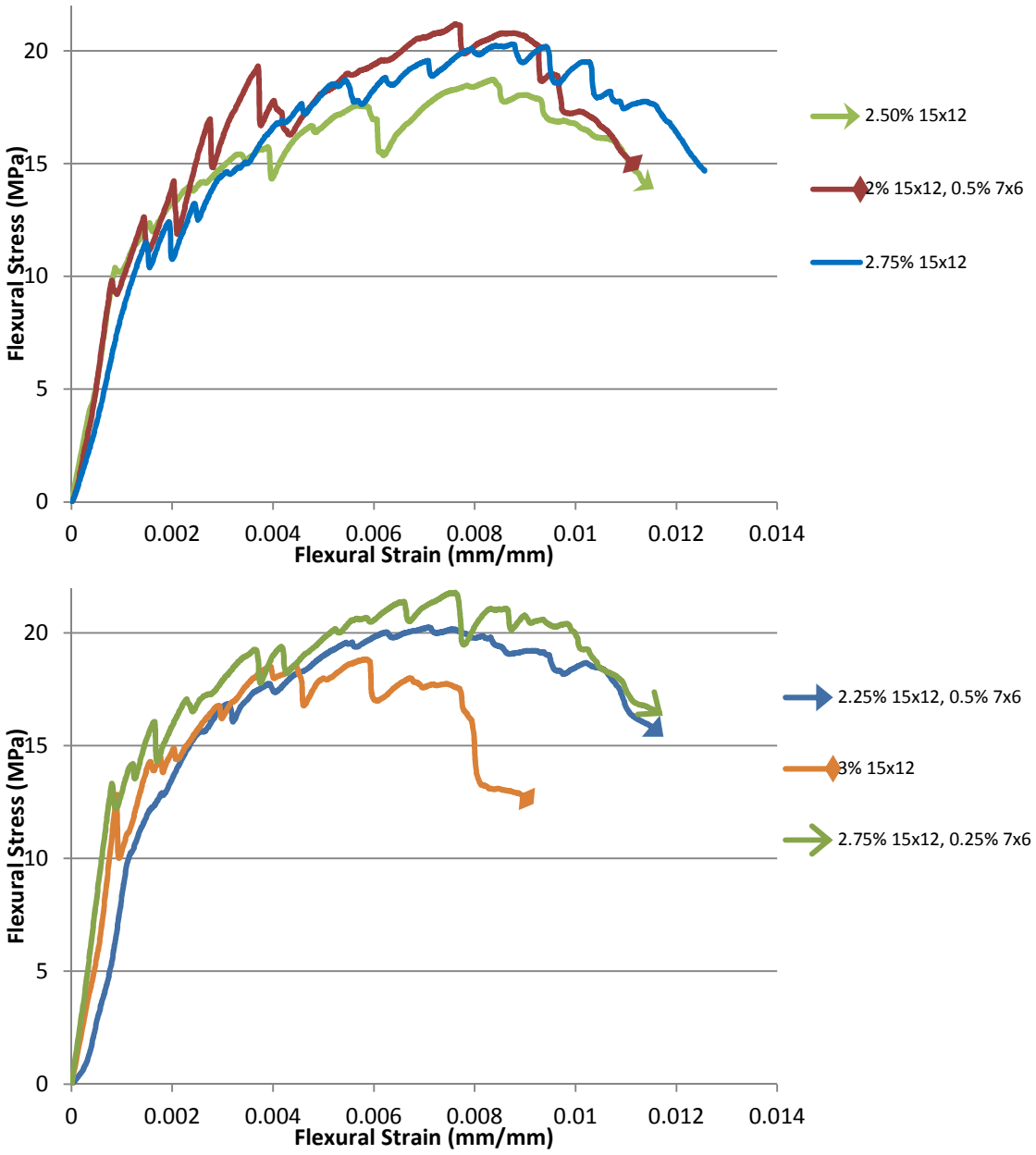

Figure 28: Flexural Behavior of ECC based on Combined Fiber Types

5.2 Phase A: the Effect of Silica Fume and Hydrophobization

5.2.1 Flow and Air Content

The flow of ECC/SECC in the fresh state can be seen in Figure 29 below. It can be seen that the two mixtures with a w/cm ratio of 0.45 have a very similar flow, showing that the addition of hydrophobic emulsions have a little effect on fresh properties. However, there is an increase in flow when the hydrophobic emulsions are added to the composite material at a lower w/cm ratio. This type of behavior was not observed in previous studies, but could be contributed to a reaction between the hydrophobic emulsions and the large quantity of supplementary cementitious material being used. Moreover, the material with a lower w/cm ratio tends to have

a higher flow. This is due to the lesser-uniform mixtures that were created at a higher w/cm ratio and higher dosages of aggregates. In these mixtures, clumping of fibers was observed, thus reducing the workability of the material. The clumping of fibers within the material is also the reason an increase in flow was not detected. In this situation, the emulsion droplets became trapped within clumps of fibers, thus not being able to interact with the SCM to improve flow and workability.

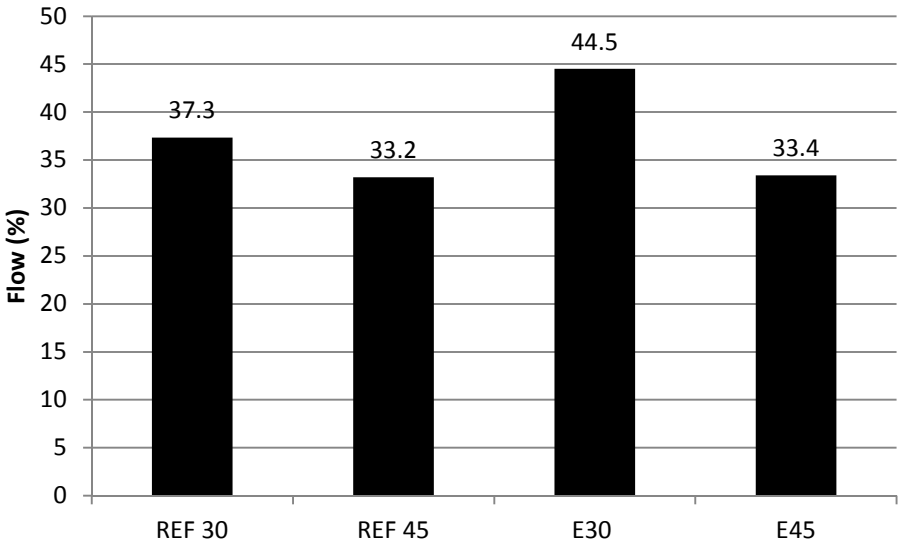

Figure 29: Flow of SECC with 50% SCM with Varying w/cm Ratios, each with and without Hydrophobic Emulsions

The air content in the fresh state remained within a relatively close band with air contents of 2.0, 2.4, 2.4, and 2.4 for REF 30, REF45, E30, and E45 respectively. One may think that with the addition of hydrophobic emulsion, which is intended to create artificial air voids, there would be an increase in air content. However, since the air content was measured immediately after mixing, the hydrophobic emulsions have not had a chance to form their air void structures yet. This process will then take place during setting of material (2+ hours), which is why there is little difference in observed fresh initial air content.

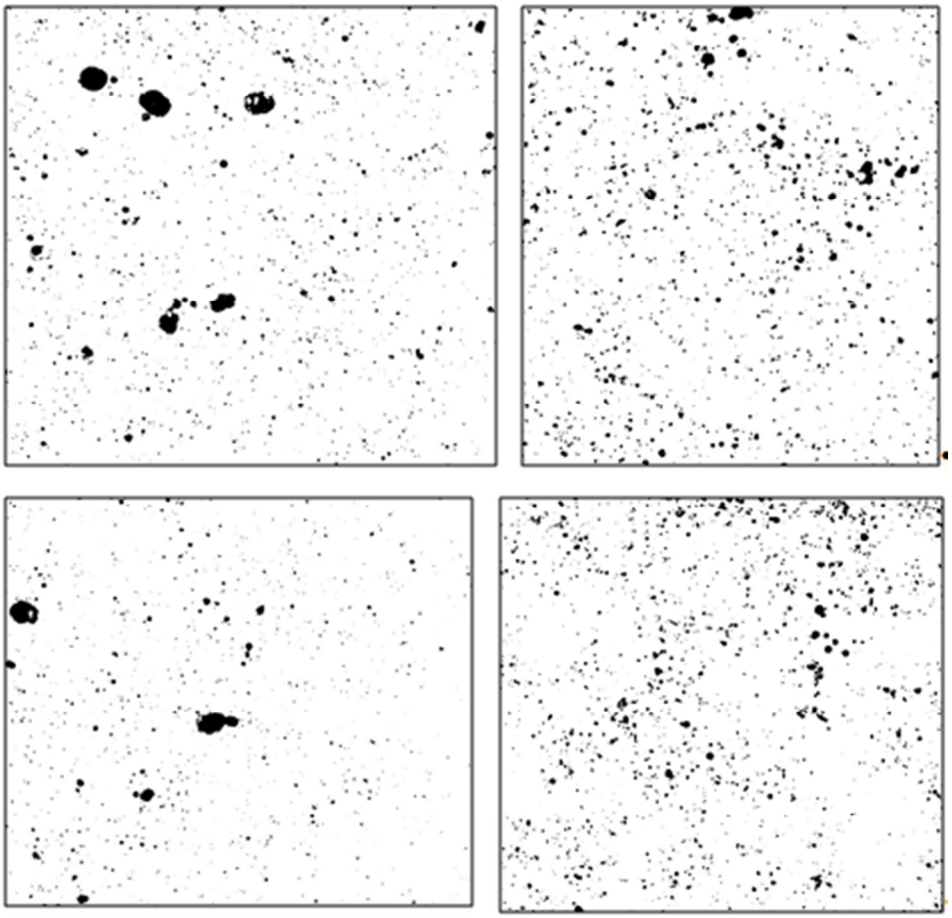

Figure 30: Air Void Analysis E30 (Top Left), E45 (Top Right), REF30 (Bottom Left), and REF45 (Bottom Right)

Figure 30 above, shows air voids (black portions) of SECC with and without hydrophobic emulsions. At first look, it appears as though the figure on the right (higher w/cm ratio) appear to have more voids. However through image analysis (Table 14), sample E30 actually has the most voids. This value was determined using Image J software. Analysis also shows that samples with higher w/cm ratios tend to display higher air void fractions, however also larger air voids. This is most likely due to the higher quantity of entrapped air that is present within higher w/cm samples. Another interesting value that was obtained through image analysis is that the amount of air present in E30 is significantly higher than REF30. This shows that the intent of hydrophobic emulsions to create air voids within the system tends to work well, while still maintaining many small air voids within this cementitious matrix.

Table 14: Air Void Characterization of SECC

MIX ID	Area size (mm^2)	Air Voids (%)	No of Voids/mm^2 (on average)	Average Void Area (mm^2)
E30	856.28	2.63	2.006	0.0131
E45	800.74	3.45	1.966	0.0175
REF30	957.07	1.49	1.345	0.0111
REF 45	1337.01	3.54	1.547	0.0229

5.2.2 Compressive Strength and Flexural Behavior

The compressive strength of the materials can be seen in Figure 31 below. It can be seen that materials with a lower w/cm ratio demonstrated much higher strengths as is to be expected. There was, however, a slight decrease in strengths when the hydrophobic emulsion was added to the material. This reduction is small enough, especially since the material exhibits extremely high strengths (approx. 100 MPa).

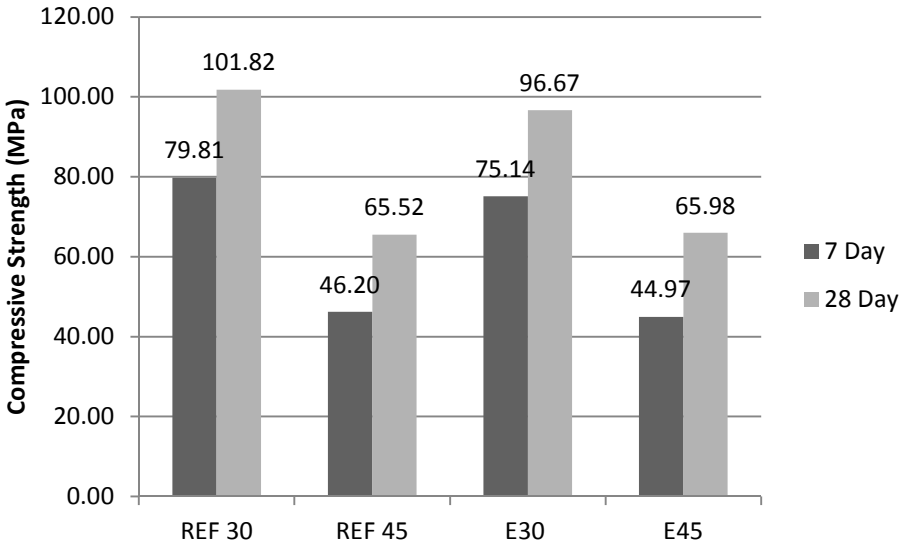

Figure 31: Compressive Strength of SECC with 50% SCM and Varying w/cm Ratios each with and without Hydrophobic Emulsions

The flexural behavior was similar as reported by previous CFIRE Report 04-09. The addition of hydrophobic emulsions improved the ductility at early ages. Moreover, even when a stronger matrix is used (w/cm ratio of 0.3), the flexural behavior displays both improvements in flexural stress and flexural strain. This is an important feature that verifies that the use of a strong matrix can still provide good ductility. In the past, other researchers have chosen to weaken the matrix to create a more ductile material, whereas in this case a stronger matrix also leads to improved ductility. This can be attributed the use of hydrophobic emulsions creating artificial flaws to allow

for strain hardening behavior. Moreover, the use of 50% supplementary cementitious materials allows for a more controlled pullout of fibers [42].

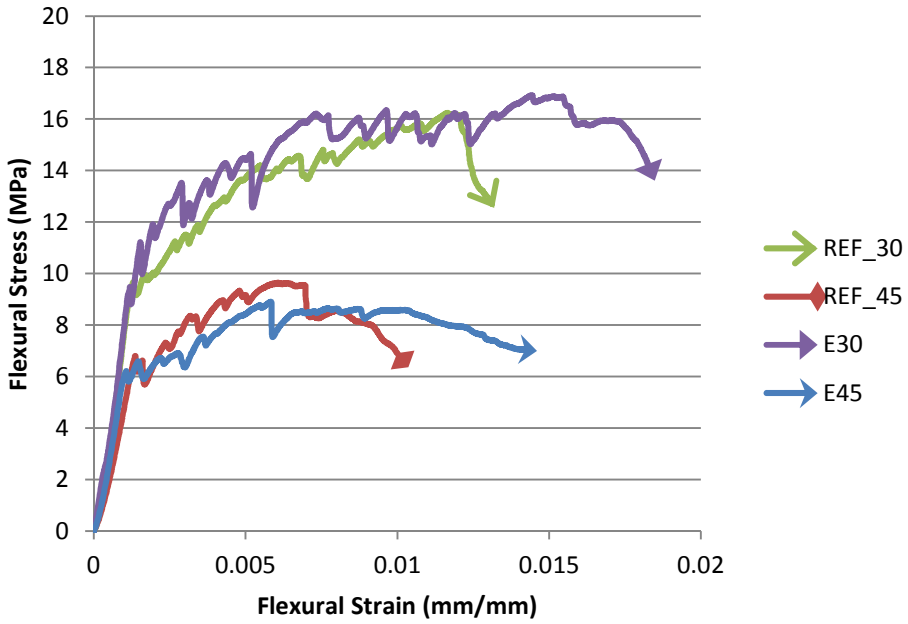

Figure 32: Flexural Behavior of SECC with 50% SCM at 7-Day Age

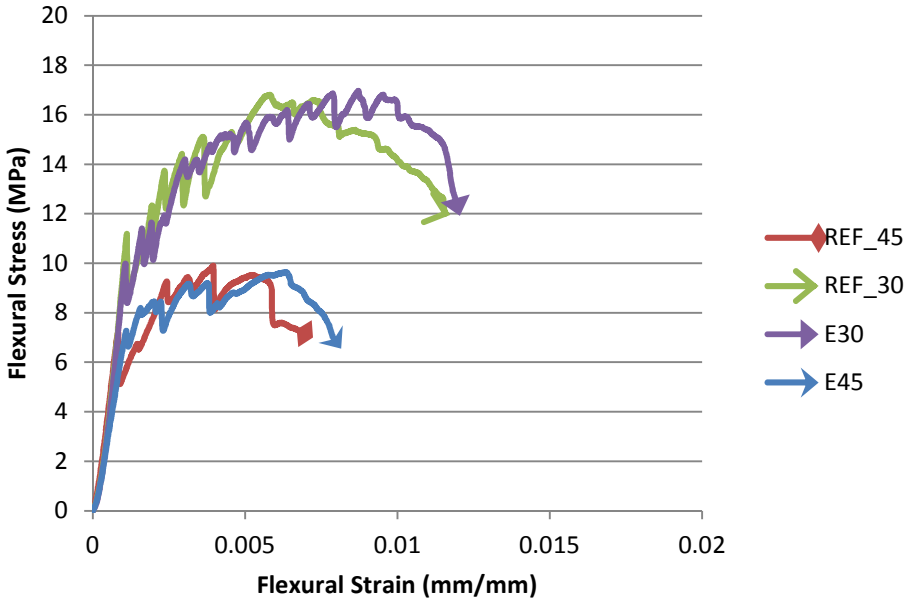

Figure 33: Flexural Behavior of SECC with 50% SCM at 14-day Age

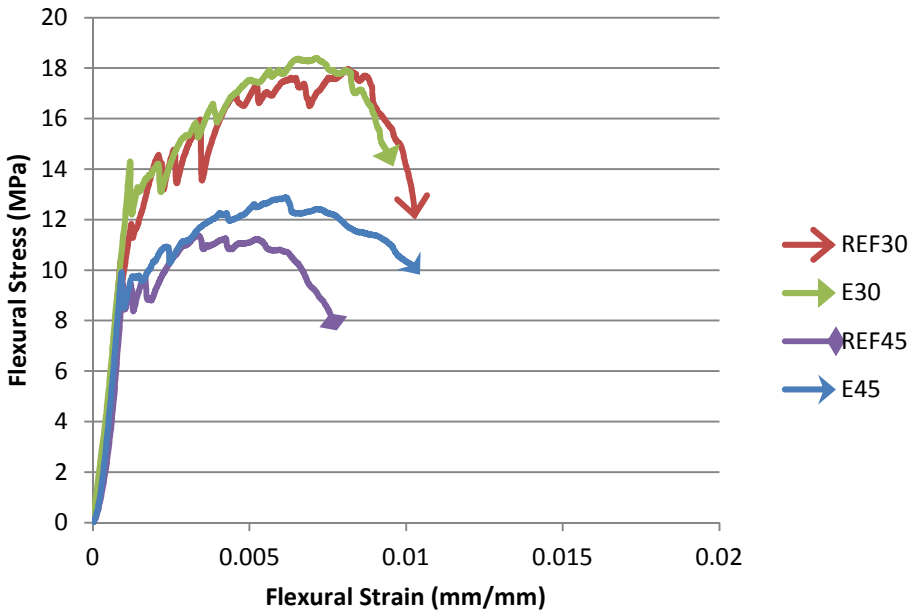

Figure 34: Flexural Behavior of SECC with 50% SCM at 28-Day Age

At earlier ages of the material (Figure 32), it can be seen that the addition of hydrophobic emulsions leads to a better strain hardening behavior and, thus, better ductility. However, at later ages (28 or more days), the addition of the hydrophobic emulsions did not improve ductility, (Figure 34). Knowing that all previous work in this study with hydrophobic emulsions improved ductility, one possible reason it is not seen here may be due to the large quantity of supplementary cementitious materials being used. Since the majority of the SCM being used is ground granulated blast furnace slag, the bond between the fiber and matrix may be improved, thus interfering with a controlled pullout of the fibers. This may be due to the dense nature of the material. This was not the case with the higher w/cm ratio. For these mixtures, the one that incorporated the hydrophobic emulsion provides a better flexural behavior at 28 days. This may be contributed to interactions between the fibers and the hydrophobic emulsions along with the higher w/cm ratio.

5.2.3 Freezing and Thawing Analysis

Two sets of freezing and thawing tests were considered when analyzing ECC/SECC. First, specimens that were created in the hydrophobic study were tested for 350 cycles. Next, optimal specimens based on the results of previous work (fiber volume and use of supplementary cementitious materials) were tested for 400 cycles.

Freeze-Thaw Resistance of ECC/SECC

Freeze-thaw resistance was considered for ECC/SECC with hydrophobic emulsions. 2% by volume PVA fibers were used in this test to better understand the effect of emulsions on SECC. It is known that PVA fibers can improve the freeze-thaw resistance of ECC/SECC, therefore adding a lower volume can help to detect the effect of the emulsions. The emulsions that were considered to be the best (E5 and E6 in the Hydrophobic Emulsions Study of Phase I of CFIRE

report) were compared against a reference specimen and tested for 350 freeze thaw cycles ranging from -50°C to 20°C. These corresponding emulsions represent a single and double dose (250 or 500 mg of siloxane per 1 liter of mixture, respectively) of the emulsions containing 25% of PMHS and 4.4% of PVA emulsifier mixed at 10,000 rpm. Cross-section change (Figure 35), mass change (Figure 36), and Young's Dynamic Modulus of Elasticity (Figure 37) were tested every 50 cycles to determine the effect of freezing and thawing. Based on the results of Young's Dynamic Modulus of Elasticity, a durability factor for the material was also determined (Figure 38). Compressive strengths after 350 cycles were also determined (Figure 39). FT1 corresponds to the reference specimen without any added air, FT2 represents a double dose of emulsions and FT3 represents a single dose of emulsion.

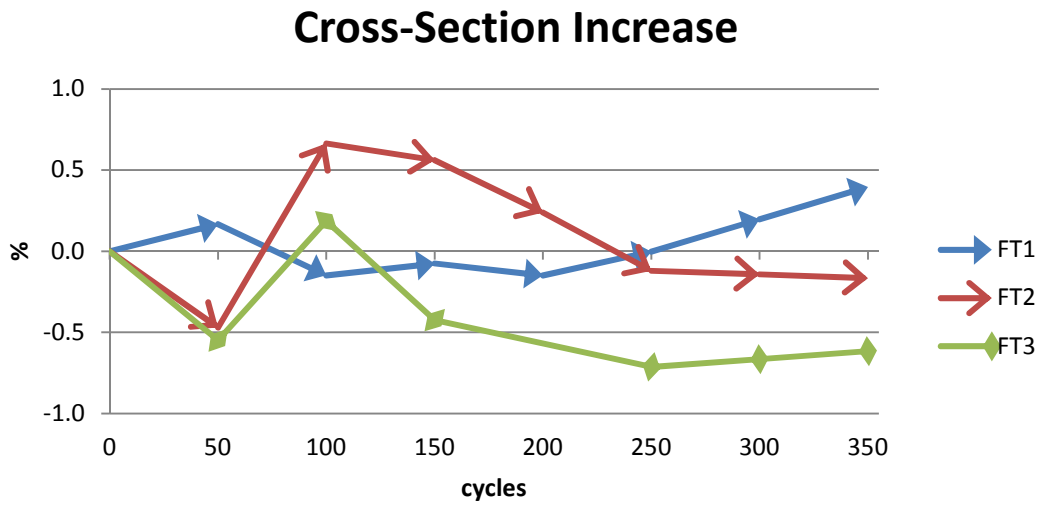

Figure 35: Cross-Sectional Change of ECC/SECC during Freezing and Thawing

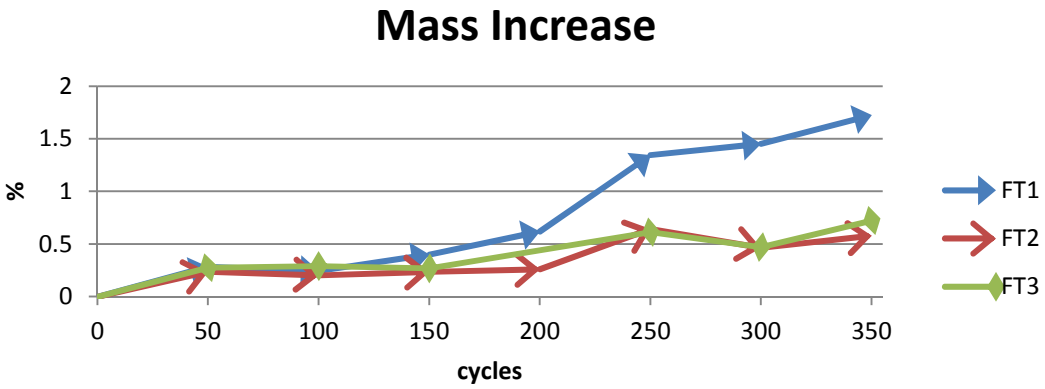

Figure 36: Mass Change of ECC/SECC during Freezing and Thawing

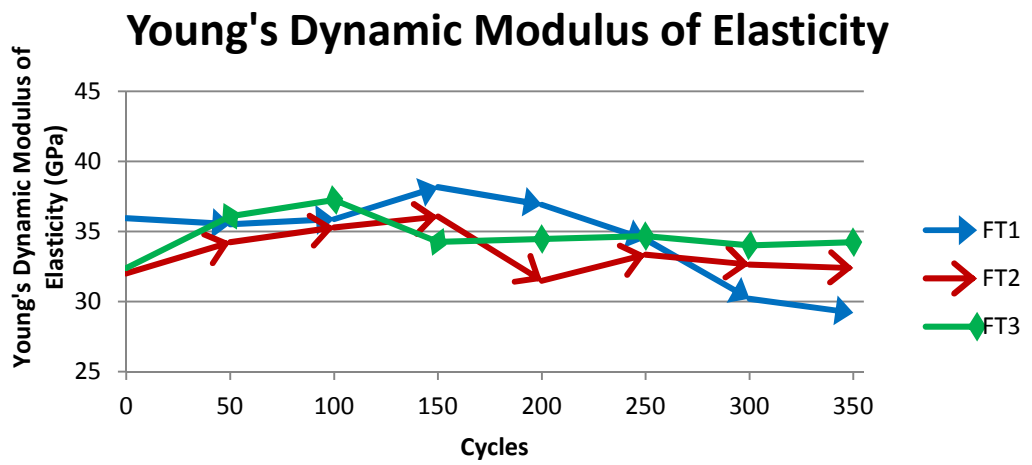

Figure 37: Young's Dynamic Modulus of Elasticity of ECC/SECC during Freezing and Thawing

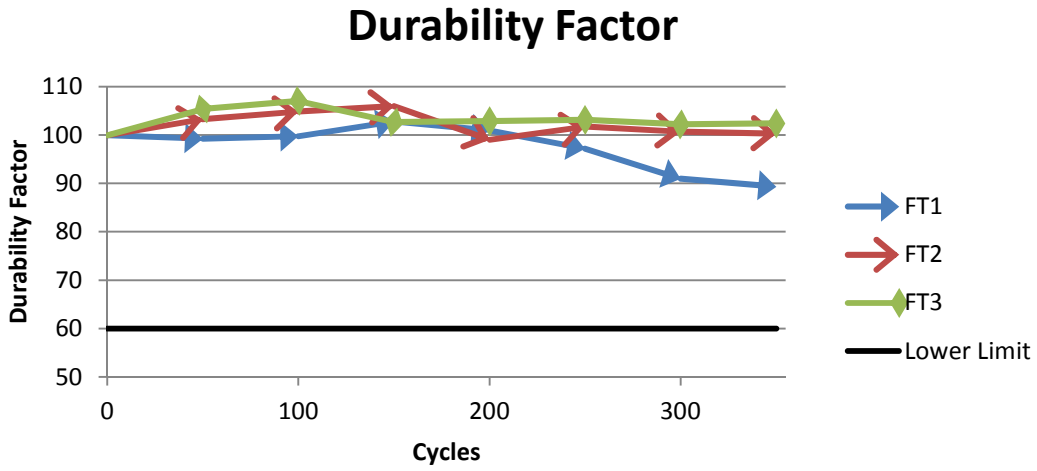

Figure 38: Durability Factor of ECC/SECC during Freezing and Thawing

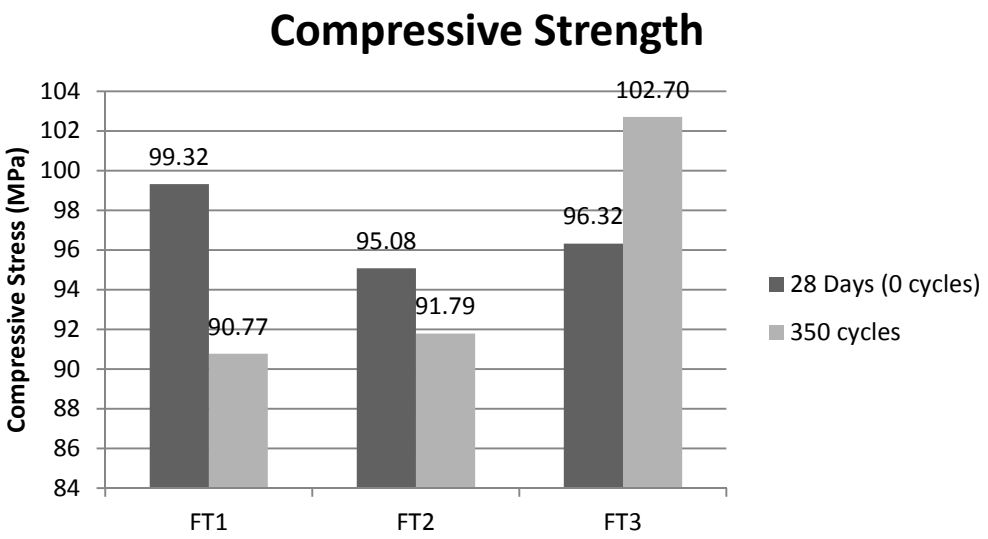

Figure 39: Compressive Strength of ECC/SECC before and after 350 Cycles of Freezing (-50°C) and Thawing

As seen in the above figures, all specimens have performed quite well through 350 freeze-thaw cycles; however, the reference ECC specimen (without any added air) has started to lose its characteristics. This can be seen from the increase in volume; showing that water is entering the entrapped air voids of the material and freezing, causing the material to expand. The Young's Dynamic Modulus of Elasticity and durability factor of this material are also dropping, showing that the larger air voids created from expanding ice are causing the stiffness of the material to decrease. The mass of the material has also significantly increased after passing 200 cycles. This is because the specimens were weighed just after coming out of the water (saturated surface dry condition); therefore water was still present within the voids, showing that larger air voids have formed within reference FT1. Even though other researchers have found that ECC is capable of withstanding 300 freeze-thaw cycles (-17°C) without any added air, the porosity within the material will inevitably be present, which will act as a home for saturated water. This water then freezes and expands creating internal stresses and inevitable loss of performance due to freeze (-50°C) and thaw cycling. The addition of hydrophobic emulsions seen above allows for a controlled access of water, allowing water to freeze and expand within spherical voids designed to handle these effects. Moreover, specimens with a single dose of emulsion displayed improved strengths after 350 cycles of freezing and thawing, while the reference specimen lost considerable strengths. Specimens with double dose of emulsions did not display the same positive results that the single dose did, showing that a double dose provides excessive generation of air. Freeze-thaw tests, along with improved ductility, show that the addition of hydrophobic emulsions to ECC can be very beneficial.

Freeze-Thaw Resistance of SECC with SCM

Freezing and thawing tests were performed on specimens with 50% of SCM at temperatures oscillating between -50°C and 20°C. The specimens were placed in the salt water to accelerate the deterioration process. To analyze the deterioration of the specimens during freezing and

thawing cycles, the change in mass, cross sectional area, deformation, dynamic modulus of elasticity, visual analysis of surface scaling, and compressive strengths before and after cycling were monitored. Each specimen was tested every 100 cycles and compressive strengths were measured at 28 days (without freezing and thawing cycles), at 300 cycles, and 400 cycles. The average of two specimens was taken for compressive strength, dynamic modulus of elasticity, and deformation while the average of 4 specimens was used for mass increase and cross sectional area change values.

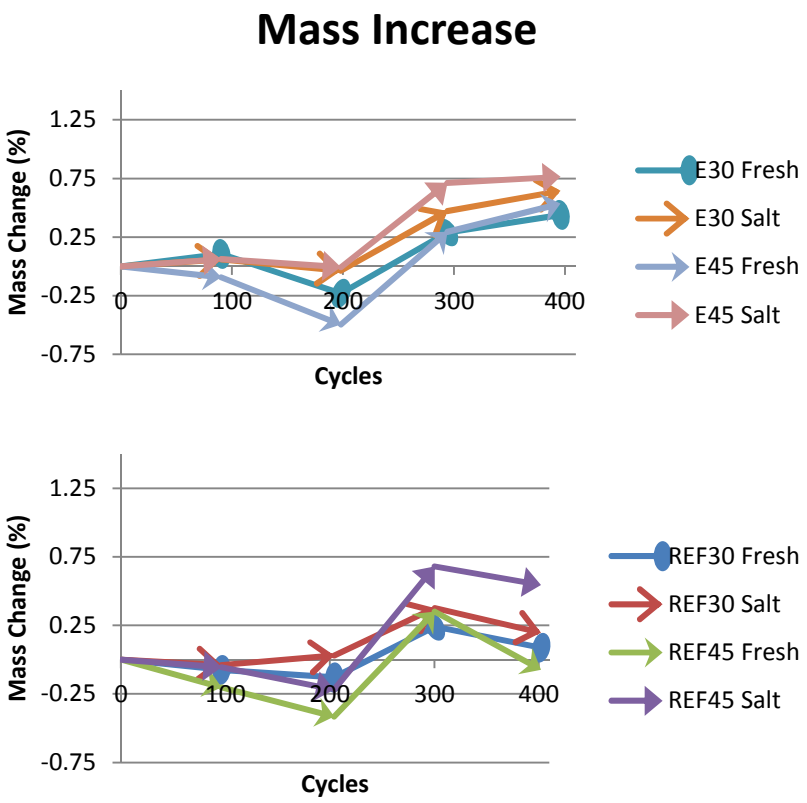

Figure 40: Mass Change of ECC/SECC after Freezing (-50°C) and Thawing (20°C) Cycles

Figure 40 above displays the increase in mass over freezing and thawing cycles. Typically when mass change is monitored during freezing and thawing cycles, mass loss is recorded by determining the amount residue left in the container. Previous researchers found that this may not be the best method for testing mass change in ECC since the fibers will hold residue meaning that even if a piece of cementitious material has detached itself from the rest of the specimen the fibers will hold it on. Moreover, the specimens were tested in saturated surface dry conditions. This allows for a better look at deterioration within the specimen. If voids within the specimen are growing in size, more water will be able fill these voids making the specimen heavier during testing. This means that specimens that display a higher mass increase can have more deterioration. As seen in the above figure, the specimens with a higher w/cm ratio

tested in salt water displayed the worst deterioration. This can be attributed to the more porous structure creating more water penetrating into the specimens causing damage during cycling.

Figure 41 displays the increase in cross sectional area of the specimens during freezing and thawing. All of the specimens performed very well showing little change during cycling. The only exception is that all of the specimens that incorporated the hydrophobic emulsion showed a relatively high increase in area during the first 100 cycles but then leveled off after that. All specimens showed little to no variations in cross sectional change after this point. This can be taken as a sign that all specimens are very durable materials.

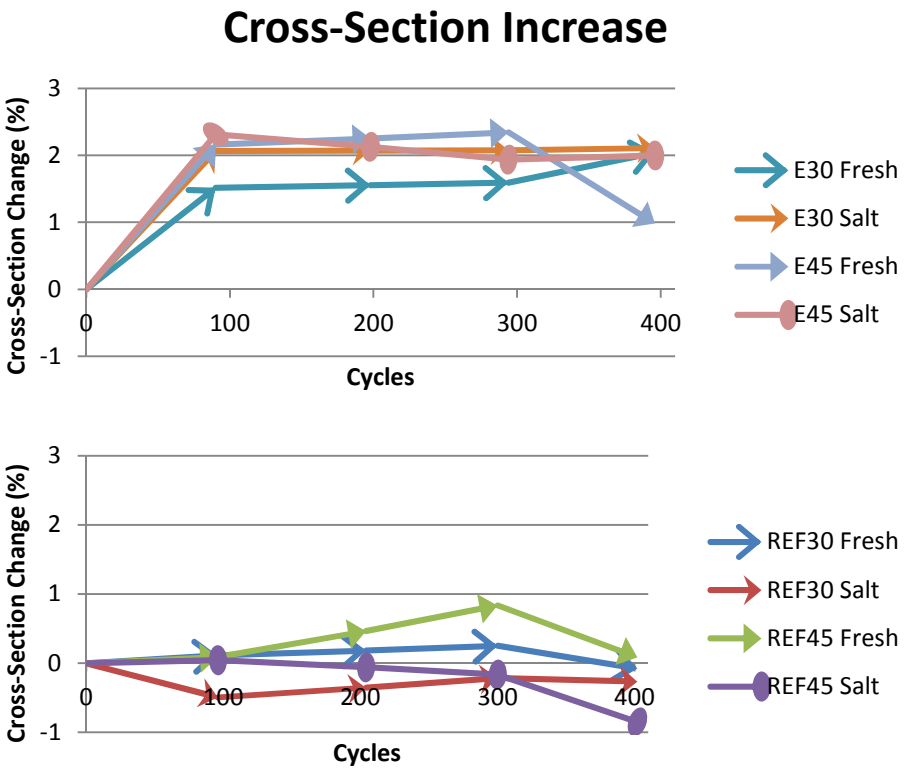

Figure 41: Cross-Section Change of ECC/SECC after Freezing and Thawing Cycles

The change in length of all the specimens remained near negligible values (Figure 42). The largest change in length was only 0.020%. This equates to only 0.0308 mm (12/10,000th of an inch) of deformation. Surprisingly, the largest deformation came from the specimen with emulsions at lower w/cm ratio and tested in salt water. Despite this, all data from deformation testing during and after 400 freeze-thaw cycles remained small enough as to be considered negligible.

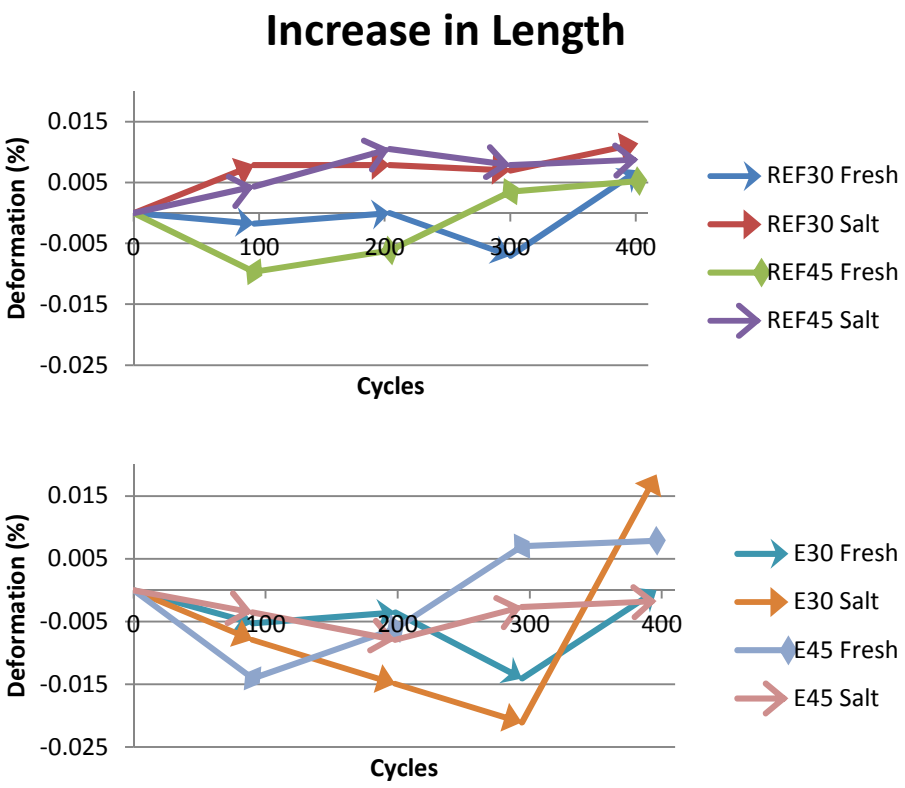

Figure 42: Deformation of ECC/SECC after Freezing and Thawing Cycles

Through monitoring of the fundamental frequency of the specimens, both Young's Dynamic Modulus of Elasticity (Figure 43) and a durability factor (Figure 44) were determined. Both of these values demonstrate the stiffness of the material after freezing and thawing cycles. Results based on Young's Dynamic Modulus of Elasticity show that the specimens with a lower w/cm ratio have a higher stiffness and tend to maintain or increase this stiffness during cycling. The specimens with a higher w/cm ratio started with a lower stiffness, which increased steadily during freezing and thawing cycles for specimens that also included an emulsion, but not for the reference specimens. This displays the continuing hardening process of the material and that freezing and thawing cycles are playing little effect on the properties of the material. The specimens with a higher w/cm ratio that did not incorporate the hydrophobic emulsion displayed scattered results and a general trend of loss in stiffness, especially after 300 cycles. These results show that specimens with a higher w/cm ratio, without the hydrophobic emulsion are beginning to reduce stiffness due to the degradation from freezing and thawing.

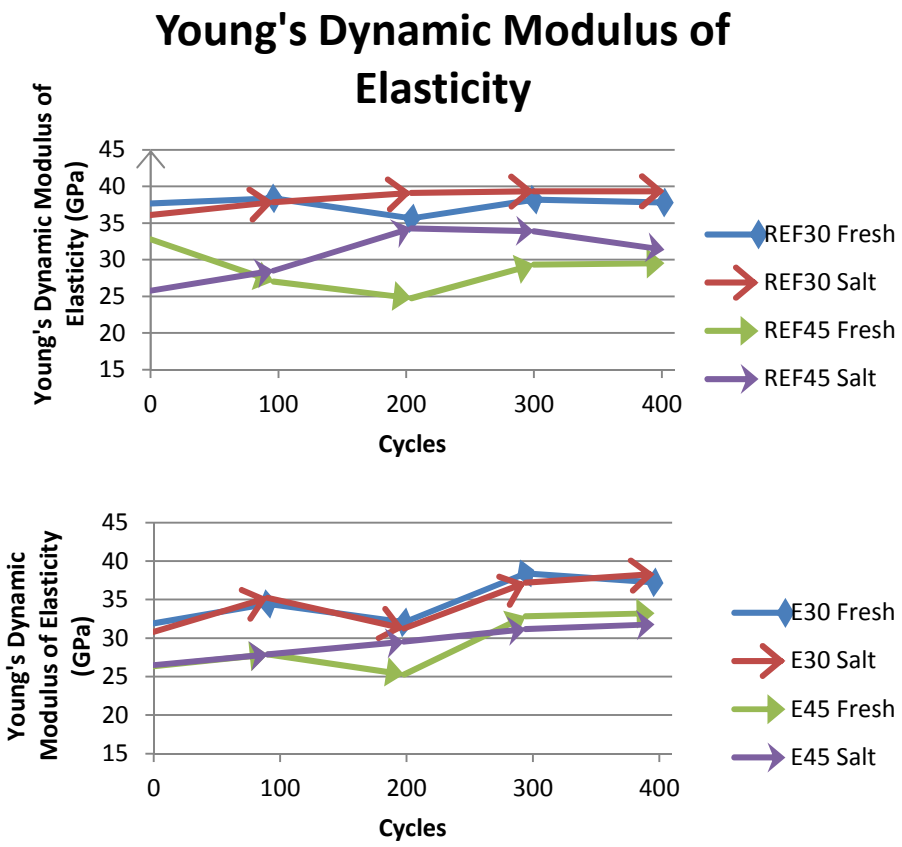

Figure 43: Young's Dynamic Modulus of Elasticity of ECC/SECC after Freezing and Thawing Cycles

The durability factor results displaying the percent change in fundamental frequency and relative dynamic modulus compared with the initial values show that all specimens that incorporated the hydrophobic emulsions performed very well. It can be seen these specimens showed a general increase in durability factor, meaning that even after 400 cycles; the material actually has a higher properties, than it did originally. This was not the case with specimens that did not incorporate the hydrophobic emulsions. Specimens with a lower w/cm maintained a relatively similar durability factor throughout cycling, but did not show an increase like the specimens with the emulsions did. The specimens with a higher w/cm ratio displayed contradictory results. It is clear that REF45 tested in fresh water is starting to degrade due to cycling, which was expected. However, the same specimen placed in salt water demonstrated a good resistance. The above results not only show the superior performance during freezing and thawing cycles of specimens with a lower w/cm ratio, but show the superior performance of specimens that incorporate hydrophobic emulsions.

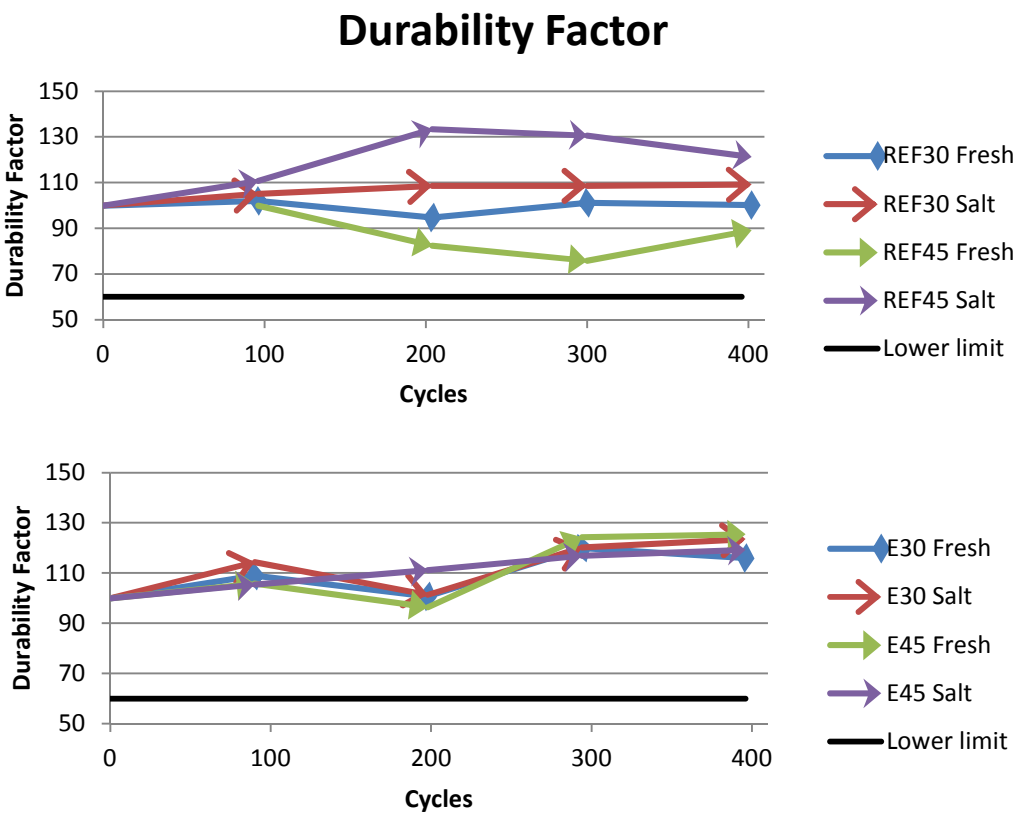

Figure 44: Durability Factor of SECC after Freezing and Thawing Cycles

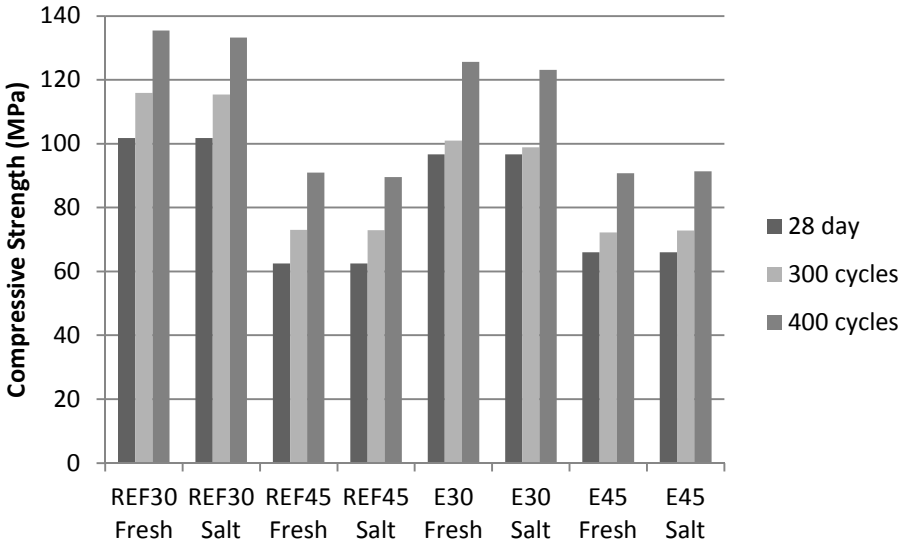

Figure 45: Compressive Strength of SECC after Freezing and Thawing Cycles

The compressive strengths of all the specimens subjected to freezing and thawing cycles displayed an improvement from their 28-day strengths. It was expected that specimens with a

higher w/cm ratio would display a drop in compressive after cycling. Additionally, the specimens that did not incorporate hydrophobic emulsions were expected to show a decrease in strength. This was not the case as seen in Figure 45. Results from other tests during freezing and thawing cycles showed similar results. There are no clear variations in any of the specimens with the exception of specimens with a lower w/cm ratio having higher strength and stiffness. The most probable cause of this is the addition of 5% silica fume. The silica fume was able to drastically improve the durability properties of all of the materials. If no silica fume had been used, the difference in deterioration between specimens with and without hydrophobic emulsions would have been clearer. However, there was significant surface scaling of the material with a higher w/cm ratio, without hydrophobic emulsions placed in salt water (Figure 46). The surface scaling of the same specimen with hydrophobic emulsions was less evident and almost negligible with the specimens with a lower w/cm ratio. It can visually be seen (Figure 46) that the addition of hydrophobic emulsions was able to reduce surface scaling of the material. The surface scaling would then lead to an accelerated erosion of materials, a further ingress of water, and would eventually lead to faster deterioration of the specimens. Based on these visual results, the addition of hydrophobic emulsions is beneficial to ECC. For Phase B testing, silica fume was not used so the benefits of hydrophobic or superhydrophobic emulsions can be determined.

Figure 46: Surface Scaling of ECC/SECC after Freezing and Thawing Cycles

5.2.4 Rapid Chloride Permeability

Rapid chloride permeability tests were performed in this study at 28 and 90 days. Results of this test are intended to give a representation of permeability of the material. At 28 days, all of the materials performed quite well with the specimens with a lower w/cm ratio performing the best. At 90 days, all of the specimens were considered to have very low permeability. Figure 47 below shows the results of rapid chloride permeability tests.

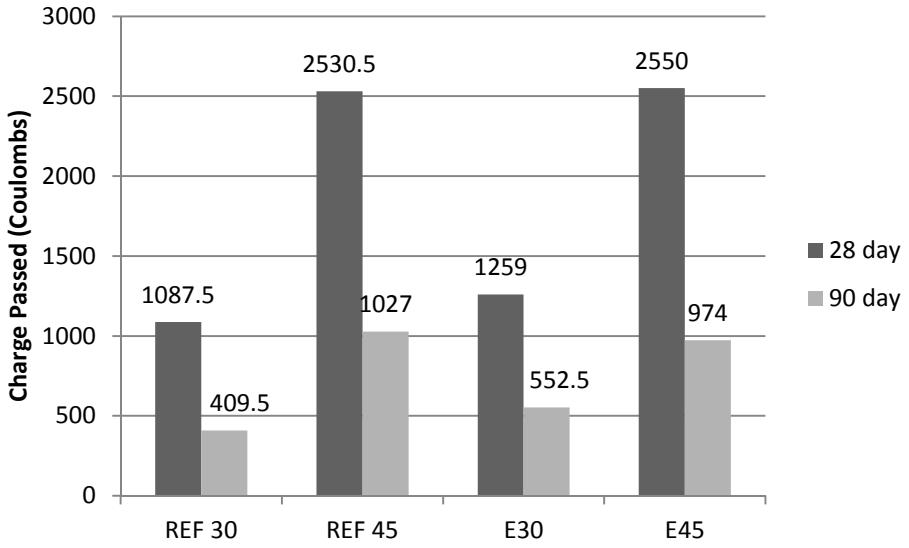

Figure 47: Rapid Chloride Permeability Tests of ECC/SECC

As can be seen in the above figure, the specimens with a lower w/cm ratio were able to reduce the charge passed by a half. These results demonstrate not only the improved durability of having a lower w/cm ratio but the impervious nature of the material. Moreover, the 90 day results displayed extremely low values showing that the addition of varying size SCM such as silica fume and ground granulated blast furnace slag improves the density of the material by improving the interfacial transition zone between cementitious materials and aggregates especially at a lower w/cm, thus reducing unneeded voids within the matrix. The specimens with hydrophobic emulsions tended to have slightly higher permeability. Since there are more air voids within the matrix, there is more opportunity for permeability. This is most likely due to the fact that this test is measuring the charge passed through the material and not the water passed through the material. Some reduction in permeability was observed at 90 days when the hydrophobic emulsions are used in higher w/cm (0.45) specimens.

5.3 Phase B: the Effect of Superhydrophobic Emulsions

5.3.1 Microstructural Analysis

Air Void Analysis

Based on the air void analysis of the specimens, the mortars produced with addition of hydrophobic agent (emulsion) had higher values of air content in the system (Table 15). Both references mortars (Ref 30 and Ref 45) had the same quantity of air content, while the specimens produced with the emulsions almost double the quantity of air. Higher value of air content in mortars with lower w/cm ratio was observed when the emulsion was used. The increase of the cementitious matrix volume in specimens produced with lower w/cm ratio may induce more complete reaction of the emulsion producing more air within the sample. On the other hand, an increase of the viscosity of the material due to the reduction of w/cm ratio (E 30) may hold more air within the sample.

Photographs of polished samples of SECC/ECC mortars are shown in Figure 48. Small cavities in the surface samples of approximately 70 µm were from PVA fibers. Orientation of the fibers was easily observed on the photographs due to the patterns they produce on the samples. In most of the surface analyzed during the test, fibers were well distributed when the w/cm ratio was lower. An increase of the viscosity of the material due to the reduction of the w/cm ratio may cause a better dispersion of the fibers within the specimens. Capillary voids and gel pores were not observed during the test due to the low magnification (50x) used, but entrained and entrapped air voids were clearly observed during the analysis. Most of the aggregate particles look transparent under the microscope and air voids were clearly observed because the edge of the voids produces a shadow. On specimens without an emulsion, voids were frequently observed close to each other (Figure 48, a).

Blue-green color of specimens was observed during the analysis due to the presence of slag in the specimens. The color is attributed to a reaction of sulfide sulfur in slag cement with other compounds in portland cement, but the color disappears with time due to the oxidation/carbonization. The degree and extent of the coloration depends on the rate of oxidation, the percentage of slag used, curing conditions, and the porosity of the concrete surfaces [5]. High w/cm ratios in concrete products increase the capillary voids and porosity in the material. The white areas were frequently observed on polished samples with higher w/cm ratio due to the oxidation of sulfur compounds, portlandite pockets, and also a higher porosity.

Table 15: Modified Point Count Parameters and Results ASTM C457

Parameters\Specimens	**Ref 30**	**E 30**	**Ref 45**	**E 45**
x, in	5	5.1	5.3	2.3
y, in	1.5	1.3	1.3	1.3
MAS, in	0.18	0.18	0.18	0.18
Traversed Area, in^2	7	7	7	7
Traversed Length, in	55	55	55	55
Total Points	1001	1003	1007	1005
w/cm ratio	0.30	0.30	0.45	0.45
Results				
Air, %	1.1	2.6	1.1	1.8
Paste, %	98.9	97.4	98.9	98.2

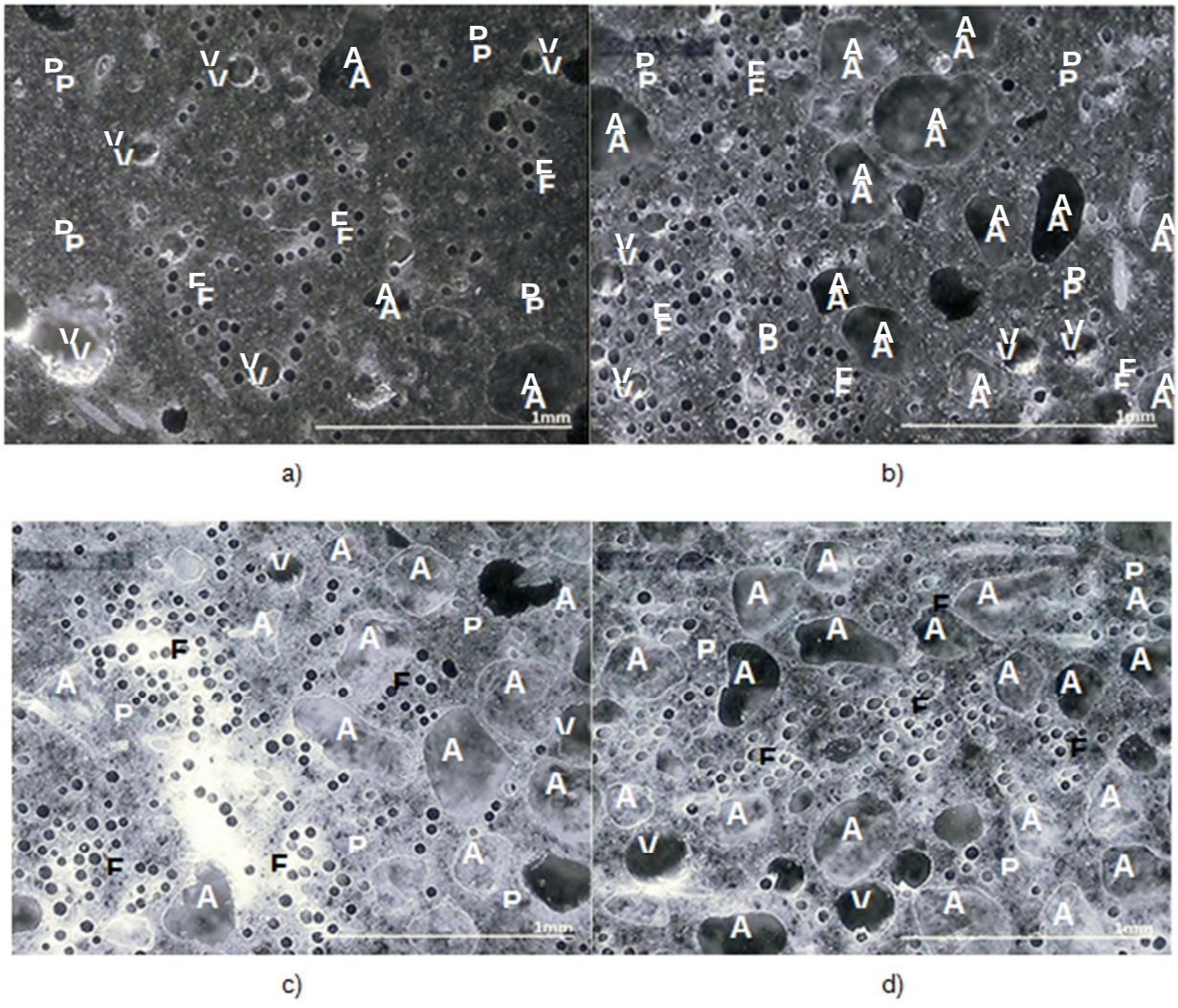

Figure 48: Photographs of Polished Surface of ECC Specimens: a) REF 30, b) E 30, c) REF 45, and d) E 45. Nomenclature - A: Aggregates, P: Paste, F: Fibers and V: Voids

5.3.2 Absorption and Rate of Absorption

Absorption values were determined by placing the samples in an oven to dry and then submerging the samples in water. Values for absorption show expected results. Samples with a lower w/cm ratio show a lower absorption (Figure 49). The other interesting data is that samples with superhydrophobic emulsions have lower absorption rates than those without. This means that the intent of created air voids that repel water tends to work. Because of the hydrophobicity of the voids, less water can enter the samples, resulting in less damage due to freezing and thawing. Additionally, if the voids are not completely saturated, no damage can occur upon freezing.

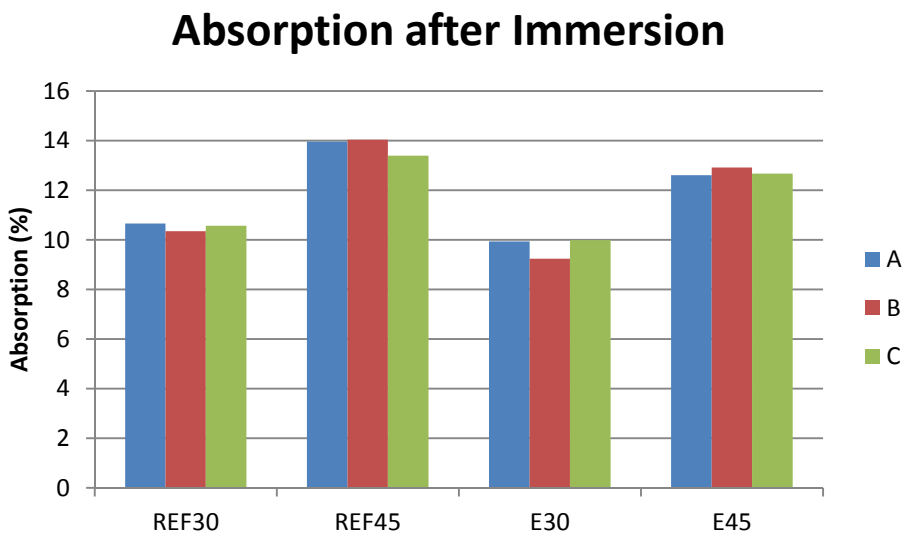

Figure 49: Absorption of ECC/SECC after Immersion in Water

Values for rate of absorption tend to show similar results. The low absorption rate (Figure 50) corresponds to a lesser total absorption (Figure 51) occurring in specimens with superhydrophobic emulsions. Again, this shows that the intent of the superhydrophobic emulsions to repel water and decrease the amount of water entering the voids is working.

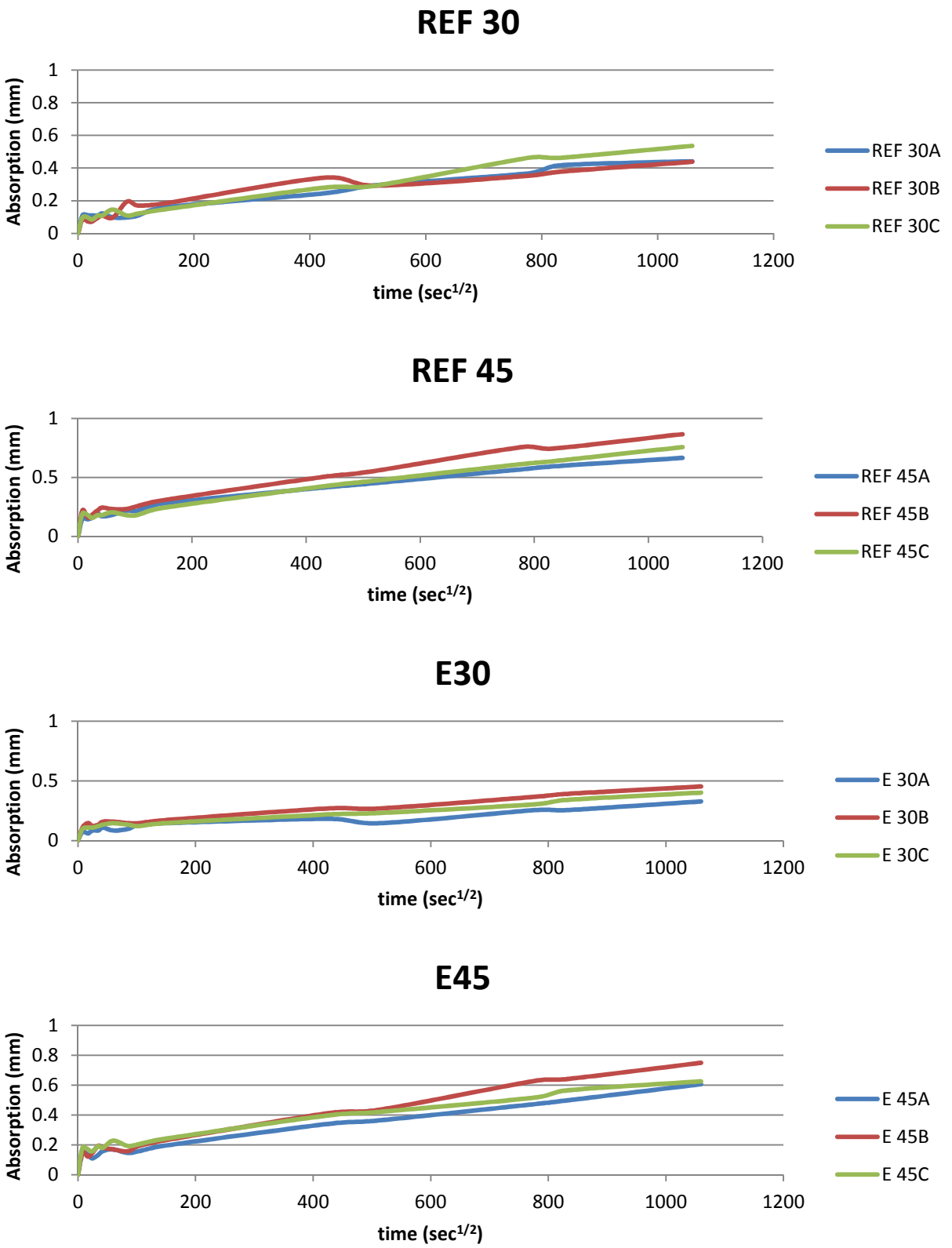

Figure 50: Rate of Absorption of ECC/SECC

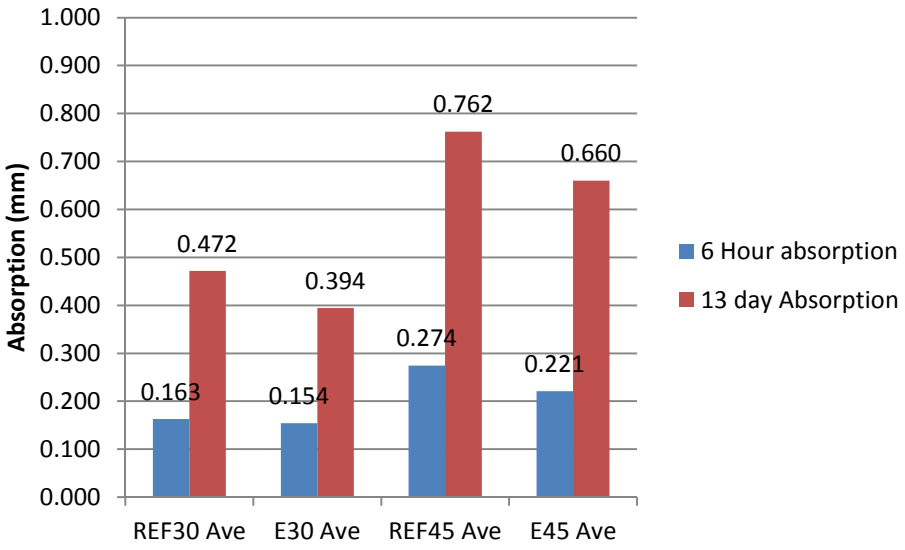

Figure 51: Total Absorption of ECC/SECC after 6 Hours and 13 Days

5.3.3 Freezing and Thawing Analysis

Results from freezing and thawing of SECC were performed with the same set of samples as in other studies in both fresh water and salt water (5% NaCl). Results clearly show that specimens with a lower w/cm ratio have a much better resistance to freezing and thawing. All of the samples with a lower w/cm ratio have survived through 700 cycles and are continuing to be tested while three of the samples at a lower w/cm ratio (E45 Fresh, REF45 Fresh, and REF 45 Salt) failed at 300 cycles, while testing of the other (E45 Salt) was stopped at 450 cycles due to excessive surface damage. Even though many of the results show that some of the specimens are still performing within a tolerable range, the surface appears to be quite damaged. This is especially evident with samples of higher w/cm ratio. This becomes even more evident with samples in salt water. Samples with a lower w/cm ratio show less surface deterioration with those in fresh water showing almost no deterioration even through 700 cycles. The photo below shows the surface deterioration throughout different cycling times.

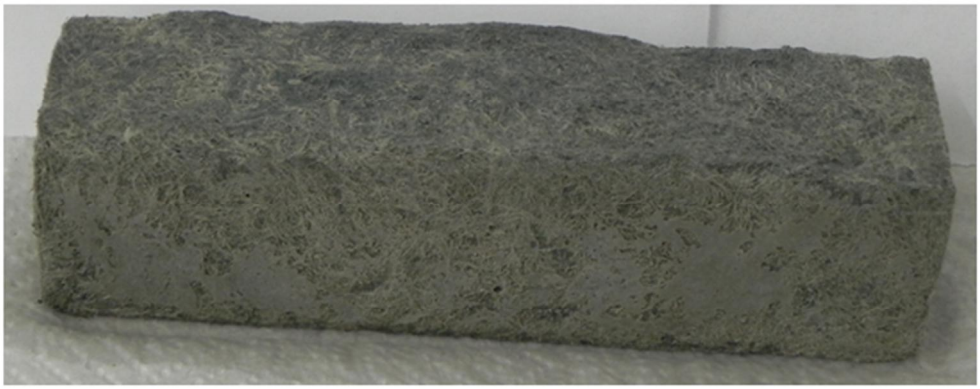

E30 Salt (500 cycles)

REF30 Salt (500 cycles)

REF45 Salt (only 250 cycles)

Figure 52: The Deterioration of the Surface of ECC/SECC after Freezing (-50°C) and Thawing cycles

Figure 52 through Figure 56 show the response of ECC/SECC during freezing and thawing cycling. As can be seen through the durability factor (Figure 53) and dynamic modulus of elasticity (Figure 55) the stiffness or integrity of the samples with a lower w/cm ratio have lower values and are decreasing at a faster rate. This again, shows the importance of lower w/cm ratio in cementitious materials to withstand freezing and thawing cycles. All samples with a lower w/cm ratio have shown great response through 700 cycles. There is little deviation between reference and samples with superhydrophobic emulsions. However, based on analysis from other durability studies, it is predicted that the samples at a lower w/cm ratio with superhydrophobic emulsions will perform well through even more freezing and thawing cycles.

There is some deviation between the samples tested in fresh water and salt water. It was assumed that specimens in fresh water would perform better than those in salt because of the harsher environment in the salt. The surface damage seen in the specimens with salt would allow for greater ingress of water into the specimens and thus more significant damage. This cannot be seen based on the data presented below. The most probable cause of this is most likely salt water is crystallizing within the samples and actually increasing dynamic response. This occurs since there is more water entering the sample, more salt can get in. Even though numerical results are showing that the dynamic response may be better, it is most likely due to the extra stiffness created by the crystallization of the salt.

Length and cross-sectional areas of the samples demonstrated consistent results as dynamic tests as well. Sample with a higher w/cm ratio are deteriorating at a faster rate than those with a lower w/cm ratio. Again, there is a little deviation between the reference and samples with emulsions.

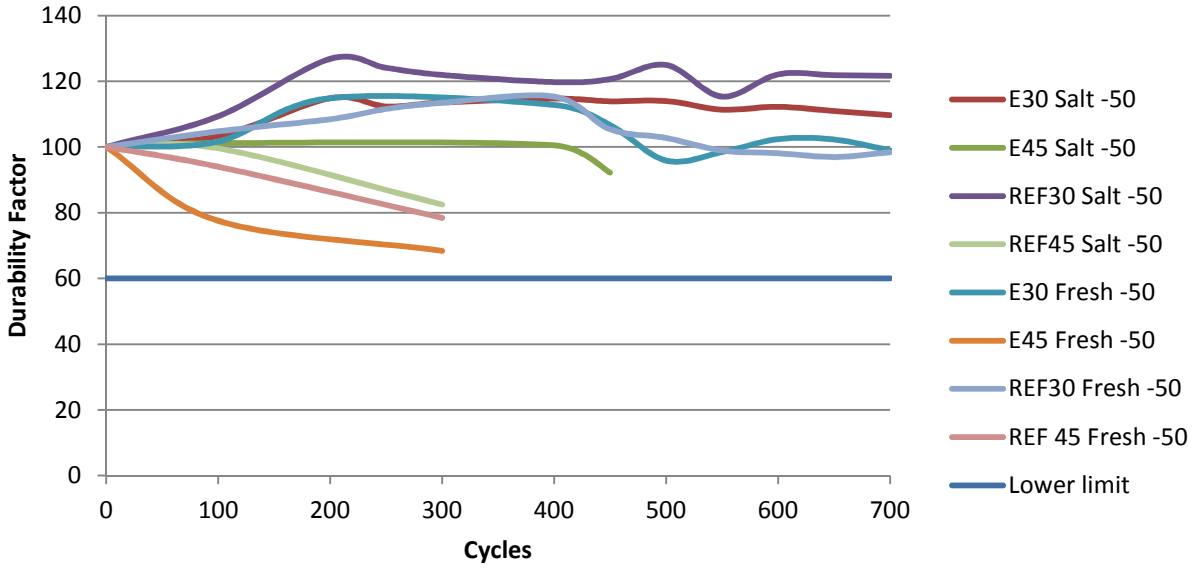

Figure 53: Durability Factor of ECC/SECC

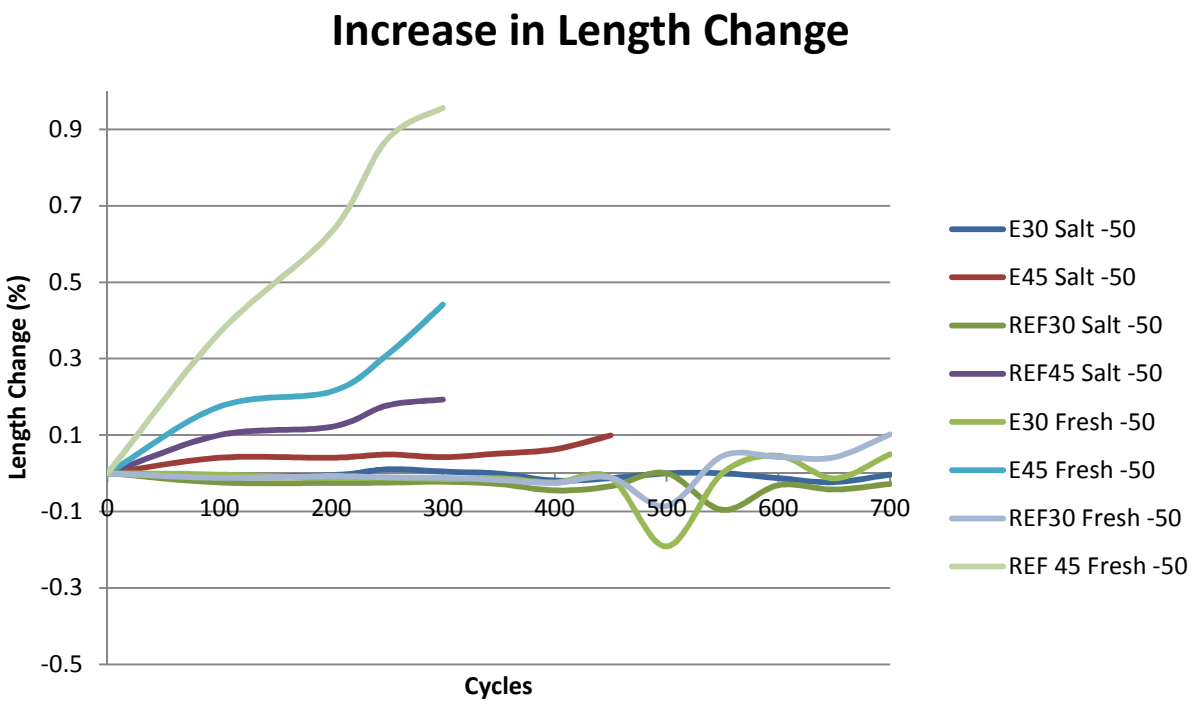

Figure 54: Increase in Length of ECC/SECC during Freezing and Thawing Cycles

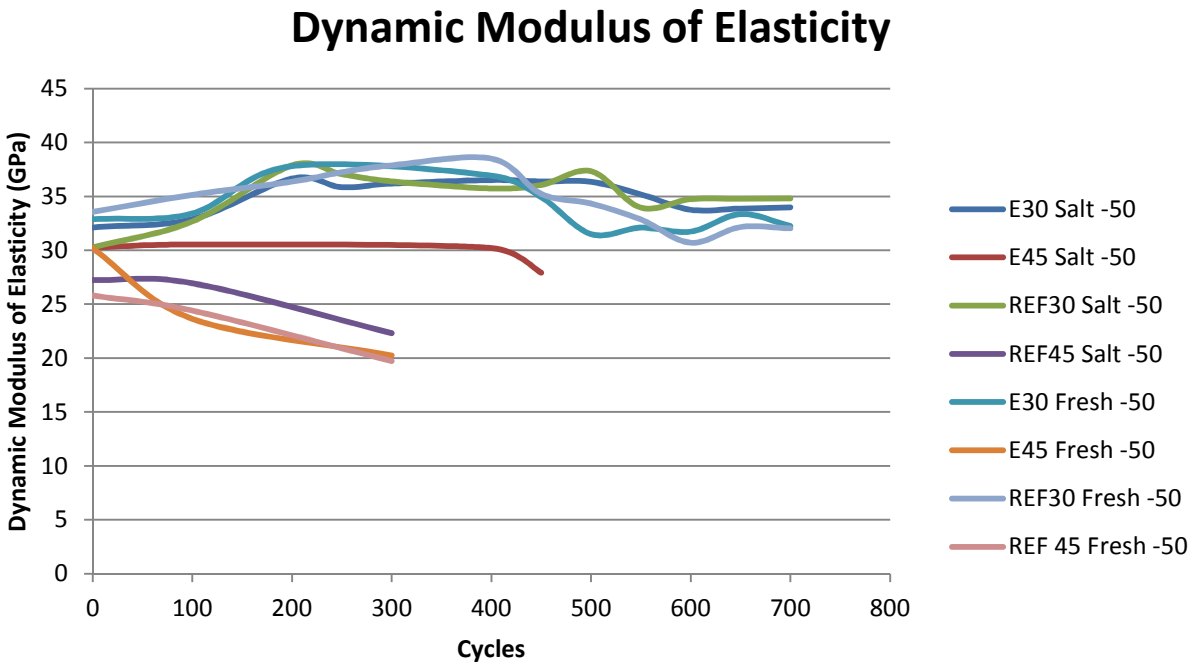

Figure 55: Dynamic Modulus of Elasticity of ECC/SECC during Freezing and Thawing Cycles

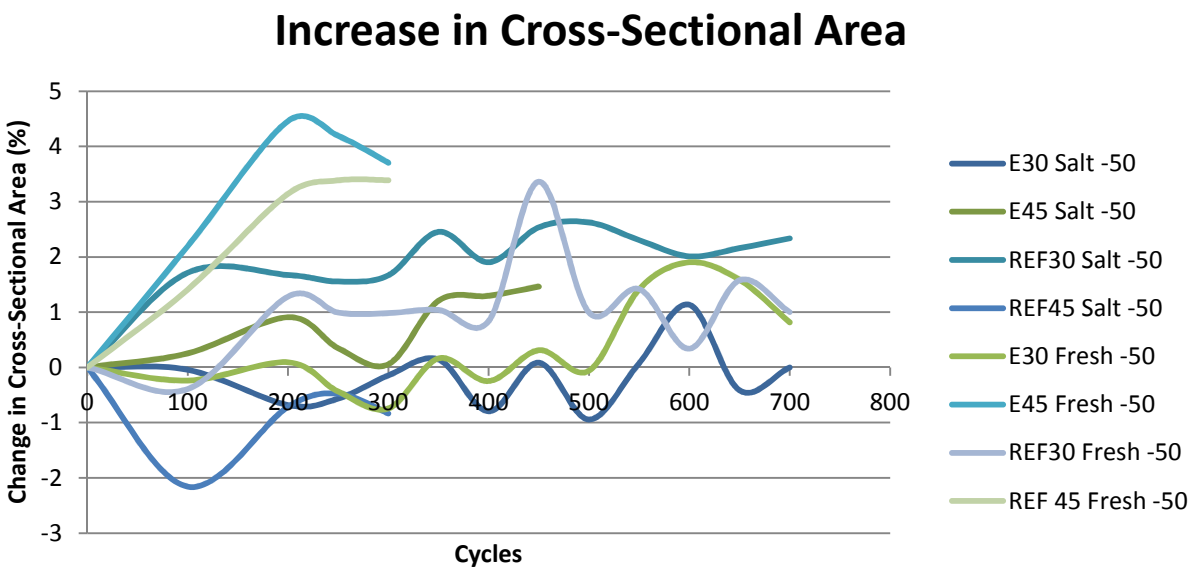

Figure 56: Increase in Cross-Section Area of ECC/SECC during Freezing and Thawing Cycles

5.3.4 Rapid Chloride Permeability

Results from 28-day rapid chloride permeability tests in samples with hydrophobic emulsions displayed results similar to those in Phase A study. Specimens with a lower w/cm ratio have a significantly lower permeability ratio. However, previously, when only hydrophobic emulsions were being considered, specimens with a lower w/cm ratio and emulsions tended to have a higher chloride permeability. Samples with the emulsions incorporating nano-particles to increase the hydrophobicity (as used in this study) actually provided lower chloride permeability values then reference specimens. These results are still interesting because rapid chloride permeability is not a true value of chloride permeability of the sample but displays the electrical resistance (which is correlated to chloride ion penetration). In the Phase A study, it was thought since there were more air voids in E30 then REF 30, it was logical that values for rapid chloride permeability would be higher. However, now that they are lower with what is expected to be a better emulsion, may be attributed to a few things. First, the air voids with the newer emulsions are intended to be smaller meaning that the smaller air voids are less conducive for chloride ion penetration. Next, the emulsions with higher hydrophobicity (reaching over-hydrophobic, $\theta > 120°$ and superhydrophobic, $\theta > 150°$ state) may hinder the mobility of chloride ions and so reduce the penetration. This could occur since the emulsions are made with different materials and were tuned for the increased hydrophobicity which lowers the permeability. Despite this, it would take further analysis, chemical tests and finite element analysis to determine the actual reasons why rapid chloride permeability values are different between these two studies. There is actually little difference between the values, but large difference between lower and higher w/cm ratios showing the importance of using a low w/cm ratio in ECC/SECC.

Table 16: Permeability Values of ECC/SECC

MIX ID	Permeability (Coulombs)			Permeability Class
	A	B	Ave	
E30	1717	1354	1535.5	Low
E45	3101	2593	2847	Moderate
REF30	1785	1575	1680	Low
REF45	4561	4363	4462	High

5.3.5 Abrasion Resistance

Results from abrasion resistance testing show that samples with a lower w/cm ratio tend to perform better under abrasion testing. This is due to the fact that these samples tend to have a better strength and particle/fiber bond to matrix and thus have fewer flaws on the surface that would get sheared off during the abrasion testing. The Figure 57 below shows the mass that was lost during the abrasion testing.

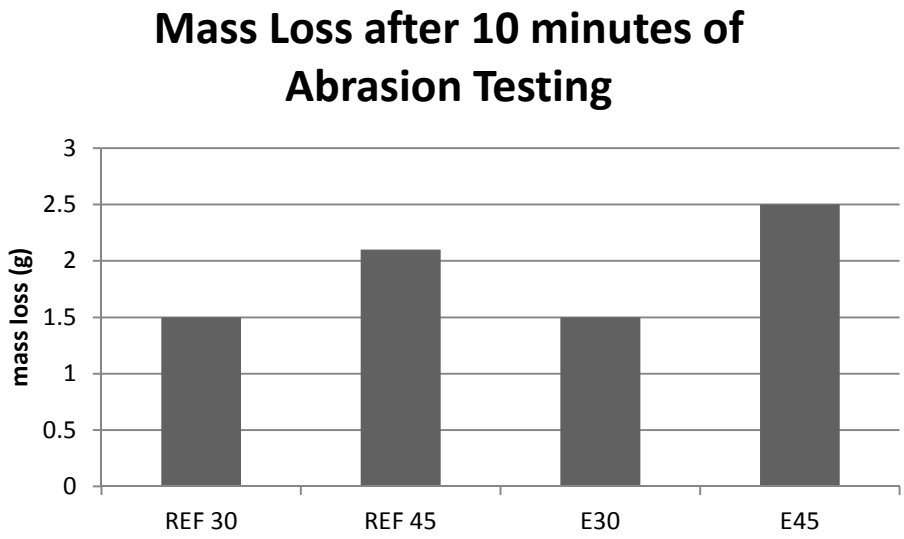

Figure 57: Mass Lost after Abrasion Testing of ECC/SECC

Even though the above results may not be considered to be definite because of the lack of repetition in trials, it can be used as an indication of how ECC/SECC would resist the abrasion from traffic.

6. Large Scale Experiment

6.1 Scope of Work

This study was primarily focused on getting a ductile workable mix as recommended after previous studies done at UW-Milwaukee and UW-Madison [17]. Parameters like material proportions, curing time, and mixing procedure were varied to meet the objectives of the project.

The beam dimensions were limited to small-scale 1 x 3 x 15-in beams and these beams were tested to failure in bending at a deflection controlled rate of 0.039 in/min. Mixing of the material was done using paint mixer in a bucket and in a planetary mixer.

Superplasticizer quantity, water/cement ratio and the fiber content were varied throughout the course of study. Ratios of sand and the binder material were kept the same as used in a mix designated as M45 [43]. Quasi-static loading was used for the purposes of this study and no cyclic loading was applied to the specimens.

The structural characteristics were determined by examining mid-span deflections and the load on small-scale beams. It was assumed that the mid-span deflection under simple loading could also represent the rotation capacity achievable at the end of an approach slab.

Although ASTM procedures were studied and often followed as closely as possible, some deviation was necessary. Testing of compression cylinders conformed to ASTM C873. All flexural tests generally followed ASTM C1609 (Standard Test Method for Flexural Performance of Fiber- Reinforced Concrete) with some modifications.

6.2 M45 Mix Design

The M45 ECC mix was designed and tested by researchers at the University of Michigan [43]. Mix proportions of this design can be found in Table 17**.** The volume fraction of fiber is 2%. ASTM Type I portland cement and low calcium ASTM class F fly ash were used in this research. Large aggregates were excluded from ECC mix design, and only fine sand was incorporated. The silica sand used here had a maximum grain size of 250 μm and an average size of 110 μm. The PVA fiber had a diameter of 39 μm, a length of 12 mm, and overall Young's modulus of 25.8 MPa. The apparent fiber strength when embedded in cementitious matrix was 900 MPa. The fiber surface was treated with oil coating to reduce the interface bond and the oiling content is 1.2% [43].

Table 17: PVA-ECC Mixture Proportioning (kg/m^3)

MIX ID	Cement	Sand	Fly ash	Water	Superplasticizer	PVA Fiber
M45	583	467	700	298	19	26

Two approaches were adopted to reduce the excessive interface bond. On the fiber aspect, surface coating by oil was investigated. With increase of oiling content, both frictional stress and interface fracture energy decrease significantly. On the matrix aspect, fly ash was introduced. A high volume fraction of fly ash tends to reduce both the interface bond and matrix toughness. Additionally, fly ash improves mixture workability and material sustainability. However, high content of fly ash leads to slower strength development at early ages. It was found that a fly ash to cement ratio of 1.2 provided best overall performance [43], and this proportion was used in this study.

6.2.1 Tensile Behavior of M45 Mix [43]

Tensile behavior was measured by direct uniaxial tension tests. The coupon specimen measured 304.8 x 76.2 x 12.7 mm. Deformation was recorded with a gage length of 180 mm. Figure 58 (left) shows the development of tensile strain capacity over age. The strain capacity at 24 hours after casting is about 2.3% [43]. At early age, the strain capacity increases with time and reaches above 4% after 7 days, and later it decreases and then plateaus after about 30 days [43]. The change in strain capacity reflects the evolutions of matrix toughness and interfacial bond properties. Figure 58 (right) presents the typical tensile stress-strain curves after 24 hours and 90 days, where the tensile strength increases from 3.0 to 5.4 MPa [43].

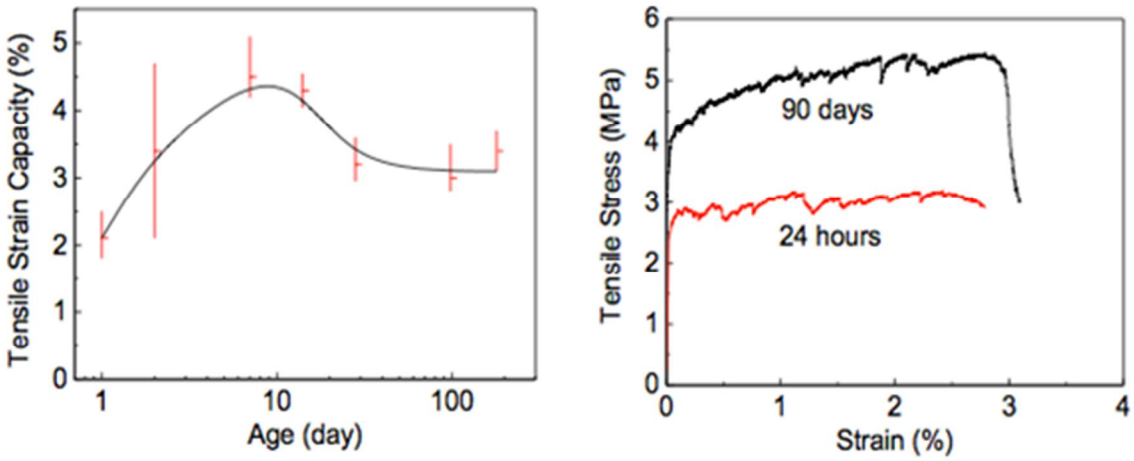

Figure 58: Age dependancy of tensile strain capacity (left) and typical tensile stress-strain curve at 24 hrs and 90 days (right) [43]

6.2.2 Flexural Behavior of M45 Mix [43]

Flexural response of the M45 material was measured by a four point bending test [43]. Figure 59 shows the typical flexural responses at 24 hours and 90 days. Significant deflection hardening can be seen and the corresponding flexural strength is 11 and 16 MPa, respectively [43]. Figure 60 shows the cracking pattern of the tensile face at the constant moment section (90 days), and the average crack spacing is below 1.5 mm [43].

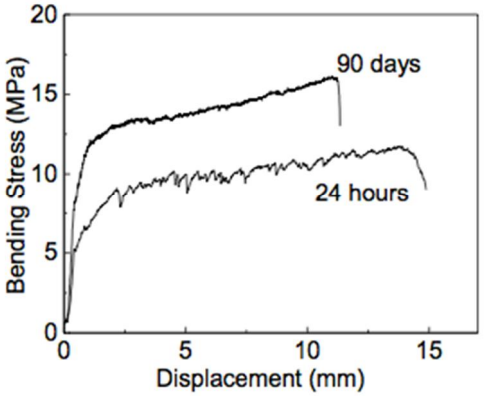

Figure 59: Flexural Behavior of PVA-ECC [43]

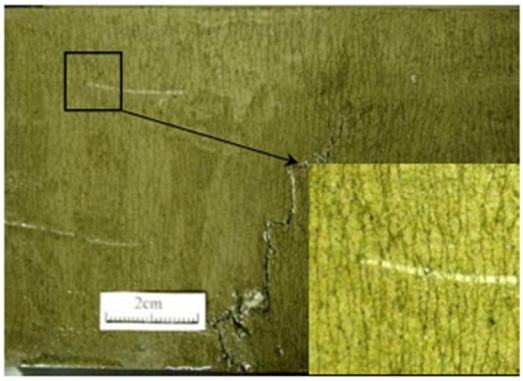

Figure 60: Multiple Cracking Pattern under Bending [43]

6.3 Mix Design, Procedure and Test Setups

6.3.1 Base Mix Design

The preliminary mix of the best performance is shown in Table 18. It was recommended making the mix more workable due to the problems with low workability and uniformity developed during mixing when a large mixer was used in order to cast 3 x 5 x 36 in beams [17]. This study was primarily focused on getting a workable mix for pilot application while keeping the bending performance ductile and getting widespread small flexural cracking.

This mix Table 18 was used as the base mix design and additional modifications were tested to attempt to improve the workability and bending performance.

Table 18: ECC Mixture Proportioning

Mix	Fly ash	Sand	Water	Superplasticizer	Fiber	w/cm
	fa/c	s/c	w/c		%	w/(c+fa)
Preliminary Mix [6]	1.2	0.8	0.53	6.07 oz/100 lb concrete	2.0	0.24
Michigan M45 mix	1.2	0.8	0.51	1.4 (% of binder content)	2.0	0.23

- M45 used sand size of 110 μm and ADVACAST 530 as superplasticizer, whereas, preliminary mix in this study used sand of 177 μm and ADVACAST 575 as superplasticizer.

6.3.2 Trial Mixes Objective

As mentioned, the objectives for the trial mixes were to come up with a mix design that provides workable consistency, and flexural performance that is ductile and shows a multiple small cracking pattern. In order to achieve these goals, several parameters were varied in different test batches. First, water/cement ratio, superplasticizer content and fiber quantity were varied to get the desired objectives. Secondly, different mixing procedures were tried in order to get the most efficient mix procedure. Ductility was measured by observing the cracking pattern, midspan deflection, and load obtained in small flexural test specimens. Once an acceptable ECC mix was achieved under these criterions, flexural specimens of larger size were tested.

6.3.3 Materials

The materials for the chosen ECC mix at the University of Wisconsin-Madison are as follows: Type I ordinary portland cement (OPC) (Lafarge), ASTM Class F fly ash (Headwaters Shufer Station, Illinois), a fine grained sand with an average grain size of 177 μm (US Silica F-80), PVA fiber (Kuraray RECS15x8 mm) [17] , and superplasticizer (MEGAPOL 40 DF from Handy Chemicals). It is to be noted that M45 mix used RECS 15x12 mm fibers. For this study RECS 15x8 mm PVA fibers were used

The change in the fiber length might affect the flexural test results and the specimens may be deformed less due to the better chance of pullout with 8 mm fibers as compared to 12 mm. Adding an oiling agent to the fibers should shift the failure mode from modified Griffith cracking to the steady-state cracking. The fibers chosen for this project (Kuraray fibers) were already pre-coated with an oiling agent at 1.2% of the fiber volume [43] to account for this factor.

6.3.4 Tested Mix Proportions

A total of 19 batches were tested with different mix proportions and mixing procedures. Table 19 shows all the mix proportions used during the course of this study and the M45 mix [43].

Table 19: Trial Mixes for 1 x 3 x 15 in Beams

Mix designation	Fly ash fa/c	Sand s/c	Water w/c	Superplasticizer % wt. of Binder content	Fiber % of Binder content	w/cm w/(c+fa)
Base	1.2	0.8	0.53	6.07 oz/100 lb of concrete	2.0	0.24
Mix 0	1.2	0.8	0.55	6.07 oz/100 lb of concrete	2.0	0.25
Mix 1	1.2	0.8	0.57	0.8	2.0	0.26
Mix 2	1.2	0.8	0.57	0.8	2.2	0.26
Mix 3	1.2	0.8	0.57	0.8	2.4	0.26
Mix 4	1.2	0.8	0.57	0.9	2.2	0.26
Mix 5	1.2	0.8	0.59	0.9	2.2	0.27
Mix 6	1.2	0.8	0.59	0.9	2.2	0.27
Mix 7, 8, 9	1.2	0.8	0.57	0.9	2.2	0.26
Mix 10, 11	1.2	0.8	0.57	0.9	2.2	0.26
Mix 12, 13, 14, 15, 16, 17	1.2	0.8	0.57	0.9	2.2	0.26
M45 mix	1.2	0.8	0.51	1.4	2.0	0.23

Legend of values in tables:

fa/c = weight of fly ash/weight of cement
s/c = weight of sand/weight of cement
w/c = weight of water/weight of cement
w/cm = weight of water/weight of cementitious materials (portland cement and fly ash)

6.3.5 Flexural Test Setup

Four point loading tests were used to examine the flexural behavior of the beams. The tests were performed three days after the being cast. Specimens were covered with plastic sheets and the curing occurred at room temperature for 3 days. Specimens were tested to failure at 3 days and the peak load and maximum mid span displacement were noted. The tests were done on the Sintech machine as shown in Figure 61 and Figure 62**.** The loading was deflection controlled and was applied at a rate of 0.039 in/min. A mechanical deflection gauge was used to measure the mid span deflections relative to machine platen. Bearing pads were used at the places where loading was applied in order to distribute the load uniformly and avoid stress concentrations.

Figure 61: Sintech Machine for Flexural Testing

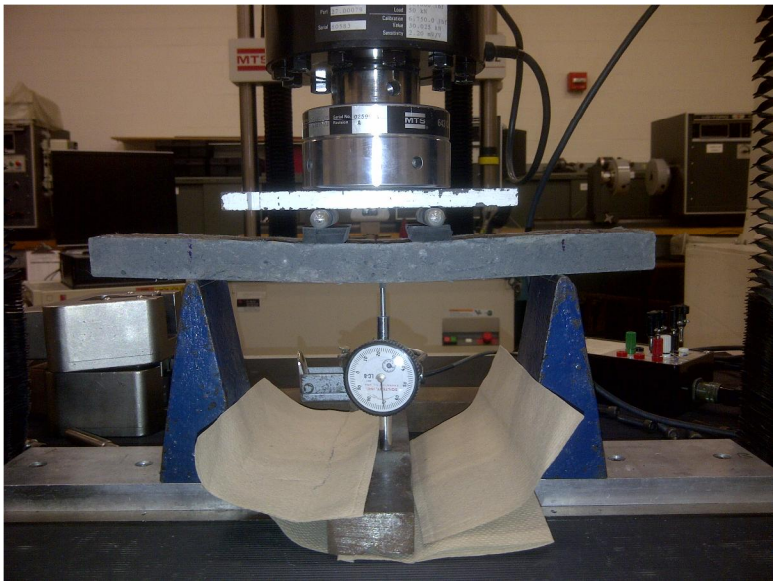

Figure 62: Flexural Test Setup

6.3.6 Mix Procedure and Workability

Mixing order was varied throughout the study to get the best possible procedure for large batches. Different types of formworks were used for the flexural test specimens and they are shown in Figure 63**.**

a) Vertical wooden forms

b) Vertical high-density polyethylene (HDPE) forms

c) Horizontal wooden forms

d) Vertical HDPE forms

Figure 63: Different Formworks used for 1 x 3 x 15 in Beams

The workability of the base mixtures (Base/Mix 0) with w/cm of 0.24 to 0.25 was poor as lumps were formed when placed; therefore theses mixture were not tested for flexure.

The w/c ratio was then increased to 0.26 and the superplasticizer content was increased to 0.8% by weight of the binder content. The mix procedure was altered and the mixture provided better workability. The mix procedure was as follow:

- Cement, sand, and fly ash were all mixed together dry in a small bucket using a paint mixer (Figure 64);
- Once it was a uniform dry mix, water was added to the mix and the paint mixer was used for mixing;
- Fibers were slowly added to the mix and it was mixed using the paint mixer until the fibers were uniformly distributed throughout the mix;
- Fresh material was then placed in horizontal wooden frames.

Figure 64: Mixing of ECC using a Paint Mixer

Beginning with Mix 2, the fiber content was increased to 2.2% from 2.0%. The fresh material was tested for workability using a standard mortar flow test apparatus (Figure 65)

Figure 65: Mortar Flow Table

The fiber content was even further increased for Mix 3 to 2.4%. This mixture displayed poor workability as lumps of fibers were forming. Due to this reason, flexural tests were not performed on this mixture. Mix 4 used a fiber content of 2.2% while the superplasticizer content was increased to 0.9% by weight of the cementitious material. The workability of this mix was not satisfactory, so the w/c content was increased to 0.27 for Mix 5. This provided a better workability, but segregation of the mixture occurred and the flexural response was with a single crack instead of the desirable multiple cracking as seen in Figure 66 below.

Figure 66: Single Crack Failure

To account for this the mixing procedure for Mix 6 was altered as follows:

- Cement and sand were mixed in a small drum using paint mixer;
- Water was added and mixed using the paint mixer;
- Fibers were slowly added to the batch and hand mixing was used;
- Finally, the mix was poured into a standard Hobart mixer and fly ash was added (Figure 67).

Figure 67: Standard Hobart Mixer used for Preparation of ECC

Workability of the previous mixture was not satisfactory, as a dry mix prevented proper compaction. Adding fly ash at the end proved to be detrimental; therefore it was decided to add portland cement at the end in place of the fly ash for mixtures 7, 8, and 9. Flexural results from these tests were however not satisfactory. It is assumed that this can be attributed to a poorly finished top surface (Figure 68) of the beams as the cracks were propagating from the defects on the unfinished surface.

Figure 68: Rough Loading Surface from Horizontally Placed Molds

To improve the surface finishing, mixes 10 and 11 were cast in vertical HDPE molds (Figure 63b). Since the molds were vertical, there was only a 1-in gap to fill the material. This made compaction difficult and posed difficulty for entrapped air to escape as finished beams displayed surface air voids. This resulted in crack propagation during testing (Figure 69). In an attempt to allow the entrapped air to escape during compaction, a vibrating table was used while pouring Mix 11.

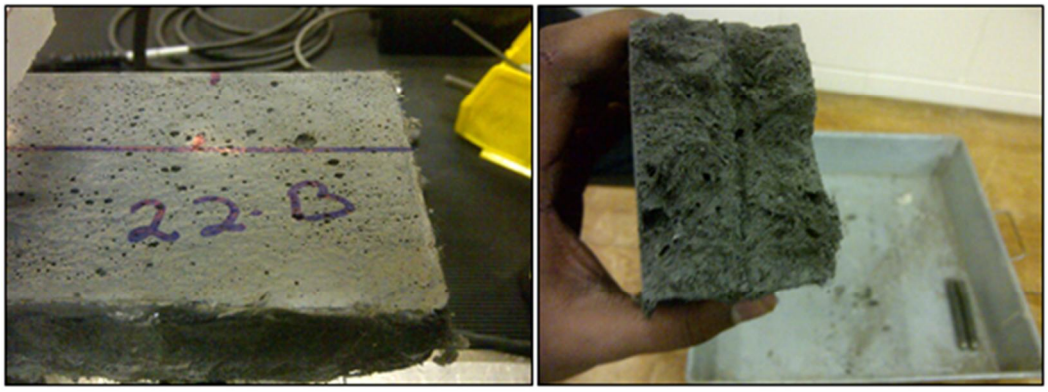

Figure 69: Surface Air Voids from Vertically Placed HDPE Molds

The use of the vertical molds did not provide an adequate compaction for ECC, therefore it was determined that horizontal HDPE molds should be used. A vibrating table was used while placing ECC in the horizontal HDPE molds as well. This procedure was used for the remaining mixtures (Mix 12-17).

6.4 Data Results and Analysis

6.4.1 Failure Criteria for Tests

The ECC beams do not normally show a brittle failure mechanism, therefore it is harder to detect. Three conditions were considered when evaluating the performance of the beams. First, the formation of large cracks (>0.05 in.) were considered. Next, the peak load resisted by the

beam. Finally, the ability of the beam to continue to deform after reaching peak the load were considered. The first two conditions were easy to define, the third is somewhat arbitrary to define and measure. The third condition, denoted as “failure” of each beam, was defined as the condition when the load capacity decreases 20% from the measured the peak load [17].

6.4.2 Load vs. Deflection of Trial Mixes

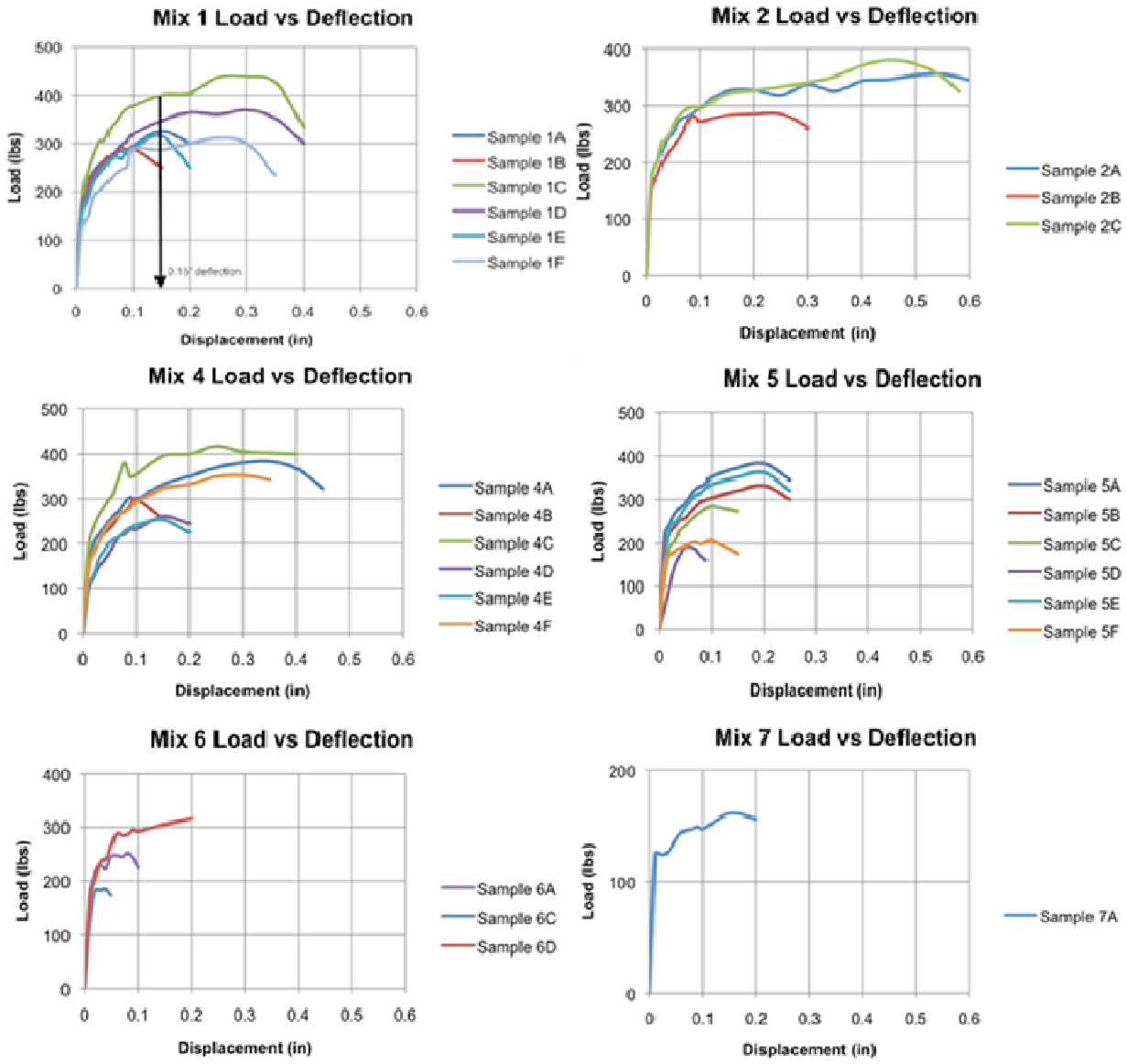

Figure 70: Load vs. Deflection Curves for Mixtures 1-7

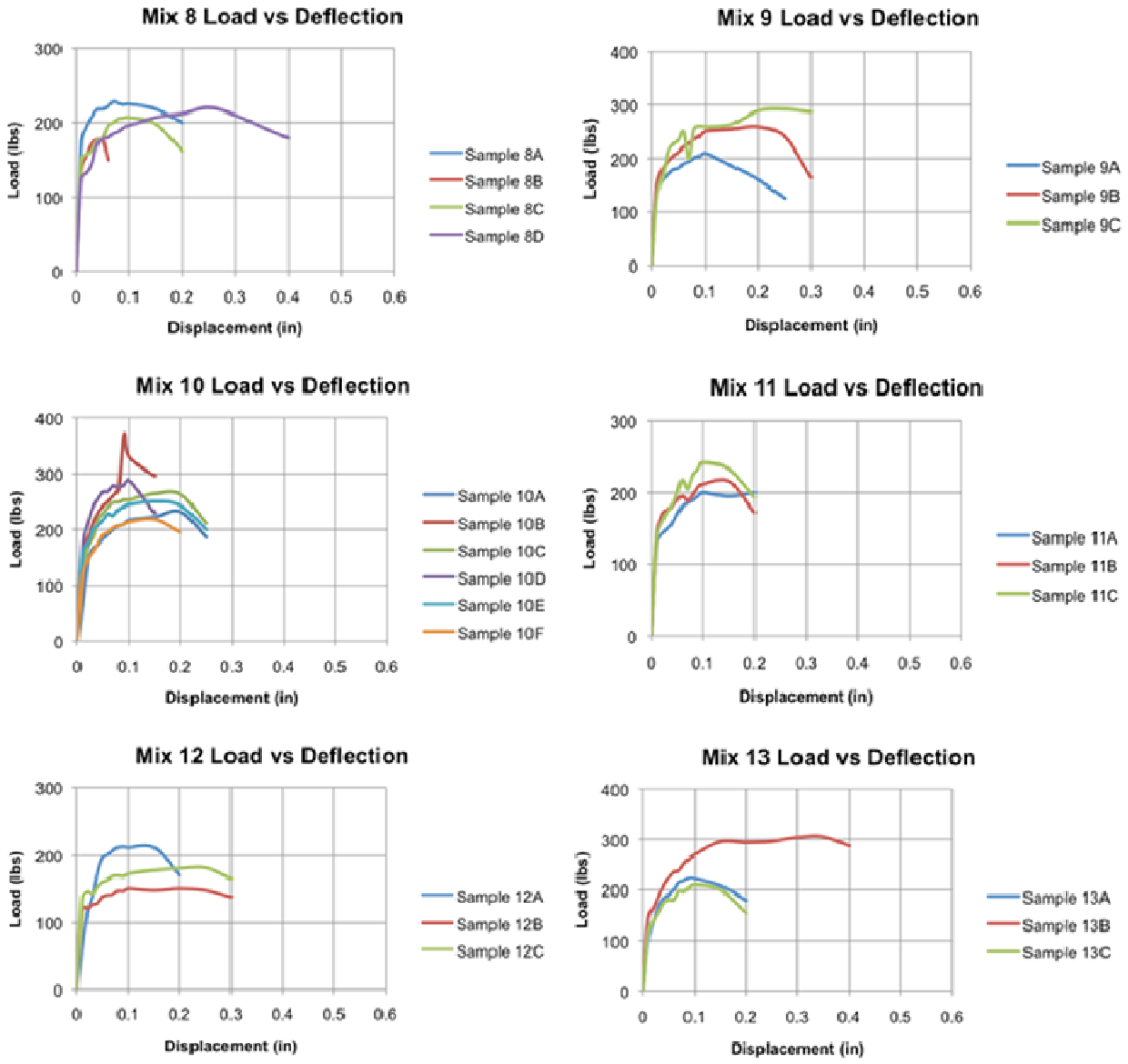

Figure 71: Load vs. Deflection Curves for Mixtures 8-13

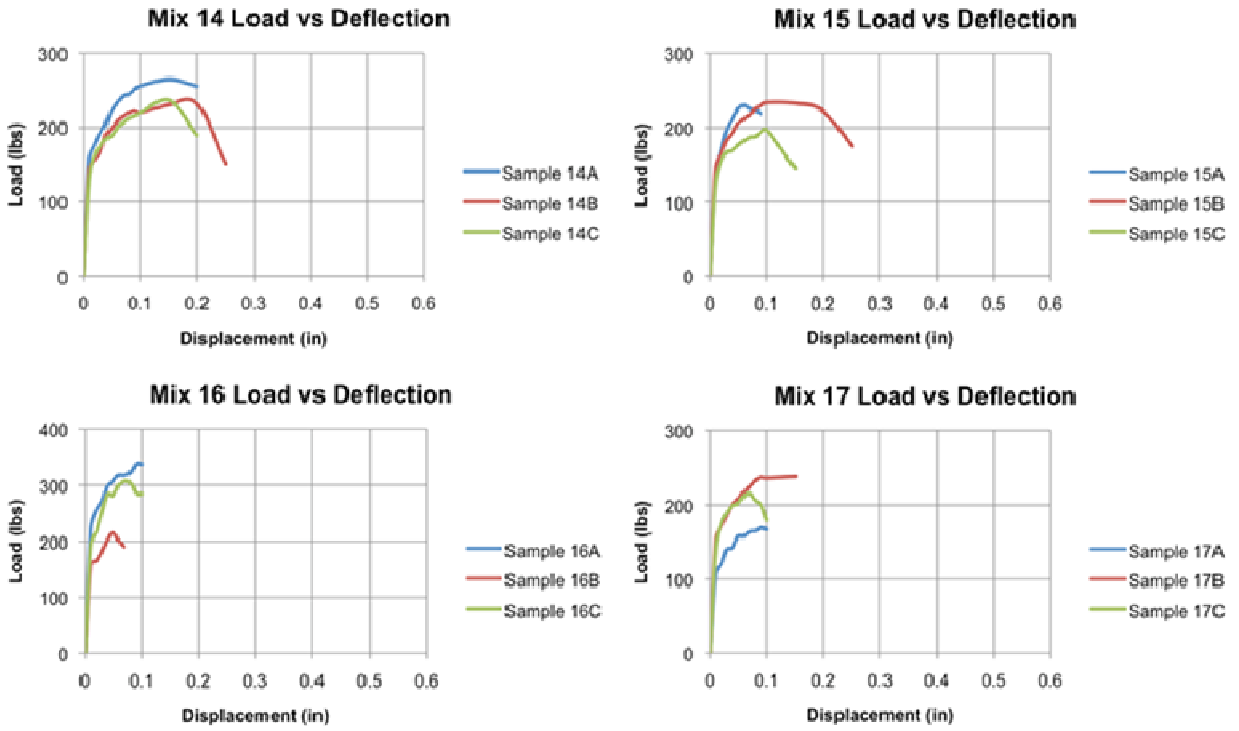

Figure 72: Load vs. Deflection Curves for Mixtures 14-17

Table 20: Summary of Loads and Deflections for all Mixtures

Mix	Max. Peak Load, lbs	Average Peak load, lbs	Max. Deflection, in	Average Deflection, in	Mortar Flow, in
Mix 1	439	335	0.4	0.28	6.0
Mix 2	380	340	0.6	0.49	5.5
Mix 3	-	-	-	-	4.0
Mix 4	383	328	0.4	0.29	5.5
Mix 5	372	293	0.25	0.19	6.5
Mix 6	315	250	0.2	0.09	5.5
Mix 7, 8, 9	292	208	0.4	0.23	7.5
Mix 10, 11	288	245	0.25	0.20	7.5
Mix 12, 13, 14, 15, 16, 17	307	231	0.4	0.20	7.5

The load deflection curves for all mixtures can be seen in Figure 70, Figure 71, and Figure 72 above. A summary of the loads and deflections can also be seen in the Table 20 above. In mix 1 there was a large variation in the deformation and strength of the beams which could be attributed to a non-uniform distribution of fibers throughout the mix. In mix 2, when the fiber volume was increased, the deformability of the specimens increased by 33% and the average peak load increased by 1.5%. The variations of load and deflection were much less in this mixture as compared with mix 1. All of the beams within this study failed due to formation of

large cracks. In mix 4 when an additional quantities of superplasticizer were added, the beams again failed due to the formation of large cracks spaced approximately 0.2 – 0.3 in apart. Again there were some variations among samples which could be attributed to non-uniformity of fiber spacing. In mix 5, four out of the six beams failed without any steady-state cracking while one large crack caused failure. The same failure pattern occurred for mix 6 while mixes 7-9 had fewer samples failing due to the formation of one large crack. This could be attributed to change in mixing procedure for these mixtures. For mixes 10 and 11, seven out of nine specimens were able to sustain 80% of the peak load without forming a big crack. The other two specimens failed by the formation of a large crack. The specimens provided fairly consistent results in terms of variability of strength. Vertical forms appeared to be reducing the variability in results. However, a steady state cracking pattern was not achieved and 2-3 small cracks (approx. 1-1.5 in apart) formed in all the specimens before failure because of the entrapped air voids not being able to escape during compaction. Finally, when horizontal HDPE molds were used, mixes 12-17 provided satisfactory results as a steady state cracking patterns were achieved. The cracks were approximately 0.2-0.5 in apart and most specimens formed 6-10 small cracks in the loading region. Figure 73 shows a beam tested that showed multiple small cracking patterns. These results display that the selected procedure creates ECC capable of forming multiple cracks.

Figure 73: Steady-State Cracking Pattern of ECC

7. Conclusions and Recommendations

There is no doubt that engineered cementitious composites (ECC) with PVA fibers can be designed as a durable material. However, past research on the material has been performed in a way to reduce the toughness of the matrix to improve ductility. Work within this research demonstrates the ability of superhydrophobic engineered cementitious composites (SECC) to create a ductile material while still maintaining high strengths and a very dense structure. The addition of hydrophobic/superhydrophobic admixtures not only creates a less permeable

material with water resistant air voids, but also creates artificial flaws that lead to multi-cracking behavior and enhanced strain-hardening ability.

Using an experimental matrix considering fibers with three different sizes at varying volumes (2.0, 2.25, 2.5, 2.75, and 3.0%), the optimal fiber type was larger (RECS 15x12 mm) PVA fibers used at a 2.75% volume.

The addition of supplementary cementitious materials (SCM) can lead to a more environmentally friendly composite by lessening the burden from cement production. This research demonstrated that the use of 5% silica fume and 45% granulated blast furnace slag creates SECC with an extremely durable matrix. These SCMs can, therefore, be used in SECC intended to last 120 or more years.

The addition of hydrophobic emulsion (0.25 g/L, single dose) to SECC mixtures resulted in an improved flexural behavior with only the slightest decrease in compressive strength due to formation of beneficial air-void structure. However, the compressive strength of this material would have dropped even more drastically if conventional air entraining admixtures had been used. The fact that these hydrophobic emulsions are capable of creating a controlled air void structure with smaller, better spaced voids contributes to this improved behavior. The addition of hydrophobic emulsions demonstrated the improvement in flexural behavior in all specimens presented within this research. Moreover, the addition of these hydrophobic emulsions demonstrated improved resistance to freezing and thawing.

When micro particles were added to the hydrophobic emulsion, the hydrophobic performance of the material was significantly improved. Even though by definition the treated concrete surfaces cannot reach the superhydrophobicity benchmark (contact angle greater than 150°), the improvement of contact angle when micro- and nano- particles were added to the admixture provided a good development towards superhydrophobicity.

Even though data shows that ECC, especially based on blended systems with SCM (5% silica fume, SF and 45% ground granulated blast furnace slag, BFS), performed extremely well through durability testing without any intentionally added air, it is a safe assumption that over the course of the intended lifespan (120 or more years), SF-BFS specimens that incorporate the hydrophobic/superhydrophobic admixtures will perform better. The addition of 5% silica fume and 45% ground granulated blast furnace slag created an extremely durable matrix, which is the reason for using them within the research; however, their performance was only monitored through 400 accelerated freeze-thaw cycles (at -50°C in 5% NaCl). The main benefit of hydrophobic emulsions that was seen during freezing and thawing cycles was the resistance to surface scaling. Even though this was not numerically evaluated within the research, it is an important durability aspect. If these specimens were to have been tested longer, it is safe to say that the ones showing surface scaling would begin to display drops in performance for other properties such as cross sectional area change and relative dynamic modulus of elasticity. This is due to the fact that when surface scaling occurs, water can more easily penetrate into the specimen and upon freezing create internal stresses leading to the deterioration of the material. The use of a lower w/cm ratio, not only displayed better compressive strength and stiffness before freezing and thawing, but provided better resistance to freezing and thawing as well. The ECC/SECC materials with a lower w/cm ratio also provided a denser matrix with lower permeability.

The addition of superhydrophobic admixtures to ECC creates a durable material by introducing a controlled air void structure that allows for higher ductility and improved freeze-thaw resistance. This material can provide a lifespan for critical elements of bridges that will be significantly longer than materials currently being used. Moreover, the use of SECC in highway infrastructure will significantly reduce repair that may be required. Despite an increased cost of production for this material, the cost throughout its lifespan will be significantly lower. With increasing freight on highways, the need for a more durable material is evident, and indeed superhydrophobic engineered cementitious composites can provide this required durability and mechanical response for critical elements of transportation infrastructure.

8. Future Work

The results of the reported research can be used to manufacture a new-generation of superhydrophobic concrete material (Figure 74) with enhanced durability required for critical infrastructure components such as highway bridges and building foundations.

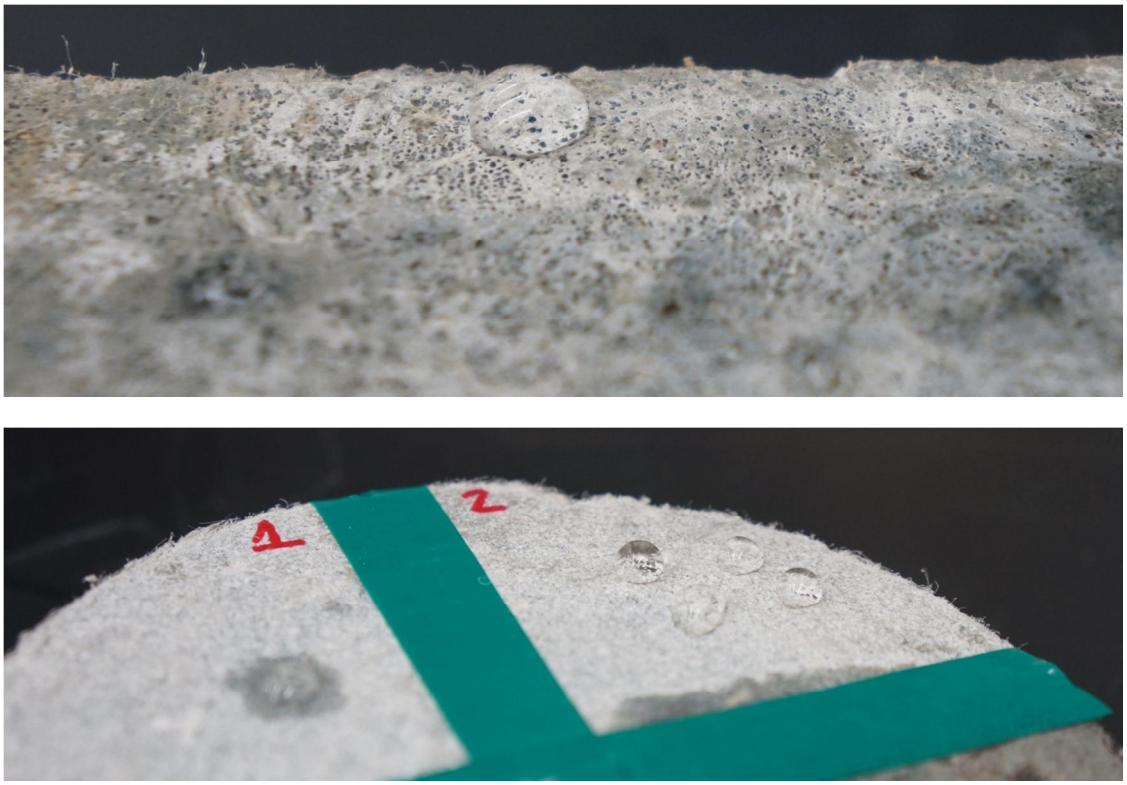

Figure 74: The Superhydrophobic Properties restored by Emulsion Application after Freeze-Thaw (top) or Abrasion (bottom, #2) Exposure

The following additional concepts such as anti-icing and de-icing properties can be investigated in the future:

a) By introducing hydrophobic fibers, particles and nanoparticles with properly selected parameters (size, volume fraction) superhydrophobic concrete with anti-icing and de-icing properties can be created;
b) The superhydrophobic concrete with anti-icing and de-icing properties can be engineered to be wear-resistant in the sense that wear (the removal of material from the surface) will not affect the performance;.
c) The superhydrophobic concrete with anti-icing and de-icing properties, capable to repel water and ice, can be designed for extreme durability.

References

[1] C. E. Report, "Poor Infrastucture Fails America," [Online]. Available: http://www.cnn.com/2009/US/01/28/infrastructure.report.car/index.html.

[2] "Deteriorating Urban Pavement Conditions Cost the Average Driver More Than $400 Annually," [Online]. Available: http://www.reuters.com/article/pressRelease/idUS101228+12-Mar-2008+PRN20080312.

[3] H. Tabatabai, A. Ghorpanpoor and A. Turnquist-Nass, "Rehabilitation techniques for concrete bridges, WHRP Report 05-01," Wisconsin Highway Research Program, 2005.

[4] F. Klaiber, K. Dunker, T. Wipt and W. Sanders, "Methods of strengthening existing highway bridges," Transportation Research Board 1180, NRC, National Academy Press, 1988.

[5] J. Hooks, "Holding it together: FHWA Bridge Plan Part 1," Roads & Bridges Magazine, 2003.

[6] H. Tabatabai, M. Tabatabai and C. Lee, "Reliability of bridge decks in Wisconsin," *ASCE Journal of Bridge Engineering,* 2010.

[7] "Trends in Highway Material Costs," [Online]. Available: http://www.wsdot.wa.gov/biz/construction/constructioncosts.cfm.

[8] M. Oliva and J. Schneider, "An innovative focus on highway bridge approach slabs," proposal funded by the FHWA CFIRE National Transportaion Center, 2009.

[9] V. Li, "Engineered cementitious composites-tailored composites through micromechanical modeling," Fiber Reinforced Concrete: Presnet and the Future, CSCE, Montreal, 1998.

[10] J. Zhang, H. Stang and V. Li, "Experimental study on crack bridging in FRC under uniaxial fatigue tension," *ASCE J. of Materials in Civil Engineering,* vol. 12, no. 1, pp. 66-73, 2000.

[11] V. LI, "Advances in ECC research," *ACI Special Publication on Concrete: Material Science to Applications,* Vols. SP206-23, pp. 373-400, 2002.

[12] L. Briaud, R. W. James and S. Hoffman, "Settlment of bridge approaches: the bump at the end of the bridge," National Cooperative Highway Reserach Program, National Reserach Council (U.S.), Transporation Reserach Board, 1997.

[13] S. J. Bok, "The bump at the endo fo the bridge: An investigation," Texas A&M University, College Station, TX, 2003.

[14] H. Walhls, "NCHRP Synthesis of highway Practices 159," Design and Construction of Bridge Approaches, National Research Council, Transportation Research Board, Washington D.C., 1990.

[15] M. Zaman and A. L. Gopalasingam, "Consolidation of settlment of bridge approach foundations," *ASCE Journal of Geotechnical Engineering,* vol. 117, 1991.

[16] T. Stark, S. Olson and J. Long, "Differential movement at the embankment/structure interface - mitigation and rehabilitation Report No. IAB=HI," Illinois Department of Transportation, Springfield, IL, 1995.

[17] K. Scharenbrock, "Use of engineering cementitious composties to improve bridge approach slab durability," Department of Civil and Environmental Engineering, University of Wisconsin-Madison, Madison, WI, 2011.

[18] G. Rajek, "Numberical modeling of the performance of highway bridge approach slabs," Department of Civil and Environmental Engineering, University of Wisconsin-Madison, Madison, WI, 2010.

[19] P. Balaguru and S. Shah, Fiber Reinforced Cement Composites, McGraw Hill, 1992.

[20] G. Batson, E. Jenkins and R. Spatney, "Steel fibers as shear reinforcement," *ACI Journal,* vol. 69, no. 10, pp. 640-644, 1972.

[21] A. Sharma, "Shear strength of steel fiber reinforced concrete beams," in *ACI*, 1986.

[22] R. Swamy and H. Bahia, "The effectiveness of steel fibers as shear reinforcement," *Concrete International,* pp. 35-40, 1985.

[23] H. Stang and T. Aarre, "Evaluation of crack width in FRC with conventional reinforcement," *Cement and Concrete Composites,* vol. 14, no. 2, pp. 143-154, 1992.

[24] H. Stang, V. Li and H. Krenchel, "Design and structural applications of stress-crack with relations in FRC," *RILEM J. Materials and Structures,* 1993.

[25] D. Mishra, "Design of pseudo strain-hardening cementitious composites for a ductile plastic hinge," Department of Civil and Environmental Engineering, University of Michigan, Ann Arbor, MI, 1995.

[26] V. Li, S. Wang and C. Wu, "Tensile strain-hardening behavior of polyvinyl alcohol engineered cementitious composites (PVA-ECC)," *ACI Matieral Journal,* vol. 98, no. 6, pp. 483-492, 2001.

[27] V. Li, H. Stang and H. Krenchel, "Micromechanics of crack bridging in fiber-reinforced concrete," Advanced Civil Engineering Materials Reserach Laboratory, University of Michigan, Ann Arbor, MI, 1993.

[28] V. Li, "On engineered cementitious composites (ECC), A review of the material and its applications".

[29] V. Li and C. Leung, "Steady state and multiple cracking of short random fiber composites," *ASCE J. Engineering Mech.,* vol. 118, no. 11, pp. 2246-2264, 1992.

[30] V. Li, C. Wu, S. Wang, A. Ogawa and T. Saito, "Interface tailoring for strain-hardening polyvinyl alcohol-engineered cementitious composites (PVA-ECC)," *ACI Materials Journal,* vol. 99, no. 5, pp. 463-472, 2002.

[31] K. Sobolev and V. Bartrakov, "The effect of a PEHSO on the durability of concrete with supplementary cementitious materials," *ASCE Journal of Materials in Civil Engineering,* vol. 19, no. 10, pp. 809-819, 2007.

[32] K. Sobolev and M. Ferrada-Guiierrez, "How nanotechnology can change the concrete world :part 2," *American Ceramic Dociety Bulletin 11,* no. 11, 2005.

[33] B. Poole, "Biomimetics: Borrowing from Biology," [Online]. Available: http://www.thenakedsciences.com/HTML/articles/articl/biomimeticsborrowingfrombiology/.

[34] K. Kock, B. Bhushan and W. Barthlott, "Diversity of structure, morphology and wetting of plant surfaces," *Soft Matter,* vol. 4, pp. 1943-1963, 2008.

[35] R. Pinto and K. Hover, "Frost Scaling resistance of high strength concrete.," Portland Cement Assocation, Research and Development Bulletin RD122, 2001.

[36] S. Mindess and J. Young, Concrete, New York: Prentice-Hall, 1981.

[37] J. Tanesi and R. Meininger, "Freeze-thaw resistance of concrete with marginal air content," US Department of Transportation, Publication No. FHWA-HRT-06-117, 2006.

[38] P. Aitcin, High Performance Concrete, New York: E & Fn Spon., 1998.

[39] D. Zolocha and J. Kasperkiewicz, "Estimation of the structure of air entrained cocnrete using a flatbed scanner," *Cement and Concrete Research,* vol. 35, no. 10, pp. 2041-2046, 2005.

[40] ASTMC465-08, "Standard test for microscopical determination of parameters of the air-void system in hardened concrete," 2008.

[41] H. Titi, A. Druckery and K. Alshili, "Characterization of aggregates for sustainable freight transportation infrastructure," CFIRE Paper No. 11-2, Milwaukee, WI.

[42] S. Wang and V. Li, "Engineered cementitious composites with high-volumes of fly ash," *ACI Matierals Journal,* vol. 104, no. 3, pp. 233-231, 2007.

[43] V. Li and S. Wang, "PVA fiber reinforced engineered cementitious composite material and design performances".

[44] E. Yang, "Designing added functions in engineered cementitious composites," Department of Civil and Environmental Engineering, University of Michigan, Ann Arbor, MI, 2008.

CFIRE

University of Wisconsin-Madison
Department of Civil and Environmental Engineering
1410 Engineering Drive, Room 270
Madison, WI 53706
Phone: 608-263-3175
Fax: 608-263-2512
cfire.wistrans.org